Improvement and Further Development in CESM/CAM5: Gas-Phase Chemistry and Inorganic Aerosol Treatments

Jian He[1] and Yang Zhang[1,*]

[1]Air Quality Forecasting Laboratory, Department of Marine, Earth, and Atmospheric Sciences, North Carolina State University, Raleigh, NC, 27695, USA

Abstract: Gas-phase chemistry and subsequent gas-to-particle conversion processes such as new particle formation (J), condensation, and thermodynamic partitioning have large impacts on air quality, climate, and public health through influencing the amounts and distributions of gaseous precursors and secondary aerosols. Their roles in global air quality and climate are examined in this work using the Community Earth System Model version 1.0.5 (CESM1.0.5) with the Community Atmosphere Model version 5.1 (CAM5.1) (referred to as CESM1.0.5/CAM5.1). CAM5.1 includes a simple chemistry that is coupled with a 7-mode prognostic Modal Aerosol Model (MAM7). MAM7 includes classical homogenous nucleation (binary and ternary) and activation nucleation (empirical first-order power law) parameterizations, and a highly-simplified inorganic aerosol thermodynamics treatment that only simulates particulate-phase sulfate (SO_4^{2-}) and ammonium (NH_4^+). In this work, a new gas-phase chemistry mechanism based on the 2005 Carbon Bond Mechanism for Global Extension (CB05_GE) and several advanced inorganic aerosol treatments for condensation of volatile species, ion-mediated nucleation (IMN), and explicit inorganic aerosol thermodynamics have been incorporated into CESM/CAM5.1-MAM7. Comparing to the simple gas-phase chemistry, CB05_GE can predict many more gaseous species, and thus could improve model performance for $PM_{2.5}$, PM_{10}, PM components, and some PM gaseous precursors such as SO_2 and NH_3 in several regions, as well as aerosol optical depth (AOD) and cloud properties (e.g., cloud fraction (CF), cloud droplet number concentration

* Email: yang_zhang@ncsu.edu, Phone: (919)-515-9688

(CDNC), and shortwave cloud forcing (SWCF)) on globe. The modified condensation and aqueous-phase chemistry could further improve the predictions of additional variables such as HNO_3, NO_2, and O_3 in some regions, and new particle formation rate (J) and AOD over globe. IMN can improve the predictions of secondary $PM_{2.5}$ components, $PM_{2.5}$, and PM_{10} over Europe, as well as AOD and CDNC over globe. The explicit inorganic aerosol thermodynamics using ISORROPIA II improves the predictions of all major $PM_{2.5}$ components and their gaseous precursors in some regions, as well as downwelling shortwave radiation, SWCF, and cloud condensation nuclei at a supersaturation of 0.5% over globe. For simulations of 2001-2005 with all the modified and new treatments, the improved model predicts that on a global average, SWCF increases by 2.7 W m^{-2}, reducing NMBs of SWCF from -5.4% to 1.2%. Uncertainties in emissions can explain largely the inaccurate predictions of precursor gases (e.g., SO_2, NH_3, and NO) and primary aerosols (e.g., black carbon (BC) and primary organic matter (POM)). Additional factors leading to discrepancies between model predictions and observations include uncertainties in model treatments such as dust emissions, secondary organic aerosol (SOA) formation, multiple-phase chemistry, cloud microphysics, aerosol-cloud interaction, dry and wet deposition, and model parameters (e.g., accommodation coefficients and prefactors of the nucleation power law), as well as uncertainties in model configuration such as the use of a coarse grid resolution.

Keywords: CESM/CAM5.1, CB05_GE, New particle formation, Aerosol thermodynamics, Ion-mediated nucleation, ISORROPIA II, Earth system modeling

1. Introduction

Atmospheric gases and aerosols play important roles in climate change due to their ability to directly or indirectly alter the Earth's radiation balance. Atmospheric chemistry determines the distribution of important oxidants and gaseous precursors for secondary air pollutants such as ozone (O_3) and fine particular matter ($PM_{2.5}$). Meanwhile, climate change can strongly influence atmospheric chemistry and air quality. Therefore, gas-phase chemistry is an important component for atmospheric and Earth system models. Different chemical reactions and kinetic parameters can lead to differences in the predictions of gases, secondary aerosols, new particle formation rate (J), as well as climatic variables such as cloud condensation nuclei (CCN), cloud droplet number concentration (CDNC), and radiative forcing (Faraji et al., 2008; Luecken et al., 2008; Sarwar et al., 2008; Kim et al., 2011a; Zhang et al., 2012a; Lamarque et al., 2013; Young et al., 2013; Shindell et al., 2013).

Aerosol can influence the Earth's radiative balance by directly scattering and absorbing radiation and indirectly affecting cloud properties through acting as CCN and ice nuclei (IN). Therefore, it is important to accurately simulate aerosol size distribution, chemical composition, and properties, which can determine the magnitude of aerosol radiative forcing (Koloutsou-Vakakis et al., 1998). Aerosol and its influence on climate have been included in many global climate models (GCMs) such as the Community Climate System Model (CCSM) (Collins et al., 2006; Gent et al., 2010), the 5th generation of global climate model modified from European Centre for Medium-Range Weather Forecasts in Hamburg (ECHAM5) (Roeckner et al., 2003, 2006a; Stier et al., 2005), and Earth system models such as the Community Earth System Model (CESM) (Ghan et al., 2012; Liu et al., 2012), the Integrated Global System Model (IGSM) (Dutkiewicz et al., 2005; Sokolov et al., 2005; Monier et al., 2013), and the Earth System Model (ESM) (Dunne et al., 2012, 2013). However, due to the complexity of aerosol microphysical

processes and their interactions with cloud processes, it remains a challenge to accurately represent those properties and processes in GCMs.

Inorganic aerosols comprise 25-50% of fine aerosol mass (Heintzenberg, 1989), which mainly includes sulfate (SO_4^{2-}), ammonium (NH_4^+), nitrate (NO_3^-), chloride (Cl^-), and sodium (Na^+). The physical and chemical properties of these aerosol constituents have been understood reasonably well, making it possible to simulate aerosol physical and chemical processes in GCMs. Major gas-to-particle conversion processes of inorganic aerosols include condensation, nucleation, and thermodynamics. An important factor that determines the condensation of gases is the mass accommodation coefficient (α), which can be measured through laboratory experiments. The measured α values, however, are subject to large uncertainty and may vary in several orders of magnitudes under different laboratory conditions. To simulate aerosol condensational growth, a constant value of α is therefore often assumed in GCMs, which is a source of uncertainty in model predictions.

Homogeneous nucleation of H_2SO_4 vapor produces new particles that can grow to form CCN. Different nucleation parameterizations are used in GCMs or global aerosol models. For example, Kulmala et al. (2006), Sihto et al. (2006), and Kuang et al. (2008) derived empirical power laws with the first- or second-order dependencies of new particle formation rates (J) on H_2SO_4 vapor concentration from observations based on cluster-activation or barrierless kinetic mechanisms, which have been used in the Community Atmosphere Model (CAM) (Wang and Penner, 2009), the Global-through-Urban Weather Research and Forecasting model with Chemistry (GU-WRF/Chem) (Zhang et al., 2012b), and Global Model of Aerosol Processes (GLOMAP) (Spracklen et al., 2006). An ion-mediated nucleation (IMN) model was developed to calculate J based on ambient atmospheric conditions, H_2SO_4 vapor concentrations, ionization

rate, and surface area of preexisting particles. It has been used in GEOS-Chem (Yu et al., 2008; Yu et al., 2010), CAM (Yu et al., 2012), and GU_WRF/Chem (Zhang et al., 2012). Different nucleation parameterizations lead to significant differences in J predictions by regional and global models (Zhang et al., 2010) and CCN/CDNC (Yu and Luo, 2009; Pierce and Adams, 2009; Kuang et al., 2009; Zhang et al., 2012; Yu et al., 2012). Limited observations make it difficult to validate predicted J values and appropriateness of various parameterizations.

A number of thermodynamic aerosol modules have been developed to understand physical and chemical properties of inorganic aerosols. For example, EQUISOLV II (Jacobson, 1999) has been used in a one-way nested (from global to local scales) gas, aerosol, transport, radiation, general circulation, mesoscale, and ocean model (GATOR-GCMOM) (Jacobson, 2010). EQUISOLV II uses analytical equilibrium iteration and mass flux iteration to solve equilibrium problems (Jacobson, 1999), which requires relatively large computational cost. SCAPE2 is used in the California Institute of Technology (CIT) model (Meng et al., 1998). ISORROPIA (Nenes et al., 1998) has been used in several global models such as GEOS-Chem (Bey et al., 2001), the GISS Caltech (Liao et al., 2003), and the GU-WRF/Chem (Zhang et al., 2012) and regional models such as the Community Multiscale Air Quality model (CMAQ) (Byun and Schere, 2006) and the Comprehensive Air Quality Model with Extensions (CAMx) (ENVIRON, 2010). An updated version, ISORROPIA II (Fountoukis and Nenes, 2007), has also been implemented in recent versions of CMAQ (e.g., CMAQ v4.7-Dust (Wang et al., 2012) and CMAQ v5.0 (Appel et al., 2013)), GEOS-Chem (Fountoukis and Nenes, 2007), and ECHAM5 with MESSy Atmospheric Chemistry and Global Modal-aerosol eXtension (EMAC/GMXe) (Metzger et al., 2011). The Multicomponent Equilibrium Solver for Aerosols (MESA) (Zaveri et al., 2005) has been used in the mesoscale WRF/Chem (Fast et al., 2006). The Equilibrium

Simplified Aerosol Model (EQSAM) has been updated in EMAC/GMXe in the past decade (Metzger et al., 2002, 2007, and 2011). These modules assume that particles simulated in a given particle size range have the same composition (i.e., internal mixture) and most of the modules assume that thermodynamic equilibrium exists between the gas and particulate phases for volatile compounds. Different aerosol thermodynamic models can lead to different aerosol predictions (Nenes et al., 1998; Zhang et al., 2000; Zaveri et al., 2005; Metzger et al., 2011). Zhang et al (2000) reported average absolute differences of 7.7% - 12.3% in total PM predictions between different thermodynamic modules under 400 test conditions but the differences could be as large as 68% under some cases (e.g., high nitrate/chloride concentrations and low/medium relative humidity (RH)). Fountoukis and Nenes (2007) found the largest discrepancies between ISORROPIA II and SCAPE2 in water concentration predictions exist under low RH conditions (RH < 60%), primarily from differences in the treatment of water uptake and solid state composition. The 3-D atmospheric models with these modules include explicit thermodynamic treatments for sulfate, ammonium, nitrate, sodium, and chloride. For comparison, some GCMs, such as CAM, use highly-simplified thermodynamics that treats sulfate and ammonium only. Most thermodynamic modules assume thermodynamic equilibrium between the gas and particulate phases for volatile compounds. However, if the time needed for the system achieving chemical equilibrium is much longer than the time step used in the model, the equilibrium assumption is not valid, which often occurs for coarse particles and cooler conditions (Wexler and Seinfeld, 1991; Meng and Seinfeld, 1996). Therefore, it remains a challenge to simulate thermodynamics for coarse particles.

In this work, a comprehensive gas-phase chemical mechanism and detailed inorganic aerosol treatments for nucleation and aerosol thermodynamics are incorporated into CAM

141 version 5.1 (CAM5.1) in the CESM version 1.0.5 (CESM1.0.5). Several modifications are also
142 made to the existing treatments such as condensation and aqueous-phase chemistry. The
143 objectives are to improve the representations of gas-phase chemistry and inorganic aerosol
144 treatments in CESM/CAM5.1, and reduce uncertainties in the chemical and radiative predictions
145 associated with those processes. The improved model with enhanced capabilities can be applied
146 for decadal simulations to study interactions among atmospheric chemistry, aerosols, and climate
147 change.
148
149 **2. Model Development and Improvement**
150 CESM is a fully-coupled global Earth system model, which includes land, ocean,
151 atmosphere, and sea ice components. The atmosphere component used in this study is CAM5.1.
152 Existing and new model treatments related to this study are described in this section. Further
153 details on CAM5.1 can be found at http://www.cesm.ucar.edu/models/cesm1.0/cam/.
154
155 2.1 Existing Gas-Phase Chemistry and Aerosol Treatments in CESM/CAM5.1
156 CAM5.1 uses a simple gas-phase chemistry for sulfur species, which includes 1
157 photolytic reaction and 7 kinetic reactions among 6 gas-phase species (i.e., hydrogen peroxide
158 (H_2O_2), sulfuric acid (H_2SO_4), sulfur dioxide (SO_2), dimethylsulfide (DMS), ammonia (NH_3),
159 and semi-volatile organic gas (SOAG)). A more comprehensive gas-phase mechanism with 40
160 photolytic reactions and 172 kinetic reactions among 103 species, i.e., the Model of OZone and
161 Related chemical Tracers version 4 (MOZART-4) of Emmons et al. (2010), has been
162 incorporated into the official released CAM5.1. It is, however, only coupled with the bulk
163 aerosol module (BAM) in CAM5.1. In addition to BAM, CAM5.1 contains the modal aerosol

model (MAM) that is based on modal representations of aerosols. In this study, MAM is used because it can represent more accurate size distributions as compared to BAM. There are two versions of MAM, one with seven lognormal modes (MAM7), and the other with three lognormal modes (MAM3) (Liu et al., 2012), and both are coupled with the simple gas-phase chemistry in the default model. MAM7 is used in this study because it contains explicit treatments for ammonium and size distributions for dust, sea-salt, and primary carbon compared to MAM3. MAM7 explicitly treats sulfate, ammonium, sea-salt, dust, BC, POM, and SOA. It simulates condensational growth of aerosol, nucleation, coagulation, dry deposition, wet removal, and water uptake. Condensation is simulated based on a kinetic approach, in which MAM7 treats H_2SO_4, NH_3, and methanesulfonic acids (MSA) as completely non-volatile species and treats SOAG as a volatile species, using a constant accommodation coefficient of 0.65 for all these condensing species based on Adams and Seinfeld (2002). NH_3 condensation stops when the NH_4^+/SO_4^{2-} molar ratio of a particle mode reaches 2 (i.e., fully neutralized by SO_4^{2-} ions). The net uptake rate, I_{net}, due to gas to particle mass transfer for each species to each mode is simulated as,

$$I_{net} = \int dx \frac{dN}{dx} I_{cond} \quad (1)$$

$$I_{cond} = 2 \times \pi \times D_g \times D_p \times F(Kn, \alpha) \quad (2)$$

$$F(Kn, \alpha) = \frac{0.75 \times (1 + Kn)}{Kn \times \left(\frac{1 + Kn}{\alpha} + 0.283 \right) + 0.75} \quad (3)$$

where D_p is the particle diameter; x is the logarithmic diameter of particle, = $ln(D_p)$; dN/dx is the log-normal particle number density distribution; I_{net} is the gas condensation rate; Kn is the Knudsen number; α is the accommodation coefficient of condensable vapor; D_g is the gas diffusivity, and F(Kn, α) is the Fuchs-Sutugin correction factor that describes the resistance to

uptake caused by gas-phase diffusion. Equation (1) is solved using the Gauss-Hermite quadrature of order 2. Based on equation (3), as α approaches zero, F(Kn, α) approaches zero. Consequently, I_{cond} (i.e., the uptake rate) approaches zero in equation (1).

There are three nucleation parameterizations in MAM7. The empirical power law of Wang and Penner (2009) (WP09) is used in the planetary boundary layer (PBL), which includes a first-order dependence on H_2SO_4 vapor with a prefactor of 1×10^{-6}. The binary H_2SO_4-H_2O homogeneous nucleation of Vehkamaki et al. (2002) (VE02) and ternary H_2SO_4-NH_3-H_2O homogeneous nucleation of Merikanto et al. (2007) (ME07) are used above PBL. MAM7 also includes simplified inorganic aerosol thermodynamics that only involves sulfate and ammonium. A more detailed description of MAM can be found in Liu et al. (2012).

2.2 New and Modified Model Treatments Implemented in This Work

2.2.1 Gas-Phase Chemical Mechanism

Highly simplified gas-phase mechanism can result in large uncertainties in the predictions of oxidants and gaseous precursors for secondary aerosols. Therefore, a new gas-phase mechanism, the 2005 Carbon Bond Mechanism for Global Extension (CB05_GE) (Karamchandani et al., 2012) has been implemented into CAM5.1 using the same chemical preprocessor as MOZART-4 (Lamarque et al., 2012) and coupled with both MAM3 and MAM7. CB05_GE was developed to simulate major chemical reactions for global-through-urban applications as illustrated in Zhang et al. (2012). A more detailed description of CB05_GE can be found in Karamchandani et al. (2012). In this study, gas precursors for SOA in CB05_GE are mapped to SOAG to make it compatible in MAM7. As the first study of CESM/CAM5.1 with CB05_GE, this work focuses on the impact of gas-phase chemistry. The heterogeneous

chemistry on the surface of aerosol is turned off. CB05_GE implemented in CESM/CAM5 contains a total of 273 reactions including 50 photolytic reactions and 223 kinetic reactions among 93 gas-phase species in this study. The gas-phase chemical system is solved using an implicit backward Euler method.

2.2.2 Ion-mediated nucleation parameterization

Ions generated by cosmic radiation and natural radioactive decay have been studied for a long time as an important source to enhance nucleation (Raes et al., 1986). An IMN model is developed by Yu (2010) (Yu10) for H_2SO_4-H_2O system, and explicitly solves the dynamic equations in terms of temperature, relative humidity, H_2SO_4 vapor concentration, ionization rate, and surface area of preexisting particles. Different from classic binary nucleation theory, which is based on the minimization of changes in Gibbs free energy (Seinfeld and Pandis, 2006), IMN is based on a kinetic model that considers the interactions among ions, neutral and charged clusters, vapor molecules, and preexisting particles (Yu and Turco, 2000, 2001; Yu, 2006, 2010). The global ionization rates due to cosmic rays are calculated based on the schemes given in Usoskin and Kovaltsov (2006) and the contribution of radioactive materials from soil to ionization rates is parameterized based on the profiles given in Reiter (1992). To reduce the computing cost using IMN in 3-D models, Yu et al. (2008) developed lookup tables with simple interpolation subroutines to calculate nucleation rates under typical atmospheric conditions. In this work, IMN based on YU10 is implemented into MAM7 and combined with default nucleation parameterizations (VE02, ME07, and WP09) in order to improve the J predictions and aerosol number concentrations in upper troposphere. The J value above PBL is taken as the maximum value among predictions from IMN (YU10) and homogeneous nucleation (VE02 or ME07), and

the J value within PBL is taken as the maximum value among predictions from IMN (YU10), homogeneous nucleation (VE02 or ME07), and the first-order parameterization (WP09).

2.2.3 Inorganic Aerosol Thermodynamics

Gas-particle partitioning is an important process in the formation and evolution of secondary aerosols. Several factors affect gas-particle partitioning, such as temperature, relative humidity, saturation vapor pressures of species, the physical state of the condensed-phase, and the way in which aerosol components interact each other (Cappa et al., 2008; Zuend et al., 2010). Most models focus on inorganic aerosols. Fountoukis and Nenes (2007) developed a computationally-efficient thermodynamics equilibrium model, ISORROPIA II, for the magnesium (Mg^{2+}) - potassium (K^{+}) - calcium (Ca^{2+}) - NH_4^{+}- Na^{+} - SO_4^{2-}- NO_3^{-}- Cl^{-}- H_2O aerosol system. An important difference between ISORROPIA II and most other thermodynamics equilibrium models is that ISORROPIA II simulates crustal species, such as Mg^{2+}, K^{+}, and Ca^{2+}, which are important constituents of atmospheric aerosols, in particular, mineral dust. Therefore, to explicitly simulate aerosol thermodynamics, ISORROPIA II has been implemented into MAM7 and applied for accumulation, Aitken, fine sea-salt, and fine dust modes to explicitly simulate thermodynamics of SO_4^{2-}, NH_4^{+}, NO_3^{-}, Cl^{-}, and Na^{+} as well as the impact of crustal species associated with fine dust modes on aerosol thermodynamics. The concentrations of K^{+}, Ca^{2+}, and Mg^{2+} as the input for ISORROPIA II are calculated from dust concentrations, using the mass ratios of 1.022×10^{-3}, 1.701×10^{-3}, and 7.084×10^{-4}, respectively (Van Pelt and Zobeck, 2007). Aerosol thermodynamics involving coarse particles (in coarse sea-salt and coarse dust modes) is currently not treated in this work, given the high computational cost (by at least a factor of 3) for solving the non-equilibrium system involving coarse particles.

253

254 2.2.4 Modifications of Existing Aerosol Treatments

255 MAM 7 does not treat NO_3^- and it treats NaCl as one species. In this work, MAM7 is
256 modified to explicitly simulate NO_3^-, Cl^-, and Na^+ using a similar method to the condensation of
257 H_2SO_4 and NH_3. NO_3^- and Cl^- are simulated in all modes except for primary carbon mode. Na^+ is
258 simulated in sea-salt modes. The source of Na^+ is calculated based on the mass ratio of Na and Cl
259 from sea-salt emissions. The source of Cl^- includes sea-salt emissions, and the condensation of
260 HCl resulted from HCl emissions and gas-particle partitioning of total chloride.

261 Species-dependent accommodation coefficients are used for H_2SO_4, NH_3, HNO_3, and
262 HCl, with the values of 0.02, 0.097, 0.0024, and 0.005 (Zhang et al., 1998; Sander et al., 2002),
263 respectively. Since by default the model treats the condensation of inorganic volatile gas species
264 as irreversible process (no evaporation) (see equation (1)), the lower limit values of mass
265 accommodation coefficients are used for these species to represent their net fluxes from the gas-
266 phase to the liquid/solid phases. Such lower limit values correspond to uptake coefficients, which
267 represent the net fluxes and are smaller than mass accommodation coefficients. To ensure
268 electroneutrality in each mode after kinetically condensing H_2SO_4, NH_3, HNO_3, and HCl at
269 different condensation (or uptake) rates, the condensation of NH_3 will stop when the mole
270 concentration of cations (i.e., NH_4^+) is equal to sum of those of anions (i.e., $[NH_4^+] = 2\times[SO_4^{2-}]+[NO_3^-]+[Cl^-]$).

272 The original MAM7 treats $NH_3(g)/NH_4^+$ in cloud water. In this work, the dissolution and
273 dissociation of HNO_3 and HCl to produce NO_3^- and Cl^- in cloud water are added in the model
274 based on Schwartz (1984), Marsh and McElroy (1985), and Seinfeld and Pandis (2006), i.e.,

275

$$HNO_{3\,(g)} \rightleftharpoons HNO_3(aq) \rightleftharpoons H^+ + NO_3^-$$

$$HCl_{(g)} \rightleftharpoons HCl_{(aq)} \rightleftharpoons H^+ + Cl^-$$

The concentration of H^+ (thus the pH value of the solution) is obtained by solving the electro-neutrality equation using the bisection method. The aqueous-phase chemical system is solved analytically.

3. Model Configurations and Evaluation Protocols

3.1 Model Setup and Simulation Design

Table 1 summarizes the CESM/CAM5.1 simulations that are designed to examine the impacts of individual new and modified treatments on model predictions. The first set of simulations includes two simulations with the same default MAM7 coupled with different gas-phase mechanisms: one uses the simple gas-phase chemistry (MAM_SIM) with a total of 37 prognostic species and one uses the CB05_GE (MAM_CB05_GE) with a total of 127 prognostic species. A comparison of the two simulations provides an estimate of the impacts of gas-phase chemical mechanisms. The second set of simulations consists of five simulations that use the same CB05_GE gas-phase mechanism but with modified and new aerosol treatments individually and jointly. The first one is MAM_CON that uses an explicit treatment for NO_3^-, Cl^-, and Na^+ and species-dependent mass accommodation coefficients for condensation and that includes the aqueous-phase chemistry of HNO_3/NO_3^- and HCl/Cl^-. This simulation includes a total of 139 prognostic species. The second one is MAM_CON/IMN that uses the same treatments as MAM_CON but with IMN as one of the nucleation mechanisms and a prefactor of 1.0×10^{-8} in WP09. The third one is MAM_CON/ISO that uses the same treatments as MAM_CON but with ISORROPIA II for aerosol thermodynamics assuming metastate

298 equilibrium (i.e., liquid only). The fourth one is MAM_NEWA that uses the same treatments as
299 MAM_CON but with all new and modified aerosol treatments and a prefactor of 1.0×10^{-9} for
300 WP09. The fifth one is MAM_NEWB that uses the same treatments as MAM_NEWA, but with
301 ISORROPIA II assuming a stable condition (i.e., solid and liquid coexist). A comparison of
302 MAM_CB05_GE with MAM_CON indicates the impact of modified condensation and aqueous-
303 phase chemistry. A comparison of MAM_CON/IMN, MAM_CON/ISO, and MAM_NEWA with
304 MAM_CON indicates the impacts of IMN, ISORROPIA II, and combined new and modified
305 aerosol treatments, respectively. Comparison of MAM_NEWB with MAM_NEWA indicates the
306 impacts of thermodynamic conditions on gas-aerosol partitioning. The 3rd set of simulation
307 includes one simulation using the same configuration as MAM_NEWA but with adjusted
308 emissions (MAM_NEW/EMIS). Its comparison with MAM_NEWA indicates the impacts of
309 uncertainties in emissions on model predictions. The 4th set of simulation includes one simulation
310 using the same configuration as MAM_SIM but with prescribed SST for a 5-yr period during
311 2001-2005 (MAM_SIM_5Y), and two simulations both using the same configuration as
312 MAM_NEW/EMIS for 2001-2005, but one with prescribed SST (MAM_NEW_5YA), and the
313 other in a fully-coupled mode (MAM_NEW_5YB).

314 All these simulations use the same approach for photolytic rates calculations based on
315 Lamarque et al. (2012), the same aqueous-phase chemistry of Barth et al. (2000), and the same
316 physical options as those in MAM_SIM. Major physical options include the cloud microphysics
317 parameterization of Morrison and Gettelman (2008), the moisture PBL scheme of Bretherton and
318 Park (2009), the shallow convection scheme and deep convection scheme of Park and Bretherton
319 (2009) and Zhang and McFarlane (1995), respectively, the aerosol activation parameterization of
320 Abdul-Razzak and Ghan (2000), and the Rapid Radiative Transfer Model for GCMs (RRTMG)

of Mlawer et al. (1997) and Iacono et al. (2003, 2008) for long and short-wave radiation. The land surface processes are simulated by the Community Land Model (CLM) of Lawrence et al. (2011) in CESM that is coupled with CAM5.1.

All simulations except for MAM_SIM_5Y and MAM_NEW_5YA are performed with fully-coupled CESM1.0.5 with standard B_1850-2000_CAM5_CN configuration, which represents 1850 to 2000 transient conditions and includes all active components in CESM with biogeochemistry in the land model. MAM_SIM_5Y and MAM_NEW_5YA are performed with standard F_AMIP_CAM5 configuration, which uses a climatological dataset for SST provided by NCAR for ocean model. The simulations are conducted for the full-year of 2001 and 2001-2005 at a horizontal resolution of $0.9^{o}\times1.25^{o}$ and a vertical resolution of 30 layers for CAM5.1. The initial conditions for ice and ocean models are from CESM default settings. The initial conditions for the land model are based on the output from the NCAR's CESM/CAM4 B_1850-2000_CN simulation. The initial conditions for CAM5 are derived from a 10-yr (1990-2000) CAM5 standalone simulation with the MOZART chemistry provided by NCAR. A 1-year (January 1-December 31, 2000) CESM/CAM5 simulation using NCAR's CESM B_1850-2000_CAM5_CN component set is performed as spinup to provide the initial conditions for meteorological variables and chemical species that are treated in both MOZART and CB05_GE. An additional 3-month (October 1-December 31, 2000) CESM/CAM5 simulation based on a 10-month (January-October, 2000) CESM/CAM5 output using initial conditions from NCAR's CESM B_1850-2000_CAM5_CN is performed as spinup to provide initial conditions for chemical species that are treated in CB05_GE but not in MOZART. All production simulations of 2001 are from January 1 - December 31, 2001 and those of 2001-2005 are from January 1, 2001- December 31, 2005. The offline anthropogenic emissions used in all simulations except

for MAM_NEW/EMIS are taken from Zhang et al. (2012) (see Table 2 of Zhang et al. (2012) for the sources of those anthropogenic emissions). Anthropogenic emissions used in MAM_NEW/EMIS are adjusted emissions based on those of Zhang et al. (2012), with adjustment factors of 0.7, 0.5, and 1.2 for SO_2 over CONUS, Europe, and Asia, respectively, and 1.2 for NH_3, BC, and organic carbon (OC), and 1.3 for carbon monoxide (CO) over all three regions. Those emissions are adjusted based on the comparison with the emission inventories from the Representative Concentration Pathways (RCPs), the MOZART version 4 (MOZART-4), the Reanalysis of the TROpospheric chemical composition (RETRO), the Global Fire Emissions Database (GFED) version 2, and preliminary evaluation of CESM/CAM5.1 with modified and new gas and aerosol treatments using available observations. The online emissions include biogenic volatile organic carbon (Guenther et al., 2006), mineral dust (Zender et al., 2003), and sea-salt (Martensson et al., 2003).

3.2 Available Measurements for Model Validation

A number of observational datasets from surface networks and satellites are used for model evaluation. They are summarized along with the variables to be evaluated in Table 2. Global surface networks include the Baseline Surface Radiation Network (BSRN) and the National Oceanic and Atmospheric Administration Climate Diagnostics Center (NOAA/CDC). The satellite datasets include the Moderate Resolution Imaging Spectroradiometer (MODIS), the Clouds and Earth's Radiant Energy System (CERES), the Total Ozone Mapping Spectrometer/the Solar Backscatter UltraViolet (TOMS/SBUV), the Measurements Of Pollution In The Troposphere (MOPITT), and the Global Ozone Monitoring Experiment (GOME). Other satellite-based data include the MODIS-derived CDNC from Bennartz (2007) (BE07).

Regional observational networks include the Clean Air Status and Trends Network (CASTNET), the Interagency Monitoring of Protected Visual Environments (IMPROVE), and the Speciation Trends Network (STN) over CONUS; the European Monitoring and Evaluation Program (EMEP), the Base de Données sur la Qualité de l'Air (BDQA), and the European air quality database (AirBase) over Europe; the Ministry of Environmental Protection of China (MEP of China), the National Institute for Environmental Studies of Japan (NIES of Japan), and Taiwan Air Quality Monitoring Network (TAQMN) over East Asia. The observational data for particle formation rate J is compiled from Kulmala et al. (2004) and Yu et al. (2008), which include land-, ship-, and aircraft-based measurements.

3.3 Evaluation Protocol

The protocols for performance evaluation include spatial distributions and statistics, following the approach of Zhang et al. (2012). The analysis of the performance statistics will focus on mean bias (MB), normalized mean bias (NMB), normalized mean error (NME), and root mean square error (RMSE). The radiative variables are evaluated annually, including downwelling shortwave radiation (SWD) and downwelling longwave radiation (LWD) from BSRN; outgoing longwave radiation (OLR) from NOAA/CDC; shortwave cloud forcing (SWCF) from CERES; cloud fraction (CF), aerosol optical depth (AOD), cloud optical thickness (COT), cloud water path (CWP), precipitating water vapor (PWV), and CCN from MODIS; as well as CDNC from BE07. Chemical concentrations evaluated include seasonal and annual averaged concentrations of CO, O_3, SO_2, NH_3, NO_2, HNO_3, PM, and its major components (i.e., SO_4^{2-}, NO_3^-, and NH_4^+, BC, OC, total carbon (TC) for CONUS and Europe). The chemical observations over East Asia are very limited, and they only include surface concentrations of CO,

390 SO_2, NO_2, O_3, and PM_{10}. Column concentrations of tropospheric CO and NO_2, and tropospheric
391 O_3 residual (TOR) are evaluated for globe.
392 All observational data used for evaluating 2001 simulations are based on 2001 only
393 except for particle formation rates (J) that are based on different years compiled from Kulmala et
394 al. (2004) and Yu et al. (2008). All observational data used for evaluating 2001-2005 simulations
395 are based on 2001-2005.
396
397 **4. Model Evaluation for MAM_SIM Based on Original Model Treatments**
398 Tables 3 and 4 show MBs and NMBs of radiative/cloud and chemical predictions,
399 respectively. The model performance of the baseline simulation, MAM_SIM, is discussed below,
400 and that for all other simulations will be discussed in section 5.
401 As shown in Table 3, radiative variables such as LWD and SWD are underpredicted by
402 3.4 W m^{-2} (~ -1.1%) and 2.0 W m^{-2} (~ -1.1%), respectively, whereas OLR and SWCF are
403 overpredicted by 8.8 W m^{-2} (~ 4.1%) and 3.2 W m^{-2} (~ 7.9%) respectively. Cloud variables such
404 as CF and PWV are slightly underpredicted, whereas COT, CWP, column CCN at a
405 supersaturation of 0.5% (CCN5), and CDNC are largely underpredicted, with NMBs of -77.8%
406 to -55.6%, which is likely due to the limitations in the current model treatments of cloud
407 microphysics and aerosol-cloud interactions in CAM5.1.
408 AOD is also underpredicted by 36.1%, which is likely due to inaccurate predictions of
409 aerosol concentrations and uncertainties in the assumed hygroscopicity of aerosol components in
410 the calculation of optical properties and water uptake. For example, as shown in Table 4, $PM_{2.5}$
411 concentrations over CONUS and Europe, and PM_{10} concentrations over CONUS, Europe, and
412 East Asia are underpredicted, with NMBs of -67.5% to -31.8%, which is due to the inaccurate

413 predictions of SO_4^{2-}, NH_4^+, and organic aerosols, and missing major inorganic aerosol species
414 such as nitrate and chloride. The concentrations of BC, OC, and TC are underpredicted (by ~
415 50%), which is likely due to the uncertainties in the BC and primary OC emissions as well as
416 treatments for SOA formation. In particular, the SOA treatment used in CAM5.1 is based on a
417 highly-simplified aerosol yield approach with a single lumped semi-volatile organic gas (i.e.,
418 SOAG). For gaseous species, SO_2 concentrations over CONUS and Europe are significantly
419 overpredicted by 10.3 μg m^{-3} (~ 264.8%) and 6.6 μg m^{-3} (~ 97.5%), respectively, whereas SO_2
420 concentrations over East Asia are largely underpredicted by 7.9 μg m^{-3} (by ~63.0%). NH_3
421 concentrations over Europe are also largely underpredicted by 82.0%. These large biases in SO_2
422 and NH_3 are likely due in part to the uncertainties in the emissions of SO_2 and NH_3, which in
423 turn affect the predictions of SO_4^{2-} and NH_4^+. The J values in PBL are highly underpredicted by
424 99.6%, which is mainly due to the inaccurate calculation of H_2SO_4 vapor concentration that
425 participates in the nucleation and uncertainties in the nucleation parameterizations used in the
426 default CESM/CAM5.1.
427
428 **5. Sensitivity Simulations**
429 5.1 Impacts of New Gas-Phase Chemistry
430 Compared to simple gas-phase chemistry, many more gaseous species and chemical
431 reactions simulated in CB05_GE can affect secondary aerosol formation through gas-to-particle
432 mass transfer and aqueous-phase chemistry and affect climatic variables through chemistry
433 feedbacks to the climate system. Figure 1a shows the absolute differences of H_2O_2, SO_2, SO_4^{2-},
434 and SOA between MAM_CB05_GE and MAM_SIM. MAM_CB05_GE treats more gaseous
435 species and chemical reactions than MAM_SIM, leading to large changes in the concentrations

436 of gaseous and PM species. Compared with MAM_SIM, MAM_CB05_GE predicts higher H_2O_2
437 by 0.4 ppb, SO_2 by 7.3 ppt, SO_4^{2-} by 0.01 μg m^{-3}, and SOA by 0.06 μg m^{-3}in terms of global
438 mean. Those changes are mainly caused by different gas-phase chemical mechanisms used in
439 MAM_SIM and MAM_CB05_GE. While MAM_CB05_GE explicitly simulates OH, HO_2, NO_3,
440 and O_3, MAM_SIM uses climatology data for these species. OH simulated by MAM_CB05_GE
441 is lower than that prescribed by MAM_SIM by up to 2.8×10^6 molecules cm^{-3}, or higher by up to
442 3.0×10^6 molecules cm^{-3} in different regions (Figure not shown), with a higher global mean by
443 MAM_CB05_GE. MAM_SIM includes the production of H_2O_2 from the self-destruction of HO_2
444 and the loss of H_2O_2 through its photolytic reaction and its reaction with OH. Higher H_2O_2 in
445 MAM_CB05_GE is mainly due to greater production of H_2O_2 from additional chemical
446 reactions (e.g., OH+OH) than loss of H_2O_2 through the reactions of OH + H_2O_2, O + H_2O_2, Cl +
447 H_2O_2, and Hg + H_2O_2. Different predictions in H_2O_2 can in turn affect OH mixing ratios in
448 MAM_CB05_GE but not in MAM_SIM. In addition, the photolytic reactions of VOCs (e.g.,
449 HCHO, peroxyacyl nitrates (PAN), and peroxyacetic and higher peroxycarboxylic acids (PACD))
450 and other gases (e.g., HNO_3, HONO, HNO_4, HOCl, and HOBR) treated in MAM_CB05_GE can
451 produce OH. Figure 1b shows the absolute differences between the mixing ratios of major
452 oxidants predicted from MAM_CB05_GE and climatology values used in MAM_SIM. The
453 global mean mixing ratios of oxidants are higher in MAM_CB05_GE than climatology data in
454 MAM_SIM, leading to more oxidation of VOCs and therefore more SOA in MAM_CB05_GE.
455 Higher O_3 predicted from MAM_CB05_GE over most of the domain is mainly due to more O_3
456 precursors (e.g., NO_2 and VOCs) treated in the model. Despite higher OH mixing ratios in
457 MAM_CB05_GE, many gaseous species such as NO_x, SO_2, HNO_3, HONO, and other VOCs are
458 oxidized by OH to form secondary inorganic and organic aerosols. Those oxidation reactions

compete for limited OH, leading to less oxidation of SO_2, thus higher SO_2 mixing ratios over most land areas by MAM_CB05_GE. Lower SO_2 mixing ratios over the oceanic areas in MAM_CB05_GE is due to the combined effects of less production of SO_2 from lower DMS mixing ratios (due to increased OH levels) and greater SO_2 oxidation from higher OH mixing ratios.

The changes in the concentrations of PM and its components are due to the change in the mixing ratios of gaseous precursors. CB05_GE contains more photolytic reactions, which affect the mixing ratios of OH, SO_2, and H_2SO_4, and subsequently the concentration of SO_4^{2-} through condensation and homogeneous nucleation. Higher SO_2 mixing ratios in MAM_CB05_GE result in more H_2SO_4 thus more SO_4^{2-}. For example, both SO_2 mixing ratios and SO_4^{2-} concentrations are higher over eastern China in MAM_CB05_GE. More SO_4^{2-} over the oceanic areas is mainly due to more oxidation of SO_2 by OH. Due to the simplification of aerosol thermodynamics in default MAM7, the concentrations of SO_4^{2-} can affect the concentrations of NH_4^+ directly and therefore NH_3 mixing ratios and PM number concentrations (PM_{num}). For example, the increase of SO_4^{2-} results in an increase in NH_4^+ and PM_{num}, and a decrease in NH_3. The increase of SO_4^{2-} and PM_{num} can increase AOD, CF, COT, CWP, PWV, and CDNC and therefore affect radiation by increasing LWD and SWD (Figures not shown, see changes in performance statistics of these affected variables in Table 3). The increase of SOA is due to the inclusion of more gaseous precursor emissions (e.g., isoprene, terpene, xylene, and toluene) in MAM_CB05_GE, which contribute to SOAG and thus SOA through gas-to-particle conversion.

Figure 2 shows the spatial distributions of CO, O_3, NO_2, HNO_3, hydrochloric acid (HCl), and isoprene (ISOP) that can be predicted by MAM_CB05_GE but not by MAM_SIM. CO mixing ratio is higher in most Asia, central Africa, South Africa, and eastern U.S., which is

482 mainly due to higher CO emissions in those regions and the production of CO from the
483 photolytic reactions of VOCs (e.g., formaldehyde, acetaldehyde, and isoprene). Higher O_3
484 mixing ratios in the northern hemisphere than southern hemisphere are mainly due to much
485 higher mixing ratios of O_3 precursors. Higher O_3 mixing ratios over Mediterranean Sea are
486 mainly due to the transport of O_3 and its precursors from source regions and less deposition onto
487 ocean surface. Higher O_3 mixing ratios over Tibet are mainly due to the stratospheric influences
488 from high altitude and no titration of O_3 due to low NO mixing ratios (< 0.2 ppb) in this region.
489 Higher mixing ratios of NO_2 over most Asia, eastern U.S, Europe, and Central Africa are mainly
490 due to higher NO_x emissions over those regions, which also result in higher HNO_3 in those
491 regions. Higher mixing ratios of HCl over Europe, India, and East Asia are mainly due to the
492 higher anthropogenic HCl emissions in those regions. In addition, MAM_CB05_GE includes
493 oceanic emissions of HCl, leading to higher HCl over ocean. Higher isoprene mixing ratios over
494 South Africa, central Africa, and Oceania are mainly due to higher isoprene emissions in those
495 regions, which also contribute to the formation of SOA in those regions.

496 The aforementioned changes in the concentrations of gaseous species and PM due to new
497 gas-phase chemistry implemented in the model and its feedbacks to radiation through the climate
498 system result in a change in predicted cloud properties and radiation balance that in turn affect
499 the predictions of all chemical species during subsequent time steps. As a consequence of
500 interwoven changes due to complex feedback mechanisms, the two simulations perform
501 differently, with noticeable improvement by MAM_CB05_GE. As shown in Table 3, compared
502 with MAM_SIM, MAM_CB05_GE reduces MB of LWD by 17.6%, OLR by 8.0%, CF by
503 28.6%, COT by 1.0%, PWV by 28.0%, AOD by 5.5%, and CDNC by 1.8%, leading to 0.3-2.2%
504 absolute reduction in their NMBs. Although MAM_CB05_GE increases MB of SWD by 26.2%,

505 the increases in their NMBs are only 1.2%. As shown in Table A1 in the supplementary material,
506 the changes in most cloud and radiative variables between MAM_SIM and MAM_CB05_GE are
507 statistically significant. As shown in Table 4, MAM_CB05_GE also reduces MBs of SO_2 by
508 2.5% and PM_{10} by 8.1% over East Asia, NH_3 by 1.3% and SO_4^{2-} by 12.5% over Europe, OC by
509 11.1%, TC by 8.3%, and $PM_{2.5}$ by 3.3% over CONUS, leading to 0.8-6.5% absolute reductions
510 in NMBs. Despite the model improvement by CB05_GE, large biases still remain for some
511 chemical species. For example, CO over East Asia is largely underpredicted with an NMB of -
512 82.1% (see Table 4), which results from the uncertainties in the CO emissions over East Asia.
513 However, the column CO over globe is predicted very well, with an NMB of -5.7%. Large biases
514 in SO_2 predictions over CONUS, Europe, and East Asia are mainly due to the uncertainties in the
515 SO_2 emissions over those regions. Large biases in O_3 over Europe are likely due to the
516 uncertainties in the O_3 precursor emissions (e.g., NO_x) and inaccurate predictions of radiation
517 over Europe. In particular, the large underpredictions in NO_2 concentrations (likely due to the
518 uncertainties in the NO_x emissions and overpredictions in radiation, see section 5.5 for more
519 detailed discussions) indicate insufficient NO_x for titration of O_3, leading to a large
520 overprediction in O_3 concentrations in Europe. The large biases in HNO_3 are due to no treatment
521 for gas-particle partitioning in both simulations.
522
523 5.2 Impacts of Condensation and Aqueous-Phase Chemistry
524 The mass accommodation coefficient (α) for H_2SO_4 vapor is subject to considerable
525 uncertainty. The calculation in the default condensation module with a default α value of 0.65
526 gives a very low concentration of H_2SO_4, resulting in very low nucleation rates and aerosol
527 number concentrations. Considering that the original model treats H_2SO_4 and NH_3 condensation

528 as an irreversible process, the default α value of 0.65 for H_2SO_4 and NH_3 is reduced to 0.02 and
529 0.097, respectively, based on Zhang et al. (1998). This change in α value provides sufficient
530 H_2SO_4 and NH_3 for nucleation with a typical H_2SO_4 concentration range of 10^6~10^8 molecules
531 cm^{-3}. Because HNO_3 and HCl are semi-volatile species, the lower limits of α (0.0024 and 0.005,
532 respectively) based on Sander et al. (2002) are selected for their irreversible condensation
533 process. NH_4^+ from NH_3 condensation will be constrained by the available SO_4^{2-}, NO_3^-, and
534 condensed Cl^-, following the approach that is used in the default simplified thermodynamics to
535 neutralize the cations in the system.

536 Figure 3 shows the absolute differences of NH_3, SO_2, HNO_3, HCl, H_2SO_4, total
537 particulate ammonium (TNH_4), total particulate sulfate (TSO_4), total particulate nitrate (TNO_3),
538 and total particulate chloride (TCL) in all the modes except primary carbon mode, and $PM_{2.5}$
539 between MAM_CON and MAM_CB05_GE in June, July, and August (JJA), 2001. Due to the
540 inclusion of HNO_3 and HCl condensation in MAM_CON, the concentrations of HNO_3 and HCl
541 decrease by 0.1 ppb (~72%) and 0.097 ppb (~84%), respectively. NO_3^- is not simulated in the
542 original model and the concentration of NO_3^- is assumed as zero in MAM_CB05_GE. Therefore,
543 the concentration of NO_3^- increases due to the condensation of HNO_3 in MAM_CON. The
544 concentration of TCL in MAM_CB05_GE is calculated from the mass ratio of chloride in sea-
545 salt. Over land, TCL increases significantly due to the condensation of HCl to form Cl^-. The
546 change of TCL over ocean is mainly due to the change of sea-salt emissions. The changes of SO_2
547 mixing ratios are mainly due to the differences in mixing ratios of species in sulfur chemistry in
548 the two simulations. For example, compared to MAM_CB05_GE, the increase of SO_2 over
549 eastern U.S. in MAM_CON is likely due to the less SO_2 oxidation in clouds (Figure not shown),
550 which results from lower CF. The decrease of SO_2 mixing ratios over most oceanic areas is likely

551 due to the combined effects of DMS oxidation and SO_2 oxidations in MAM_CON. More SO_2
552 can result in more H_2SO_4 and therefore more SO_4^{2-} through condensation and homogeneous
553 nucleation of H_2SO_4. The changes in H_2SO_4 concentrations are the results of changes of SO_2
554 mixing ratios. The mass accommodation coefficient of H_2SO_4 is reduced significantly (by a
555 factor of 32.5), allowing more H_2SO_4 to participate in binary/ternary homogeneous nucleation
556 and produce more secondary SO_4^{2-}, improving predictions of SO_4^{2-} over CONUS but degrading
557 the performance of SO_4^{2-} over Europe (see Table 4). Although the mass accommodation
558 coefficient of NH_3 is reduced significantly (by a factor of 67), more available NH_3 can participate
559 in the ternary homogeneous nucleation and produce secondary NH_4^+. Meanwhile, the secondary
560 NH_4^+ formed from NH_3 condensation is also constrained by available SO_4^{2-}, NO_3^-, and
561 condensed Cl^-. As a result, the concentrations of NH_3 decrease and those of NH_4^+ increase. Due
562 to more available H_2SO_4 participating in the nucleation, J has been improved significantly,
563 reducing the NMB from -99.5% to -12.8%. With an inclusion of the dissolution and dissociation
564 of HNO_3 and HCl in cloud water, more NH_3 is required to dissolve to maintain cation-anion
565 equilibrium in the cloud water, which further reduces the mixing ratios of NH_3, HNO_3, and HCl.
566 As shown in Table 4, compared with MAM_CB05_GE, MAM_CON gives better
567 performance against observations in terms of CO, NO_2, O_3, HNO_3, $PM_{2.5}$, and PM_{10} over Europe,
568 CO and PM_{10} over East Asia, O_3, HNO_3, SO_4^{2-}, NH_4^+, BC, OC, TC, and $PM_{2.5}$ over CONUS, and
569 column CO, column NO_2, TOR, and J over globe. As also shown in Table 3, the improved
570 chemical predictions improve the predictions of OLR, SWCF, CF, COT, CWP, AOD, and CDNC.
571 As shown in Table A1, the changes in most cloud /radiative variables between MAM_CB05_GE
572 and MAM_CON are statistically significant, indicating the significant impacts of the modified
573 condensation and aqueous-phase chemistry treatments on radiation. Treating condensation and

574 aqueous-phase chemistry of HNO_3 and HCl enables an explicit simulation of NO_3^- and Cl^- in
575 MAM7. However, the mass concentrations of SO_2 remain significant overpredictions, with
576 NMBs of 301.2% for CONUS, and 123.0% for Europe, mainly because of the uncertainties in
577 SO_2 emissions over those regions. Due to the simplified irreversible treatment for gas
578 condensation, the mass concentrations of SO_4^{2-}, NH_4^+, NO_3^-, and Cl^- are overpredicted, although
579 the lower limit of mass accommodation coefficient for each precursor is used in MAM_CON. As
580 shown in Table 4, the concentrations of SO_4^{2-}, NH_4^+, NO_3^-, and Cl^- from MAM_CON are
581 overpredicted by 1.7%, 20.0%, 198.2%, and 359.9%, respectively, for CONUS, and 40.3%,
582 85.0%, 67.8%, and 102.8%, respectively, for Europe. The large NMBs of NO_3^- and Cl^- in
583 MAM_CON are due to the small observed values for NO_3^- (i.e., 1.0 μg m^{-3} over CONUS and 2.0
584 μg m^{-3} over Europe) and Cl^- (i.e., 0.1 μg m^{-3} over CONUS and 0.7 μg m^{-3} over Europe), the
585 uncertainties in treating HNO_3 and HCl as non-volatile species using their lower limits of
586 accommodation coefficients, and lack of treatments for NO_3^- and Cl^- thermodynamics.
587
588 5.3 Impacts of New Particle Formation
589 Figure 4 shows the annual-mean vertical distributions of particle formation rate (J) values
590 and aerosol number concentrations, and simulated J values averaged between the ground level
591 and 1000-m overlaid with observations within the same layers. In MAM_CON/IMN, IMN is
592 combined with three default nucleation parameterizations to predict J throughout the atmosphere.
593 In MAM_CON, J over ocean is overpredicted by factors of 5-50, despite a seeming good NMB
594 of -12.8% in the globe mean (see Table 4). J values at several sites over land are underpredicted
595 by factors of 1-10, which compensates the large overpredictions at most sites over ocean. The
596 large underpredictions at those sites are likely due to the uncertainties in SO_2 emissions and

nucleation parameterizations, and the missing species that may have participated in nucleation. For example, several other species may contribute to the new particle formation, including methanesulfonic acid (van Dingenen and Raes, 1993), hydrochloric acid (Arstila et al., 1999), organic compounds (Berndt, et al., 2013), iodine-containing compounds (Hoffmann et al., 2001; O'Dowd et al., 2002; Burkholder, et al., 2004; Pechtl et al., 2006), and amines (Kurtén et al., 2008; Berndt et al., 2013). Limited observations also introduce some uncertainties in the model validation. The overprediction of J over ocean is mainly due to the use of the prefactor of 1×10^{-6} in WP09. This prefactor is derived from limited in-situ measurements (Sihto et al., 2006). It can vary by up to 3-4 orders of magnitude based on measurements in different areas and seasons (Zhang et al., 2010), introducing a large uncertainty for its application to the global scale. In MAM_CON/IMN, a prefactor of 1×10^{-8} is used in WP09 in PBL over the globe, which then decreases J and aerosol number concentrations in PBL (see Figure 4). J in PBL is very sensitive to the prefactor in WP09, and the uncertainty of the prefactor can result in a large bias in predictions of J and aerosol number in PBL. With the implementation of IMN, J values in the troposphere increase by factors of 2-10, which in turn increase the aerosol number concentrations in the troposphere. Due to a stronger radiation in the upper layer, more available ions can contribute to the new particle formation, therefore increasing the aerosol number concentrations in the middle/upper troposphere and lower stratosphere by factors of 2-4.

Figure 5 shows the absolute differences of $PM_{2.5}$, AOD, column CCN5, CF, SWCF, and SWD between MAM_CON and MAM_CON/IMN for 2001. Aerosol number can directly affect CCN, which can affect cloud formation and properties as well as radiation. Changes of PM concentrations also have impacts on AOD, CCN, CF, COT, and SWCF through both aerosol direct and indirect effects. As a net result of all those interwoven changes initially triggered by

620 the increase of aerosol number concentrations in troposphere/stratosphere, AOD and column
621 CCN5 increase by 0.004 (or by 3.3%) and 2.1×10^7 cm^{-2} (or by 11.9%), respectively, and SWCF
622 and SWD decrease by 0.1 W m^{-2} (or by 0.2%) and 0.8 W m^{-2} (or by 0.5%), respectively, in terms
623 of global mean. As shown in Table A1, the changes in SWD, AOD, and cloud variables such as
624 column CCN5, CDNC, and COT between MAM_CON and MAM_CON/IMN are statistically
625 significant, indicating the significant impacts of IMN on aerosol number concentration and cloud
626 prediction.

627 Compared with MAM_CON, IMN (MAM_CON/IMN) improves the predictions of SO_2,
628 NO_3^-, and $PM_{2.5}$ over CONUS, SO_2, SO_4^{2-}, NH_4^+, NO_3^-, Cl^-, $PM_{2.5}$, and PM_{10} over Europe, PM_{10}
629 over East Asia (see Table 4). The improved performance in aerosol concentrations and increased
630 aerosol numbers in the troposphere and lower stratosphere contribute to the improved
631 performance of aerosol and cloud parameters, with increased AOD, CCN, and CDNC, and
632 consequently increased CF, COT, CWP, and SWCF, as shown in Table 3. However, there are still
633 large biases for some chemical species predictions. For example, CO mixing ratio is
634 underpredicted over East Asia, which is mainly due to the uncertainty in CO emissions in this
635 region. Large biases in SO_2 predictions over CONUS, Europe, and East Asia are mainly due to
636 the uncertainties in SO_2 emissions in those regions. Large biases in NO_2 and HNO_3 predictions
637 over Europe are mainly due to the uncertainties in NO_x emissions and inaccurate predictions of
638 radiation over this region. The performance of J degrades with NMBs from -21.8% to -49.6% in
639 the globe, which is due to the use of a smaller prefactor of WP09 in MAM_CON/IMN than in
640 MAM_CON. J in PBL is very sensitive to the prefactor in WP09. Although the prediction of J
641 over ocean in PBL has been improved in MAM_CON/IMN, J over land areas in PBL is largely
642 underpredicted by factors of 1-100, resulting in degraded J performance in terms of globe mean.

643 The underprediction of J over land in PBL is likely due to the uncertainties in the nucleation
644 parameterizations (e.g., the missing species as mentioned previously). Large NMBs still remain
645 for COT, CWP, and CCN, indicating the uncertainties in the treatments of related atmospheric
646 processes such as cloud microphysics and aerosol-cloud interactions.
647
648 5.4 Impacts of Gas-Aerosol Partitioning
649 The inclusion of ISORROPIA II changes the mass concentrations of major $PM_{2.5}$ species
650 and their gaseous precursors. Changes in PM concentrations then affect predictions of cloud
651 variables and therefore radiation. Changes of radiation can also affect SO_2 oxidation by OH,
652 which affects H_2SO_4 concentrations. Figure 6a shows the absolute differences of H_2SO_4, fine
653 particulate sulfate (SO4f), NH_3, fine particulate ammonium (NH4f), HNO_3, fine particulate
654 nitrate (NO3f), HCl, and fine particulate chloride (CLf) for summer 2001 between MAM_CON
655 and MAM_CON/ISO. Similar plots for winter (December, January, and February (DJF)) 2001
656 are shown in Figure 6b. Compared to MAM_CON, MAM_CON/ISO gives higher H_2SO_4 mixing
657 ratios but lower SO4f concentrations. SWD increases with the global mean of 8.9 W m^{-2} (~
658 5.8%) in MAM_CON/ISO, which allows more production of OH from photolytic reactions of
659 VOCs, HONO, HNO_3, HNO_4, H_2O_2, HOCl, and HOBr, and therefore enhanced oxidation of SO_2
660 to form H_2SO_4. As shown in Figure 6a, the mixing ratios of H_2SO_4 either increase up to 0.76 ppt
661 or decrease as large as 1.14 ppt, leading to a net increase of 0.002 ppt in terms of global mean.
662 The mass concentration of SO4f is mainly affected by H_2SO_4 condensation. Although the mixing
663 ratios of H_2SO_4 increase with the global mean change of 0.002 ppt, SO4f concentrations decrease
664 with the global mean of 0.02 μg m^{-3}, which are mainly due to less condensation of H_2SO_4 under
665 higher temperature conditions. In summer, the increase or decrease of H_2SO_4 can result in an

666 increase or a decrease of SO4f (e.g., over most oceanic areas). However, the decrease of SO4f
667 with the increase of H_2SO_4 over the India Ocean is mainly due to less H_2SO_4 condensation. For
668 the regions where SO4f increases over land, the increase of SO4f is due to more oxidation of SO_2
669 by OH.

670 Compared to MAM_CON, the concentrations of NH_3, HNO_3, and HCl increase
671 significantly over most land areas, whereas NH4f, NO3f, and Clf decrease significantly over
672 most land areas in MAM_CON/ISO. The chemical regimes is the controlling factor for gas-
673 aerosol equilibrium partitioning, which is determined based on the ratio of SO_4^{2-} molar
674 concentrations to total molar concentrations of cations and their respective gases (referred to as
675 TCAT/TSO4) (Zhang et al., 2000). Three regimes are defined based on the values of
676 TCAT/TSO4: (1) if TCAT/TSO4 < 2, the system contains excess sulfate and is in a sulfate-rich
677 regime; (2) if TCAT/TSO4 = 2, the system contains just sufficient sulfate to neutralize the cation
678 species and is in sulfate-neutral regime; (3) if TCAT/TSO4 > 2, the system contain insufficient
679 sulfate to neutralize the cation species and is in sulfate-poor regime. Over land, the major cation
680 is NH_4^+, and there are also crustal species (K^+, Ca^{2+}, and Mg^{2+}) associated with dust emissions,
681 whereas over ocean, the major cation is Na^+, which is a non-volatile species. Therefore, the gas-
682 aerosol equilibrium partitioning behaves differently over land and over ocean. Figure 7 shows
683 the distributions of TCAT/TSO4 in MAM_CON and MAM_CON/ISO, and their absolute
684 differences for summer and winter, 2001. In summer, compared to MAM_CON, TCAT/TSO4 in
685 MAM_CON/ISO either increases up by 80.1 (mostly over ocean) or decreases up by 51.8 (over
686 both land and ocean), leading to a net increase of 0.7. In MAM_CON, most regions are in
687 sulfate-poor regime, whereas Greenland, southeast U.S., North Africa, a small portion of Asia
688 and North Atlantic Ocean, and some areas in North Pole are in sulfate-rich regime in summer.

689 However, due to the simplified thermodynamics treatment in MAM_CON, NH_3 is
690 underpredicted and NH_4^+ is overpredicted (see Table 4). With the inclusion of ISORROPIA II,
691 most sulfate-poor regions over land and over part of Pacific Ocean and most Atlantic Ocean
692 become less sulfate-poor. The sulfate-poor regime can drive HNO_3/HCl to produce NO_3^-/Cl^- by
693 neutralizing excess NH_4^+. If the amount of NO_3^-/Cl^- is insufficient to neutralize NH_4^+, sulfate-
694 poor regime can drive NH_4^+ to the gas phase to produce NH_3. Therefore, the increase of NH_3 and
695 decrease of NH_4^+ in MAM_CON/ISO are mainly due to insufficient NO_3^-/Cl^- to neutralize NH_4^+
696 under sulfate-poor regime. Insufficient NO_3^-/Cl^- results from the thermodynamic partitioning
697 under higher temperature conditions that favors the production of HNO_3 and HCl from NO_3^-/Cl^-
698 to produce HNO_3 and HCl under higher temperature conditions. The slight increase of NO_3^- over
699 Pacific Ocean and South Atlantic Ocean is due to much higher Na^+ concentrations yet
700 insufficient SO_4^{2-} in those regions compared with those over the land areas. Unlike a sulfate-poor
701 regime, a sulfate-rich regime (e.g., small portion of North Atlantic Ocean, South China Sea, and
702 Greenland), requires more cations such as NH_4^+ and Na^+ to neutralize excess SO_4^{2-} in the system
703 and the thermodynamics favors the partitioning of volatile species such as NO_3^- and Cl^- in the
704 gas phase as HNO_3 and HCl. Therefore, despite the increased temperatures, the decrease of NH_4^+
705 due to its evaporation back to the gas-phase is not as significant as that of NO_3^- and Cl^-, because
706 NH_4^+ needs to stay in the system to neutralize SO_4^{2-}. In winter, as shown in Figure 6b, compared
707 with MAM_CON, the mixing ratios of H_2SO_4 in MAM_CON/ISO either increase by up to 4.3
708 ppt, or decrease by up to 1.0 ppt, leading to a net increase with the global mean of 0.001 ppt.
709 NH_3 increases over most regions except Europe, eastern China, and some regions in North Pole.
710 HNO_3 decreases over most oceanic areas, Northeastern China, and East Europe, whereas
711 increases over South Asia, North Pole, southern U.S., Africa, and most land areas in southern

712 hemisphere. HCl increases over most areas except the northeastern portion of Asia and eastern
713 Europe.

714 Compared with MAM_CON, MAM_CON/ISO predicts higher HNO_3 and HCl over some
715 land areas. As shown in Figure 7, in MAM_CON, most regions are in sulfate-poor regime,
716 whereas Greenland, North Pole, North Africa, some portions of Asia and western Pacific Ocean
717 are in sulfate-rich regime. For example, northeastern China is in sulfate-poor regime, driving
718 HNO_3 and HCl partitioning to the aerosol phase to neutralize excess NH_4^+. This results in an
719 increase in NO3f and Clf, changing sulfate-poor regime to less sulfate-poor. North Pacific Ocean
720 and southern oceanic areas are also in sulfate-poor regime, and the increase of NO3f is due to the
721 partitioning HNO_3 to the aerosol phase to neutralize Na^+, whose concentration is relatively
722 higher compared to that over land areas. Therefore, more anions such as NO_3^- are needed to
723 neutralize the system. However, the decrease Cl^- over these regions is due to the equilibrium
724 state of HCl under different atmospheric conditions. The western Pacific Ocean is in sulfate-rich
725 regime, driving NO_3^- and Cl^- partition to the gas phase, which results in a decrease in NO3f and
726 Clf, and an increase in HNO_3 and HCl over this region. With the inclusion of ISORROPIA II, the
727 western Pacific Ocean changes from sulfate-rich regime to less sulfate-rich regime.

728 Compared to MAM_CON, the prediction of SWD in MAM_CON/ISO is improved with
729 the NMB decreasing from -6.5% to -2.2%. The predictions of involved species such as NH_4^+,
730 NO_3^-, and Cl^- are improved significantly by 13.6%~345.4%, although there is a slight
731 degradation in the predictions of SO_4^{2-} and O_3 over CONUS, CO, O_3, $PM_{2.5}$, and PM_{10} over
732 Europe, PM_{10} over East Asia, and column CO, NO_2, TOR, and J over globe. MAM_CON/ISO
733 improves the predictions of HNO_3, NH_4^+, NO_3^-, Cl^-, BC, OC, TC, and $PM_{2.5}$ over CONUS, SO_2,
734 NH_3, NO_2, SO_4^{2-}, NH_4^+, NO_3^-, and Cl^- over Europe, and CO and SO_2 over East Asia, which leads

735 to improved performance in SWD, column CCN5, and SWCF over globe, as shown in Table 3.
736 As shown in Table A1, the changes in most radiative and cloud variables between MAM_CON
737 and MAM_CON/ISO are statistically significant, indicating the significant impacts of
738 ISORROIA II on the predictions of radiation, aerosol, and cloud. ISORROPIA II calculates gas-
739 aerosol partitioning under different atmospheric conditions, significantly improving predictions
740 of major gas precursor (e.g., HNO_3) over CONUS and secondary aerosols (e.g., NO_3^- and Cl^-)
741 over CONUS and Europe. Large decreases in the concentrations of NO_3^- and Cl^- result in a
742 decrease in NH_4^+, $PM_{2.5}$, and PM_{10}, thus decreasing CCN, CDNC, AOD, and the absolute value
743 of SWCF.
744 Figure 8 shows the absolute differences of major inorganic gas and aerosol species
745 between metastable (MAM_NEWA) and stable (MAM_NEWB) conditions. Compared with
746 MAM_NEWA, the global average changes predicted by MAM_NEWB are overall small (within
747 5%) for most gaseous and aerosol species. For example, the global average changes are 0.01 μg
748 m^{-3} (by 4.2%) for SO_4^{2-}, 0.005 μg m^{-3}(by 12.8%) for NH_4^+, 0.006 μg m^{-3}(by -0.01%) for NO_3^-,
749 and -4×10^{-4} μg m^{-3} (by 2.0%) for Cl^-. The increase of SO_4^{2-} results in an increase in NH_4^+ (e.g.,
750 East Asia and Northeast U.S.). The differences between stable and metastable conditions may be
751 more significant under low RH conditions (RH < 50% for nitrate, Fountoukis et al., 2009).
752 However, based on the simulated global annual mean RH values, most regions have RH values >
753 60-70% (exceptions are over desert/arid regions such as Australia, the northern Africa, Arabian
754 Desert, northwestern China, and western U.S.). These results indicate that the assumption of
755 metastable conditions is not a significant sources of uncertainty for global model predictions of
756 gaseous and aerosol species.
757

758 5.5 Overall Impacts of All New and Modified Model Treatments

759 Compared to MAM_CB05_GE, the simulations with modified or new aerosol treatments
760 (MAM_CON, MAM_CON/IMN, MAM_CON/ISO, MAM_NEWA) slightly degrade the
761 prediction of LWD (increasing NMB from -0.9% to -1.4%), but improve the predictions of OLR,
762 CF, COT, and CWP slightly (with 0.6% - 10.4% decreases in their NMBs) and CDNC
763 significantly (reducing NMBs from -57.5% up to -13.4%). Although the CCN predictions are
764 somewhat degraded in MAM_CON and MAM_CON/IMN, they are improved significantly in
765 MAM_CON/ISO and MAM_NEWA (reducing NMBs from -61.6% to 1.8-6.3%). As shown in
766 Table A1, changes in most radiative and cloud variables between MAM_SIM and MAM_NEWA
767 are statistically significant, indicating the significant impacts of new and modified treatments on
768 predictions of radiation and cloud. Among all new and modified model treatments, the new gas-
769 phase chemistry simulates more gaseous species and improves the predictions of NH_3 over
770 Europe, $PM_{2.5}$ over CONUS and PM_{10} over East Asia. The modified condensation and aqueous-
771 phase chemistry simulate more aerosol species (NO_3^- and Cl^-) and improve the prediction of
772 HNO_3. MAM_CON also improves J in the PBL due to more available H_2SO_4 involving in the
773 homogeneous nucleation using an accommodation coefficient of 0.02 for H_2SO_4 condensation,
774 and improves the predictions of CDNC and AOD significantly. MAM_CON/IMN increases
775 PM_{num} above PBL and $PM_{2.5}$ and PM_{10} over Europe and improves the prediction of $PM_{2.5}$ over
776 CONUS and Europe. MAM_CON/ISO improves the predictions of HNO_3, NH_4^+, $PM_{2.5}$, NO_3^-,
777 and Cl^- over CONUS, NO_3^- and Cl^- over Europe, and CCN over globe, and improves the
778 predictions of SWCF most (with an NMB of 1.6%).

779 Large biases in some variables remain in MAM_NEWA due to uncertainties in model
780 inputs (e.g., meteorology and emissions) and model treatments (e.g., multi-phase chemistry, dust

781 emission scheme, cloud microphysics, aerosol activation, SOA formation, and dry and wet
782 deposition). The large NMBs of CO and SO_2 over East Asia, SO_2, NH_3, and NO_2 over Europe,
783 SO_2, and BC over CONUS are likely due to the uncertainties of emissions and the interpolation
784 of emissions from a fine-grid scale in the original emission inventories (e.g., county-based
785 emissions over CONUS) to a large-grid scale used in this work, which can result in large NMBs
786 in secondary aerosols (e.g., SO_4^{2-}, NH_4^+, NO_3^-, thus $PM_{2.5}$ and PM_{10}). Heterogeneous reactions
787 are not included in this work, which may help explain to some extent less oxidation and
788 underpredictions for PM species predictions (e.g., sulfate and nitrate) and overpredictions for
789 gaseous species. The large NMB of O_3 predictions over Europe in MAM_NEWA (with an NMB
790 of 62.7%) is mainly due to a lack of NO_x titration (as indicated by large underpredictions in NO_2)
791 and more production of O_3 from the photolytic reaction of NO_2 resulted from overpredictions of
792 SWD particularly in autumn and winter. Table 5 shows the seasonal statistics for O_3, NO_2, and
793 HNO_3 over Europe in MAM_NEWA. During autumn and winter, O_3 is overpredicted by about
794 100% ~ 140%, whereas NO_2 is underpredicted by about -85% ~ -20%, indicating insufficient
795 NO_x for titration of O_3 titration. SWD is overpredicted by 45.0 W m^{-2} (or by 58.4%), favoring the
796 photolytic reactions of NO_2 to produce O_3.Due to the uncertainties in the NO_x emissions, NO_2 is
797 underpredicted, causing less NO_2 to be oxidized to produce HNO_3, which results in an
798 underprediction of HNO_3 in winter. In autumn, SWD is overpredicted by 42.8 W m^{-2} (or by
799 37.9%). However, in autumn, although NO_2 is underpredicted due to the uncertainties in the NO_x
800 emissions, HNO_3 mixing ratios are overpredicted. SWD is stronger in autumn than in winter, and
801 mixing ratios of OH are higher due to photolytic reactions of overpredicted O_3 and additional
802 photolytic reactions of VOCs. Therefore, OH can oxidize NO_2 to produce HNO_3, resulting in the
803 overprediction of HNO_3. Simple aqueous-phase chemistry is included in this work, which could

804 result in high uncertainty in predicting aerosols in clouds. Decreased aerosol number
805 concentrations can result in a decrease of CCN and AOD directly. The underpredictions of
806 CDNC are likely due to uncertainties in the model treatments for aerosol activation and cloud
807 microphysics, which then result in large NMBs in COT and CWP. The large biases in OC and TC
808 indicate the uncertainties in the emissions of BC and primary OC, and the treatments for SOA
809 formation. The large NMB in particle formation rate J is likely due to uncertainties in model
810 inputs (e.g., SO_2 emissions) and model treatments (e.g., the accommodation coefficient of H_2SO_4
811 and missing participants in the current nucleation schemes).
812
813 5.6 Impacts of Adjusted Emissions
814 The evaluation and analyses of MAM_NEWA indicate that some large biases are caused
815 by inaccuracies in the emissions of CO, SO_2, BC, OC, and NH_3. The sensitivity simulation with
816 adjusted emissions of CO, SO_2, BC, OC, and NH_3 (MAM_NEW/EMIS) is performed to further
817 look into such impacts. For example, with 30% increase in CO emissions and 20% increase in
818 NH_3 emissions over Europe, the NMBs of surface concentrations of CO and NH_3 change from-
819 3.4% to 12.1%, -84.3% to -77.5%, respectively. On a global scale, the increased CO emissions
820 result in 3.0% absolute reduction in the NMB of column CO. The 30% reduction in SO_2
821 emissions and 20% increase in OC and BC emissions over CONUS result in 139.6%, 8.6%, and
822 24.9% absolute reduction in their NMBs. The 30% increase in CO emissions and 20% increase
823 in SO_2 over East Asia result in 3.3% and 7.8% absolute reduction in their NMBs.
824 As shown in Table 4, compared with MAM_NEWA, MAM_NEW/EMIS shows an
825 improved performance in the concentrations of SO_2, HNO_3, SO_4^{2-}, NH_3, and NH_4^+ over Europe,
826 SO_2, HNO_3, BC, OC, TC, NO_3^-, and Cl^- over CONUS, CO and SO_2 over Asia, and column CO

827 over globe. However, it degrades to some extent the performance of SO_4^{2-} and NH_4^+ over
828 CONUS, $PM_{2.5}$ and PM_{10} over Europe, PM_{10} over Asia, and J over globe. Decreased SO_2
829 emissions over CONUS result in a decrease of H_2SO_4 and therefore a decrease of SO_4^{2-}. Based
830 on aerosol thermodynamic treatments, decreased SO_4^{2-} will result in decreased NH_4^+. Therefore,
831 $PM_{2.5}$ and PM_{10} decrease as well. Adjusted emissions can affect secondary aerosol formations
832 and therefore radiative variables can be affected due to the direct and indirect effects of aerosols.
833 As shown in Table 3, compared with MAM_NEWA, MAM_NEW/EMIS reduces MB of LWD
834 by 9.3%, SWD by 37.5%, and CF by 18.9%, leading to 0.1% - 1.6% absolute reduction in their
835 NMBs. This illustrates the sensitivity of radiation to the perturbations in emissions through
836 chemistry feedbacks to the climate system. As shown in Table A1, only column CCN5 and AOD
837 are significantly different between MAM_NEWA and MAM_NEW/EMIS, indicating the
838 impacts of emissions are more significant on predictions of gas and aerosol than radiative
839 variables.
840
841 6. Evaluation of the Five-Year Simulations
842 6.1. Performance Evaluation
843 Tables 6 and 7 show the statistical performance for radiative/cloud variables and
844 chemical predictions, respectively, from the 5-yr simulations using three different configurations.
845 Compared with MAM_SIM_5Y, MAM_NEW_5YA improves the predictions of aerosol and
846 cloud variables such as AOD, COT, CWP, CCN5, and CDNC (with 4.8% to 23.4% absolute
847 reduction in their NMBs), and radiative variables such as SWD, LWD, OLR, and SWCF (with
848 0.4-4.2% absolute reduction in their NMBs). MAM_NEW_5YA also shows slight improvement
849 for the predictions of SO_4^{2-} and BC over CONUS and SO_2 over East Asia (with 0.3-2.3%

absolute reduction in their NMBs), but moderate-to-large improvements for the predictions of OC, TC, and $PM_{2.5}$ over CONUS, PM_{10} over East Asia, and SO_2, $PM_{2.5}$, and PM_{10} over Europe (with 5.2-20.1% absolute reduction in their NMBs). Compared to TOR calculated based on O_3 climatology used in MAM_SIM_5Y, TOR predicted from MAM_NEW_5YA is slightly improved with 1.2%, 1.3%, and 0.3 absolute reduction in its NMB, NME, and RMSE, respectively. Evaluation of major radiative/cloud variables and chemical predictions are also conducted for June, July, and August (JJA) of 2001-2005, which is shown in Tables A2 and A3 in the supplementary material. Compared with full 5-year (2001-2005) average, the simulation for JJA gives similar predictions for chemical species but better model predictions for radiation (e.g., LWD, SWD, and OLR) and cloud (e.g., COT, CWP, column CCN5, and CDNC) variables.

Tables 6 and 7 also show the performance of MAM_NEW_5YB in which CAM5 is fully coupled with land, ocean, and ice models. The performance is overall similar for all radiative variables and most chemical species between MAM_NEW_5YA and MAM_NEW_5YB (most within 5% differences in the absolute values of their NMBs). The performance of HNO_3 over CONUS and Europe, NH_4^+, NO_3^-, and Cl^- over Europe, PM_{10} over Europe and East Asia is improved appreciably (with 4.2-17.9% reduction in the absolute values of their NMBs), and that of SO_2 over CONUS and Europe and NH_4^+, NO_3^-, and Cl^- over CONUS degrades appreciably (with 4.3-8.5% increase in the absolute values of their NMBs). Those changes are mainly due to the interactions among Earth's components, particularly at the interface of earth components (e.g., air-sea, air-land, and sea-ice interfaces) and feedbacks to the climate system, which in turn affects gaseous and aerosol concentrations in the coupled system.

Large biases remain for some variables in MAM_NEW_5YA and MAM_NEW_5YB due to uncertainties in model inputs (e.g., meteorology and emissions) and model treatments (e.g.,

873 multi-phase chemistry, dust emission scheme, cloud microphysics, aerosol activation, SOA
874 formation, and dry and wet deposition), which have been illustrated in Section 5.5. Large biases
875 in Cl^- predictions over Europe are likely due to the combined effects of a low concentration of
876 observed Cl^-, uncertainties in HCl emissions, and inaccurate predictions of coarse Cl^- in the
877 model since ISORROPIA II is only implemented for fine particles. Uncertainties in the mass
878 accommodation coefficients of volatile gas species can also result in uncertainties in predictions
879 of condensable gases.
880
881 6.2 Impact of New and Modified Treatments on 5-year (2001-2005) Simulations
882 Figure 9 shows the absolute differences of surface SO_2, NH_3, SO_4^{2-}, NH_4^+, TC, $PM_{2.5}$,
883 PM_{10}, J, and aerosol number (PM_{num}) and Figure 10 shows the absolute differences of radiative
884 variables between MAM_SIM_5Y and MAM_NEW_5YA. The new and modified model
885 treatments in MAM_NEW_5YA cause changes in the concentrations of PM and precursor gases,
886 which affect radiative variables through aerosol direct and indirect effects. The changes in
887 radiative variables in turn affect gas-phase chemistry and aerosol processes. As shown in Figure
888 9, the difference of SO_2 between the two simulations varies from -1.7 to 3.8 ppb, with a global
889 mean difference of 4.2 ppt. The decrease of SO_2 over most oceanic area is mainly due to the
890 decrease of DMS resulted from less oxidation by OH radicals. The increase of SO_4^{2-} over East
891 Asia and eastern U.S. drives more NH_3 from gas-phase to particulate phase to form NH_4^+
892 through thermodynamic equilibrium, increasing the concentrations of NH_4^+ over these regions.
893 However, the concentrations of SO_4^{2-} decrease over Europe due in part to less oxidation of SO_2.
894 Despite such a decrease, the concentrations of NH_4^+ are higher over Europe due to the
895 neutralization of NH_3 by Cl^- and NO_3^- that are treated in MAM_NEW_5YA but not treated in in

MAM_SIM_5Y. Compared with MAM_SIM_5Y, J from MAM_NEW_5YA increases over globe with a global mean difference of 0.066 cm^{-3} s^{-1}, due to the use of a lower mass accommodation coefficient of H_2SO_4 in MAM_NEW_5YA, resulting in more available H_2SO_4 vapor participating in nucleation. The increases in J result in an increase in aerosol mass and number concentrations and thus higher concentrations of $PM_{2.5}$ and PM_{10} (which improve appreciably their performance, see Table 6).

As shown in Figure 10, compared with MAM_SIM_5Y, AOD increases by 0.007, column CCN5 increases by 3.8×10^7 cm^{-2}, and CDNC increases by 16.1 cm^{-3} in MAM_NEW_5YA. Higher PM_{num} in MAM_NEW_5YA allows more aerosol to grow into the CCN size, leading to higher CCN in MAM_NEW_5YA. Higher aerosol concentrations in MAM_NEW_5YA result in higher AOD. The increased aerosol number and mass concentration result in an increase in the predictions of cloud variables through the aerosol-cloud interactions. For example, with all the modified and new treatments, COT increases by 0.8, CWP increases by 4.1 g m^{-2}, and PWV increases by 0.026 cm on global average. Due to the aerosol direct and indirect effects, the difference in simulated SWD varies from -19.3.0 to 10.4 W m^{-2} and decreases by 3.4 W m^{-2} (~ 2.0%) on a global average. The difference in LWD varies from -4.2 to 8.5 W m^{-2} and increases by 1.0 W m^{-2} (~ 0.4%) on a global average (Figure not shown). The difference in SWCF varies from -8.4 to 17.9 W $m^{-2,}$ with a net increase of 2.7 W m^{-2} (~ 6.4%) on a global average. The absolute differences of surface chemical species and major cloud/radiative variables for JJA average of 2001-2005 are shown in Figures A1 and A2 in the supplementary material. Compared with 5-year average, the absolute changes of most radiative variables are smaller in JJA. The absolute changes of PM_{10} are smaller in JJA, which is mainly due to the dust events during other months (e.g., March-May over East Asia).

919

920 6.3 Global Burden Analysis

921 Table 8 shows the simulated global burdens of major gas and aerosol species for 2001-
922 2005. The global burdens of most gaseous precursors of aerosol are higher in MAM_NEW_5YA
923 than MAM_SIM_5Y (except for NH_3), due mainly to the incorporation of ISORROPIA II in
924 MAM_NEW_5YA. The global burden of tropospheric O_3 is higher in MAM_NEW_5YA than
925 MAM_SIM_5Y, which is due to higher mixing ratios of O_3 precursors (e.g., NO_2 and VOCs) that
926 are simulated in MAM_NEW_5YA. The global burdens of most gas species are comparable with
927 previous studies (Horowitz et al.2006; Larmarque et al., 2006; Williams et al., 2009; Liu et al.,
928 2012) with absolute differences of less than 20%. One exception is H_2SO_4, which is higher by a
929 factor 5 in MAM_NEW_5YA than in MAM_SIM_5Y. The higher burden of H_2SO_4 in
930 MAM_NEW_5YA is likely due to the less condensation of H_2SO_4 resulted from the use of a
931 lower mass accommodation coefficient. SO_4^{2-} burden is higher by 8.3% in MAM_NEW_5YA
932 than MAM_SIM_5Y, which is likely due to greater SO_2 oxidation in MAM_NEW_5YA. Higher
933 SO_4^{2-} burden results from higher SO_2 burden. Higher SO_2 burden leads to more SO_2 to be
934 oxidized to produce SO_4^{2-}, which overweighs the impacts from less H_2SO_4 condensation due to
935 lower mass accommodation coefficient. More SO_4^{2-} results in more NH_4^+. The burdens of BC
936 and POM are lower by 16.5% and 23.8%, respectively, in MAM_NEW_5YA than in
937 MAM_SIM_5Y, which is likely due in part to greater dry deposition fluxes and in part to a
938 slower primary carbon aging rate resulted from reduced condensation of gas species in
939 MAM_NEW_5YA. Condensation onto the primary carbon mode produces aging of the particles
940 in this mode. A lower accommodation coefficient is used in MAM_NEW_5YA, which results in
941 less condensation. Therefore, the fraction of aged particles has decreased. The global burdens of

most aerosol species are in the range of previous studies. For example, global burdens of SO_4^{2-} and NH_4^+ from MAM_SIM_5Y and MAM_NEW_5YA are 23.4% and 17.0%, respectively, and 16.7% and 12.5%, respectively, lower than Liu et al. (2012), which is likely because MAM_SIM_5Y contains no SO_4^{2-} emissions but Liu et al. (2012) included additional SO_4^{2-} emissions of 1.66 Tg S yr^{-1}. Higher SO_4^{2-} emission leads to more SO_4^{2-} concentrations thus more NH_4^+ in Liu et al. (2012). Compared with Horowitz et al. (2006), global burdens of BC and OC from MAM_NEW_5YA are lower by 72.9% and 52.3%, respectively. Compared with Liu et al. (2012), MAM_NEW_5YA gives comparable BC and POM burdens but much lower SOA (by a factor of 3.0). Compared with Textor et al. (2006), POM burden is a factor of 3.5 lower in MAM_NEW_5YA. The lower BC, OC, POM, and SOA burdens are likely due to the uncertainties in the BC and OC emissions used as well as differences in the model treatments for SOA formation and POM aging.

7. Conclusions and Future work

In this work, a new gas-phase chemistry mechanism and several advanced inorganic aerosol treatments have been incorporated into CESM/CAM5.1-MAM7. These include (1) the CB05_GE gas-phase chemical mechanism coupled with MAM7; (2) the condensation and aqueous-phase chemistry involving HNO_3/ NO_3^- and HCl/ Cl^-; (3) an ion-mediated nucleation (IMN) parameterization for the new particle formation from ions, (4) an inorganic thermodynamic module, ISORROPIA II, that explicitly simulates thermodynamics of SO_4^{2-}, NH_4^+, NO_3^-, Cl^-, and Na^+ as well as the impact of crustal species, such as Ca^{2+}, K^+, and Mg^{2+}, on aerosol thermodynamics. CB05_GE with new and modified inorganic aerosol treatments in MAM7 simulates 139 species with 273 chemical reactions, which is more accurate than simple

965 gas chemistry coupled with default MAM7. Seven 1-yr simulations for 2001 and three 5-yr
966 simulations for 2001-2005 with different model configurations are performed to evaluate the
967 capabilities of the original and improved CESM/CAM5 and the mechanisms underlying
968 differences among model predictions.

969 Comparing to the simple gas-phase chemistry, the 2001 simulation with CB05_GE can
970 predict many more gaseous species, and give improved performance for predictions of organic
971 carbon and $PM_{2.5}$ over CONUS, NH_3 and SO_4^{2-} over Europe, SO_2 and PM_{10} over East Asia, and
972 cloud properties such as CF, CDNC, and SWCF. MAM_CON simulates NO_3^- and Cl^-, which are
973 important inorganic aerosols. With species-dependent accommodation coefficients for gas
974 condensation, more H_2SO_4 can participate in homogeneous nucleation, resulting in the
975 improvement of predictions of $PM_{2.5}$, PM_{10}, J, CDNC, and SWCF. IMN can increase the
976 predictions of J and PM_{num} in the upper atmosphere and thus improve the predictions of AOD,
977 CCN, and cloud properties, and SWCF over globe, $PM_{2.5}$ over CONUS and Europe, PM_{10} over
978 Europe and East Asia, and PM composition over Europe. The 2001 simulation with ISORROPIA
979 II can improve the predictions of major gas and aerosol species significantly, including HNO_3,
980 NH_4^+, NO_3^-, Cl^-, BC, OC, TC, and $PM_{2.5}$ over CONUS, SO_2, NH_3, NO_2, SO_4^{2-}, NH_4^+, NO_3^-, and
981 Cl^- over Europe, and CO and SO_2 over East Asia. Such improvements lead to improved
982 predictions of SWD, SWCF, and CCN5 over globe. The 2001 simulation with the new and
983 modified inorganic aerosol treatments appreciably improve the predictions of OLR, CF, COT,
984 CWP, PWV, CCN, CDNC, SWCF, J over globe, and HNO_3, NH_4^+ (CONUS), $PM_{2.5}$, and PM_{10}.
985 The 2001 sensitivity simulation with adjusted emissions further improves model predictions of
986 CO and SO_2 over East Asia, SO_2, HNO_3, NO_3^-, Cl^-, BC, OC, and TC over CONUS, SO_2, NH_3,
987 NH_4^+, HNO_3, NO_3^-, and Cl^- over Europe, and column CO and SWD over globe. The change of

emissions can affect primary gaseous precursors directly, and secondary gaseous species indirectly through gas-phase chemistry. Meanwhile, secondary aerosols can be affected by gaseous precursors, and therefore have impacts on cloud properties as well as direct and indirect effects on radiation. Reducing the uncertainty of emissions can thus help reduce the model biases significantly.

The comparison of the 5-yr simulations with prescribed SST shows that MAM_NEW_5YA with CB05_GE can appreciably improve the predictions of AOD, COT, CWP, CCN5, CDNC, SWD, LWD, OLR, and SWCF on global scale and OC, TC, and $PM_{2.5}$ over CONUS, PM_{10} over East Asia, and SO_2, $PM_{2.5}$, and PM_{10} over Europe. The performance is overall similar for all radiative variables and most chemical species between MAM_NEW_5YA with prescribed SST and MAM_NEW_5YB in a fully-coupled mode.

In addition to uncertainties in emissions, additional uncertainties exist in the model treatments. For example, the large biases in the predictions of O_3 over Europe and East Asia are mainly due to insufficient NO_x titration resulting from the uncertainties in the NO_x emissions. The large biases in PM_{10} over East Asia and Europe may be mainly due to the inaccurate predictions of dust. The large bias in Cl^- over Europe may be due to the inaccurate predictions of HCl and coarse Cl^- as well as the uncertainty in the mass accommodation coefficient of HCl used. In the default and modified nucleation treatments, it only considers H_2SO_4, NH_3, H_2O, and ions involving in the new particle formation. Missing species (e.g., organics, iodine compounds, and DMS) may also contribute to the new particle formation. Uncertainties in treating organic gas-aerosol partitioning may contribute to the inaccurate predictions of SOA, OC, TC, and PM. The large biases in CDNC, COT, and LWP indicate the uncertainties in cloud microphysics schemes and aerosol-cloud interaction parameterizations, which also limit the ability of climate

and Earth system models to quantify aerosol indirect effects (Stephens, 2005; Lohmann et al., 2007; Gettelman et al., 2008). In addition to uncertainties in the model treatments, uncertainties in the model simulation settings such as the use of a coarse grid resolution and a large model time step of 1800 seconds for solving the chemical system in this work may contribute to the model biases. The representations of some of the aforementioned uncertain processes in CESM/CAM5.1 are being further improved by the authors' group. Decadal simulations using improved CESM/CAM5.1 will be conducted in the future to study the interactions among atmospheric chemistry, aerosol, and climate change and reduce associated uncertainties

Acknowledgments

This work is sponsored by the U.S. NSF EaSM program AGS-1049200. The authors would like to thank Fangqun Yu for providing the IMN scheme, Athanasios Nenes for providing ISORROPIA II, Xiaohong Liu for providing a version of MAM7 that works in CAM5.0 and CAM5.1, Ralf Bennartz and John Rausch for providing CDNC data, Steve J. Ghan and Richard C. Easter for insightful discussions, and Shuai Zhu, a former postdoc researcher of the air quality forecasting laboratory at NCSU for early work on the incorporation of CB05_GE and its coupling with MAM3. The authors would also like to thank the four reviewers for their valuable suggestions that help improve the technical quality of this work. MODIS data and CERES data are provided by NASA via http://ladsweb.nascom.nasa.gov and http://ceres.larc.nasa.gov/order_data.php, respectively. Other surface network data were downloaded from their respective web sites. We would like to acknowledge high-performance computing support from Yellowstone (ark:/85065/d7wd3xhc) provided by NCAR's

Computational and Information Systems Laboratory, sponsored by the U.S. National Science Foundation.

References

Abdul-Razzak, H. and Ghan, S. J.: A Parameterization of Aerosol Activation, Part 2: Multiple Aerosol Types, J. Geophys. Res., 105, 6837-6844, 2000.

Adams, P. J. and Seinfeld, J. H.: Predicting global aerosol size distributions in general circulation models, J. Geophys. Res., 107(D19), 4370, doi:10.1029/2001JD001010, 2002.

Appel, K.W., Pouliot, G. A., Simon, H., Sarwar, G., Pye, H. O. T., Napelenok, S. L., Akhtar, F., and Roselle, S. J.: Evaluation of dust and trace metal estimates from the Community Multiscale Air Quality (CMAQ) model version 5.0, Geosci. Model Dev., 6, 883-899, 2013.

Arstila, H., Korhonen, P., and Kulmala, M.: Ternary nucleation: Kinetics and application to water-ammonia-hydrochloric acid system, J. Aerosol Sci., 30, 131-138, doi:10.1016/S0021-8502(98)00033-0, 1999.

Barth, M. C., Rasch, P. J., Kiehl, J. T., Benkovitz, C. M., and Schwartz, S. E.: Sulfur chemistry in the National Center for Atmospheric Research Community Climate Model: Description, evaluation, features and sensitivity to aqueous chemistry, J. Geophys. Res., 105, 1387-1415, 2000.

Berndt, T., Sipilä, M., Stratmann, F., Petäjä, T., Vanhanen, J., Mikkilä, J., Patokoski, J., Taipale, R., Lee Mauldin III, R., and Kulmala, M.: Enhancement of atmospheric H_2SO_4/H_2O nucleation: organic oxidation products versus amines, Atmos. Chem. Phys. Discuss., 13, 16301-16335, doi:10.5194/acpd-13-16301-2013, 2013.

Bennartz, R.: Global assessment of marine boundary layer cloud droplet number concentration from satellite, J. Geophys. Res., 112, D02201, doi: 10.1029/2006JD007547, 2007.

Bey, I., Jacob, D. J., Yantosca, R. M., Logan, J. A., Field, B. D., Fiore, A. M., Li, Q., Lui, H. Y., Mickley, L. J., and Schultz, M. G.: Global modeling of tropospheric chemistry with assimilated meteorology: Model description and evaluation, J. Geophys. Res., 106(D19), 23073-23095, 2001.

Bretherton, C. S. and Park, S.: A new moist turbulence parameterization in the community atmosphere model, J. Climate, 22, 3422-3448, 2009.

Burkholder, J. B., Curtius, J., Ravishankara, A. R., and Lovejoy, E. R.: Laboratory studies of the homogeneous nucleation of iodine oxides, Atmos. Chem. Phys., 4, 19-34, 2004.

Byun, D. W. and Schere, K. L.: Review of the governing equations, computational algorithms, and other components of the Models-3 Community Multiscale Air Quality (CMAQ) Modeling System, Appl. Mech. Rev., 59, 51-77, 2006.

1068 Cappa, C. D., Lovejoy, E. R., and Ravishankara, A. R.: Evidence for liquid-like and nonideal
1069 behavior of a mixture of organic aerosol components, P. Natl. Acad. Sci. USA, 105, 18687-
1070 18691, doi:10.1073/pnas.0802144105, 2008.

1071 Collins, W. D., Bitz, C. M., Blackmon, M. L., Bonan, G. B., Bretherton, C. S., Carton, J. A.,
1072 Chang, P., Doney, S. C., Hack, J. J., Henderson, T. B., Kiehl, J. T., Large, W. G., McKenna, D.
1073 S., Santer, B. D., and Smith, R. D.: The Community Climate System Model version3
1074 (CCSM3), J. Clim., 19, 2122-2143, doi:10.1175/JCLI3761.1, 2006.

1075 Dunne, J. P., John, J. G., Adcroft, A. J., Griffies, S. M., Hallberg, R. W., Shevliakova, E.,
1076 Stouffer, R. J., Cooke, W., Dunne, K. A., Harrison, M. J., Krasting, J. P., Malyshev, S. L.,
1077 Milly, P. C. D., Phillipps, P. J., Sentman, L. T., Samuels, B. L., Spelman, M. J., Winton, M.,
1078 Wittenberg, A. T., and Zadeh, N.: GFDL's ESM2 global coupled climate-carbon earth system
1079 models. Part I: Physical formulation and baseline simulation characteristics, J. Climate, 25,
1080 6646-6665, 2012.

1081 Dunne, J. P., John, J. G., Shevliakova, E., Stouffer, R. J., Krasting, J. P., Malyshev, S. L., Milly,
1082 P. C. D., Sentman, L. T., Adcroft, A. J., Cooke, W., Dunne, K. A., Griffies, S. M., Hallberg, R.
1083 W., Harrison, M. J., Levy, H., Wittenberg, A. T., Phillips, P. J., and Zadeh, N.: GFDL's ESM2
1084 global coupled climate-carbon earth system models. Part II: Carbon system formulation and
1085 baseline simulation characteristics, J. Climate, 26, 2247-2267, 2013.

1086 Dutkiewicz, S., Sokolov, A. P., Scott, J., and Stone, P. H.: A Three-Dimensional Ocean-Seaice-
1087 Carbon Cycle Model and its Coupling to a Two-Dimensional Atmospheric Model: Uses in
1088 Climate Change Studies. MIT JPSPGC Report 122, May, 47 p, 2005.

1089 Emmons, L. K., Walters, S., Hess, P. G., Lamarque, J.-F., Pfister, G. G., Fillmore, D., Granier, C.,
1090 Guenther, A., Kinnison, D., Laepple, T., Orlando, J., Tie, X., Tyndall, G., Wiedinmyer, C.,
1091 Baughcum, S. L., and Kloster, S.: Description and evaluation of the Model for Ozone and
1092 Related chemical Tracers, version 4 (MOZART-4), Geosci. Model Dev., 3, 43-67,
1093 doi:10.5194/gmd-3-43-2010, 2010.

1094 ENVIRON: Comprehensive Air Quality Model with extensions User's Guide, Novato,
1095 California, USA, 5.3 edn., 2010.

1096 Faraji, M., Kimura, Y., McDonald-Buller, E., and Allen, D.: Comparison of the carbon bond and
1097 SAPRC photochemical mechanisms under conditions relevant to southeast Texas, Atmos.
1098 Environ., 42, 5821–5836, doi:10.1016/j.atmosenv.2007.07.048, 2008.

1099 Fast, J. D., Gustafson Jr., W. I., Easter, R. C., Zaveri, R. A., Barnard, J. C., Chapman, E. G.,
1100 Grell, G. A., and Peckham, S. E.: Evolution of ozone, particulates, and aerosol direct radiative
1101 forcing in the vicinity of Houston using a fully coupled meteorology-chemistry-aerosol
1102 model, J. Geophys. Res., 111, D21305, doi:10.1029/2005JD006721, 2006.

1103 Fountoukis, C and Nenes, A.: ISORROPIA II: a computationally efficient thermodynamic
1104 equilibrium model for K^+- Ca^{2+} -Mg^{2+} -NH_4^+ -Na^+-SO_4^{2-}-NO_3^--Cl^--H_2O aerosols, Atmos.
1105 Chem. Phys., 7, 4639–4659, doi:10.5194/acp-7-4639-2007, 2007.

1106 Fountoukis, C., Nenes1, A., Sullivan, A., Weber, R., Farmer, D., and Cohen, R. C., 2009,
1107 Thermodynamic characterization of Mexico City aerosol during MILAGRO 2006, Atmos.
1108 Chem. Phys., 9, 2141–2156, 2009.

1109 Gent, P. R., Yeager, S. G., Neale, R. B., Levis, S., and Bailey, D. A.: Improvements in a half
1110 degree atmosphere/land version of the CCSM, Climate Dyn., 34, 819-833,
1111 doi:10.1007/s00382-009-0614-8, 2010.

1112 Gettelman, A., Morrison, H., and Ghan, S. J.: A new two-moment bulk stratiform cloud
1113 microphysics scheme in the community atmosphere model, version 3 (CAM3). Part II:
1114 Single-column and global results, J. Climate, 21(15), 3660-3679, 2008.

1115 Ghan, S. J., and Zaveri, R. A.: Parameterization of optical properties for hydrated internally
1116 mixed aerosol, J. Geophys. Res., 112, D10201, doi:10.1029/2006JD007927,2007.

1117 Ghan, S. J., Liu, X., Easter, R. C., Zaveri, R., Rasch, P. J., and Yoon, J.-H.: Toward a minimal
1118 representation of aerosols in climate models: comparative decomposition of aerosol direct,
1119 semidirect, and indirect radiative forcing, J. Climate, 25, 6461-6476, 2012.

1120 Guenther A., Karl, T., Harley, P., Wiedinmyer, C., Palmer, P. I., and Geron, C.: Estimates of
1121 global terrestrial isoprene emissions using MEGAN (Model of Emissions of Gases and
1122 Aerosols from Nature), Atmos. Chem. Phys., 6, 3181-3210, 2006.

1123 Heald, C. L., Henze, D. K., Horowitz, L. W., Feddema, J., Lamarque, J.-F., Guenther, A., Hess, P.
1124 G., Vitt, F., Seinfeld, J. H., Goldstein, A. H., and Fung, I.: Predicted change in global
1125 secondary organic aerosol concentrations in response to future climate, emissions, and land
1126 use change, J. Geophys. Res., 113, D05211, doi:10.1029/2007JD009092, 2008.

1127 Heintzenberg, J.: Fine particles in the global troposphere, A review. Tellus, 41B, 149-160, 1989.

1128 Hoffmann, T., O'Dowd, C. D., and Seinfeld, J. H.: Iodine oxide homogeneous nucleation: An
1129 explanation for coastal new particle production, Geophys. Res. Lett., 28(10), 1949-1952,
1130 2001.

1131 Horowitz, L. W.: Past, present, and future concentrations of tropospheric ozone and aerosols:
1132 methodology, ozone evaluation, and sensitivity to aerosol wet removal, J. Geophys. Res., 111,
1133 D22211, doi:10.1029/2005JD006937, 2006.

1134 Iacono, M. J., Delamere, J. S., Mlawer, E. J., and Clough, S. A.: Evaluation of upper tropospheric
1135 water vapor in the NCAR Community Climate Model (CCM3) using modeled and observed
1136 HIRS radiances, J. Geophys. Res., 108(D2), 4037, doi:10.1029/2002jd002539, 2003.

1137 Iacono, M. J., Delamere, J. S., Mlawer, E. J., Shephard, M. W., Clough S. A., and Collins, W. D.:
1138 Radiative forcing by long-lived greenhouse gases: Calculations with the AER radiative
1139 transfer models, J. Geophys. Res., 113(D13), D13103, doi:10.1029/2008jd009944, 2008.

1140 Jacobson, M. Z.: Studying the effect of calcium and magnesium on size-distributed nitrate and
1141 ammonium with EQUISOLV II, Atmos. Environ., 33, 3635-3649, 1999.

1142 Jacobson, M. Z.: Short-term effects of Controlling Fossil-Fuel Soot, Biofuel Soot and Gases, and
1143 Methane on Climate , Arctic Ice, and Air Pollution Health, J. Geophys. Res., 115, D14209,
1144 doi:10.1029/2009JD013795, 2010.

1145 Karamchandani, P., Zhang, Y., Chen, S.-Y., and Balmori-Bronson, R.: Development of an
1146 extended chemical mechanism for global-through-urban applications, Atmospheric Pollution
1147 Research, 3, 1-24, 2012.

1148 Kim, Y., Sartelet, K., and Seigneur, C.: Formation of secondary aerosols: impact of the gas-phase
1149 chemical mechanism, Atmos. Chem. Phys., 11, 583-598, doi:10.5194/acp-11-583-2011,
1150 2011a.

1151 Koloutsou-Vakakis S., Rood, M. J., Nenes, A., and Pilinis, C.: Modeling of aerosol properties
1152 related to direct climate forcing, J. Geophys. Res., 103(D14), 17009-17032, doi:
1153 10.1029/98JD00068, 1998.

1154 Kuang, C., McMurry, P. H., McCormick, A. V., and Eisele, F. L.: Dependence of nucleation rates
1155 on sulfuric acid vapor concentration in diverse atmospheric locations, J. Geophys. Res., 113,
1156 D10209, doi:10.1029/2007JD009253, 2008.

1157 Kuang, C., McMurry, P. H., and McCormick, A. V.: Determination of cloud condensation nuclei
1158 production from measured new particle formation events, Geophys. Res. Lett., 36, L09822,
1159 doi:10.1029/2009GL037584, 2009.

1160 Kulmala, M., Lehtinen, K., and Laaksonen, A.:, Cluster activation theory as an explanation of the
1161 linear dependence between formation rate of 3 nm particles and sulphuric acid concentration,
1162 Atmos. Chem. Phys., 6, 787-793, doi:10.5194/acp-6-787-2006, 2006.

1163 Kulmala, M., Vehkamaki, H., Petaja, T., Dal Maso, M., Lauri, A., Kerminen, V.-M., Birmili, W.,
1164 and McMurry, P.: Formation and growth rates of ultrafine atmospheric particles: A review of
1165 observations, J. Aerosol Sci., 35, 143-176, 2004.

1166 Kurtén, T., Loukonen, V., Vehkamaki, H., and Kulmala, M.: Amines are likely to enhance neutral
1167 and ion-induced sulfuric acid-water nucleation in the atmosphere more effectively than
1168 ammonia, Atmos. Chem. Phys., 8, 4095-4103, doi:10.5194/acp-8-4095-2008, 2008.

1169 Lamarque, J.-F., Kiehl, J. T., Hess, P. G., Collins, W. D., Emmons, L. K., Ginoux, P., Luo, C., and
1170 Tie, X. X.: Response of a coupled chemistry-climate model to changes in aerosol emissions:
1171 global impact on the hydrological cycle and the tropospheric burdens of OH, ozone, and NOx,
1172 J. Geophys. Res., 32, L16809, doi:10.1029/2005GL023419, 2005.

1173 Lamarque, J. F., Shinedell, D. T., Josse, B., Young, P. J., Cionni, I., Eyring, V., Bergmann, D.,
1174 Cameron-Smith, P., Collins, W. J., Doherty, R., Dalsoren, S., Faluvegi, G., Folberth, G., Ghan,
1175 S. J., Hiriwutz, L. W., Lee, Y. H., MacKenzie, I. A., Nagashima, T., Naik, V., Plummer, D.,
1176 Righi, M., Rumbold, S. T., Schulz, M., Skeie, R. B., Stevenson, D. S., Strode, S., Sudo, K.,
1177 Szopa, S., Voulgarakis, A., and Zeng, G.: The atmospheric chemistry and climate model
1178 intercomparison project: overview and description of models, simulations and climate
1179 diagnostics, Geosci. Model Dev., 6, 179-206, doi:10.5194/gmd-6-179-2013, 2013.

1180 Lamarque, J. F., Emmons, L. K., Hess, P. G., Kinnison, D. E., Tilmes, S., Vitt, F., Heald, C. L.,
1181 Holland, E. A., Lauritzen, P. H., Neu, J., Orlando, J. J., Rasch, P. J., and Tyndall, G. K.:CAM-
1182 chem: description and evaluation of interactive atmospheric chemistry in CESM, Geosci.
1183 Model Dev., 5, 369-411, doi:10.5194/gmd-5-369-2012, 2012.

1184 Lawrence, D. M., Oleson, K. W., Flanner, M. G., Thornton, P. E., Swenson, S. C., Lawrence, P.
1185 J., Zeng, X., Yang, Z.-L., Levis, S., Sakaguchi, K., Bonan, G. B., and Slater, A. G.:
1186 Parameterization improvements and functional and structural advances in version 4 of the
1187 Community Land Model, J. Adv. Model. Earth Syst., 3, Art. 2011MS000045, 27 pp, doi:
1188 10.1029/2011MS000045, 2011.

1189 Liao, H., Adams, P. J., Chung, S. H., Seinfeld, J. H., Mickley, L. J., and Jacob, D. J.: Interactions
1190 between tropospheric chemistry and aerosols in a unified general circulation model, J.
1191 Geophys. Res., 108(D1), 4001, doi:10.1029/2001JD001260, 2003.

1192 Liu, X., Easter, R. C., Ghan, S. J., Zaveri, R., Rasch, P., Shi, X., Lamarque, J.-F., Gettleman, A.,
1193 Morrison, H., Vitt, F., Conley, A., Park, S., Neale, R., Hannay, C., Ekman, A. M. L., Hess, P.,
1194 Mahowald, N., Collins, W., Iacono, M.J., Bretherton, C. S., Flanner, M. G., and Mitchell,
1195 D.L.: Toward a minimal representation of aerosols in climate models: description and
1196 evaluation in the Community Atmosphere Model CAM5, Geosci. Model Dev., 5, 709-739,
1197 2012.

1198 Lohmann, U., Stier, P., Hoose, C., Ferrachat, S., Kloster, S., Roeckner, E., and Zhang, J.: Cloud
1199 microphysics and aerosol indirect effects in the global climate model ECHAM5-HAM,
1200 Atmos. Chem. Phys., 7, 3425-3446, 2007.

1201 Luecken, D. J., Phillips, S., Sarwar, G., and Jang, C.: Effects of using the CB05 vs. SAPRC99 vs.
1202 CB4 chemical mechanism on model predictions: Ozone and gas-phase photochemical
1203 precursor concentrations, Atmos. Environ., 42, 5805–5820,
1204 doi:10.1016/j.atmosenv.2007.08.056, 2008.

1205 Marsh, A. R. W., and McElory, W. J.: The dissociation constant and Henry's law constant of HCl
1206 in aqueous solution, Atmos. Environ., 19, 1075-1080, 1985.

1207 Martensson, E. M., Nilsson, E. D., deLeeuw, G., Cohen, L. H., and Hansson, H. C.: Laboratory
1208 simulations and parameterization of the primary marine aerosol production, J. Geophys. Res.,
1209 108(D9), 4297, doi:10.1029/2002JD002263, 2003.

1210 Meng, Z. and Seinfeld, J. H.: Time scales to achieve atmospheric gas-aerosol equilibrium for
1211 volatile species, Atmos. Environ., 30, 2889-2900, 1996.

1212 Meng, Z, Dabdub, D., and Seinfeld, J.H.: Size- and chemically-resolved model of atmospheric
1213 aerosol dynamics. J. Geophys. Res., 103, 3419-3435, 1998.

1214 Merikanto, J., Napari, I., Vehkamaki, H., Anttila, T., and Kulmala, M.: New parameterization of
1215 sulfuric acid-ammonia-water ternary nucleation rates at tropospheric conditions, J. Geophys.
1216 Res., 112, D15207, doi: 10.1029/2006JD007977, 2007.

1217 Metzger, S. M., Dentener, F. J., Lelieveld, J., and Pandis, S. N.: Gas/aerosol partitioning I: A
1218 computationally efficient model, J. Geophys. Res., 107(D16), 4312, doi:
1219 10.1029/2001JD001102, 2002.

1220 Metzger, S. and Lelieveld, J.: Reformulating atmospheric aerosol thermodynamics and
1221 hygroscopic growth into fog, haze and clouds, Atmos. Chem. Phys., 7, 3163-3193, doi:
1222 10.5194/acp-7-3163-2007, 2007.

1223 Metzger, S., Steil, B., Xu, L., Penner, J. E., and Lelieveld, J.: New representation of water
1224 activity based on a single solute specific constant to parameterize the hygroscopic growth of
1225 aerosols in atmospheric models, Atmos. Chem. Phys., 12, 5429-5446, doi:10.5194/acp-12-
1226 5429-2012, 2012.

1227 Mlawer, E. J., Taubman, S. J., Brown, P. D., Iacono, M. J., and Clough, S. A.: Radiative transfer
1228 for inhomogeneous atmospheres: RRTM, a validated correlated-k model for the longwave, J.
1229 Geophys. Res., 102(D14), 16663-16682, 1997.

1230 Monier, E., Scott, J. R., Sokolov, A. P., Forest, C. E., and Schlosser, C. A.: An integrated
1231 assessment modeling framework for uncertainty studies in global and regional climate
1232 change: the MIT IGSM-CAM (version 1.0), Geosci. Model Dev. Discuss., 6, 2213-2248,
1233 2013.

1234 Morrison, H. and Gettelman, A.: A new two-moment bulk stratiform cloud microphysics scheme
1235 in the community atmosphere model, version 3 (CAM3). Part I: Description and numerical
1236 tests, J. Climate, 21(15), 3642-3659, 2008.

1237 Nenes, A., Pandis, S.N., and Pilinis, C.: ISORROPIA: A new thermodynamic equilibrium model
1238 for multiphase multicomponent inorganic aerosols, Aquatic Geochemistry, 4, 123-152, 1998.

1239 O'Dowd, C. D., Jimenez, J. L., Bahreini, R., Flagan, R. C., Seinfeld, J. H., Hämeri, K., Pirjola,
1240 L., Kulmala, M., Jennings, S. G., and Hoffmann, T.: Marine aerosol formation from biogenic
1241 iodine emissions, Nature, 417, 632-636, doi:10.1038/nature00775, 2002.

1242 Olerud, D. and Sims, A. (2004). MM5 2002 Modeling in Support of VISTAS (Visibility
1243 Improvement – State and Tribal Association of the Southeast), Report, Baron Advanced
1244 Meteorological Systems, LLC, Raleigh, NC, August.

1245 Park, S. and Bretherton, C. S.: The university of Washington shallow convection and moist
1246 turbulence schemes and their impact on climate simulations with the community atmosphere
1247 model, J. Climate, 22, 3449-3469, 2009.

1248 Pechtl, S., Lovejoy, E. R., Burkholder, J. B., and von Glasow, R.: Modeling the possible role
1249 iodine oxides in atmospheric new particle formation, Atmos. Chem. Phys., 6, 505-523, 2006.

1250 Pierce, J. R. and Adams, P. J.: Uncertainty in global CCN concentrations from uncertain aerosol
1251 nucleation and primary emission rates, Atmos. Chem. Phys., 9, 1339-1356, 2009.

1252 Raes, F., Augustin, J., and Vandingenen, R.: The role of ion-induced aerosol formation in the
1253 lower atmosphere, J. Aerosol Sci., 17, 466-470, doi: 10.1016/0021-8502(86)90135-7, 1986.

Reiter, R.: Phenomena in atmospheric and environmental electricity, Elsevier, New York, 1992.

Roeckner, E., Bauml, G., Bonaventura, L., Brokopf, R., Esch, M., Giorgetta, M., Hagemann, S., Kirchner, I., Kornblueh, L., Manzini, E., Rhodin, A., Schlese, U., Schulzweida, U., and Tompkins, A.: The atmospheric general circulation model ECHAM 5. PART I: model description, MPI Technical Report 349, Max Planck Institute for Meteorology, Hamburg, Germany, 2003.

Roeckner, E., Brokopf, R., Esch, M., Giorgetta, M. A., Hagemann, S., Kornblueh, L., Manzini, E., Schlese, U., and Schulzweida, U. : Sensitivity of Simulated Climate to Horizontal and Vertical Resolution in the ECHAM5 Atmosphere Model, Journal of Climate, 19, 3771-3791, 2006a.

Sander S. P., Friedl, R. R., Golden, D. M., Kurylo, M. J., Huie, R. E., Orkin, V. L., Moortgat, G. K., Ravishankara, A. R., Kolb, C. E., Molina, M. J., and Finlayson-Pitts, B. J.: Chemical Kinetics and Photochemical Data for Use in Atmospheric Studies, National Aeronautics and Space Administration, Jet Propulsion Laboratory California Institute of Technology Pasadena, California, 2003.

Sarwar, G., Luecken, D., Yarwood, G., Whitten, G., and Carter, W. P. L.;, Impact of an updated carbon bond mechanism on predictions from the Community Multiscale Air Quality Model, J. Appl. Meteorol. Climatol., 47, 3-14, doi:10.1175/2007JAMC1393.1, 2008.

Schwartz, S. E.: Gas- and aqueous-phase chemistry of HO_2 in liquid water clouds, J. Geophys. Res., 89, 11589-11598, 1984.

Seinfeld, J. H. and Pandis, S. N.: Atmospheric chemistry and physics: From air pollution to climate change, 2 ed., John Wiley & Sons, Inc, 2006.

Shindell, D. T., Lamarque, J.-F., Schulz, M., Flanner, M., Jiao, C., Chin, M., Young, P. J., Lee, Y. H., Rotstayn, L., Mahowald, N., Milly, G., Faluvegi, G., Balkanski, Y., Collins, W. J., Conley, A. J., Dalsoren, S., Easter, R., Ghan, S., Horowitz, L., Liu, X., Myhre, G., Nagashima, T., Naik, V., Rumbold, S. T., Skeie, R., Sudo, K., Szopa, S., Takemura, T., Voulgarakis, A., Yoon, J.-H., and Lo, F.:, Radiative forcing in the ACCMIP historical and future climate simulations, Atmos. Chem. Phys., 13, 2939-2974, doi:10.5194/acp-13-2939-2013, 2013.

Sihto, S. L., Kulmala, M., Kerminen, V. M., Maso, M. D., Petaja, T., Riipinen, I., Korhonen, H., Arnold, F., Janson, R., Boy, M., Laaksonen, A., and Lehtinen, K. E. J.: Atmospheric sulphuric acid and aerosol formation: implications from atmospheric measurements for nucleation and early growth mechanisms, Atmospheric Chemistry and Physics, 6, 4079-4091, 2006.

Sokolov, A. P., Schlosser, C. A., Dutkiewicz, S., Paltsev, S., Kicklighter, D., Jacoby, H. D., Prinn, R. G., Forest, C. E., Reilly, J. M., Wang, C., Felzer, B., Sarofim, M. C., Scott, J., Stone, P. H., Melillo, J. M., and Cohen, J.: The MIT Integrated Global System Model (IGSM) Version 2: Model Description and Baseline Evaluation. MIT JPSPGC Report 124, July, 40 p, 2005.

Spracklen, D. V., Carslaw, K. S., Kulmala, M., Kerminen, V.-M., Mann, G. W., and Sihto, S.-L.: The contribution of boundary layer nucleation events to total particle concentrations on regional and global scales, Atmos. Chem. Phys., 6, 5631-5648, 2006.

1293 Stephens, G. L.: Cloud feedbacks in the climate system: A critical review, J. Climate, 18(2), 237-
1294 273, 2005.

1295 Stier, P., Feichter, J., Kinne, S., Kloster, S., Vignati, E., Wilson, J., Ganzeveld, L., Tegen, I.,
1296 Werner, M., Balkanski, Y., Schulz, M., Boucher, O., Minikin, A., and Petzold, A.: The aerosol-
1297 climate model ECHAM5-HAM, Atmos. Chem. Phys., 5, 1125-1156, doi:10.5194/acp-5-1125-
1298 2005, 2005.

1299 Textor, C., Schulz, M., Guibert, S., Kinne, S., Balkanski, Y., Bauer, S., Berntsen, T., Berglen, T.,
1300 Boucher, O., Chin, M., Dentener, F., Diehl, T., Easter, R., Feichter, H., Fillmore, D., Ghan, S.,
1301 Ginoux, P., Gong, S., Grini, A., Hendricks, J., Horowitz, L., Huang, P., Isaksen, I., Iversen, I.,
1302 Kloster, S., Koch, D., Kirkevag, A., Kristjansson,J. E., Krol, M., Lauer, A., Lamarque, J. F.,
1303 Liu, X., Montanaro, V., Myhre, G., Penner, J., Pitari, G., Reddy, S., Seland, Ø., Stier, P.,
1304 Takemura, T., and Tie, X.: Analysis and quantification of the diversities of aerosol life cycles
1305 within AeroCom, Atmos. Chem. Phys., 6, 1777–1813, doi:10.5194/acp-6-1777-2006, 2006.

1306 Tsigaridis. K., Krol, M., Dentener, F. J., Balkanski, Y., Lathiere, J., Metzger, S., Hauglustaine, D.
1307 A., and Kanakidou, M.: Change in global aerosol composition since preindustrial times,
1308 Atmos. Chem. Phys., 6, 5143-5162, 2006.

1309 Usoskin, I. G. and Kovaltsov, G. A.: Cosmic ray induced ionization in the atmosphere: full
1310 modeling and practical applications, J. Geophys. Res., 111, D21206,
1311 doi:10.1029/2006JD007150, 2006.

1312 van Dingenen, R. and Raes, F.: Ternary nucleation of methane sulphonic acid, sulphuric acid and
1313 water vapour, J. Aerosol Sci., 24, 1-17, doi:10.1016/0021-8502(93)90081-J, 1993.

1314 Van Pelt, R. S. and Zobeck, T. M.: Chemical constituents of fugitive dust, Environ. Monit.
1315 Assess., 130, 3-16, doi:10.1007/s10661-006-9446-8, 2007.

1316 Vehkamaki, H., Kulmala, M., Napari, I., Lehtinen, K. E. J., Timmreck., C., Noppel, M., and
1317 Laaksonen, A.: an improved parameterization for sulfuric acid-water nucleation rates for
1318 tropospheric and stratospheric conditions, Journal of Geophysical Research-Atmospheres,
1319 107(D22), 4622, doi:10.1029/2002JD002184, 2002.

1320 Wang, M. and Penner, J. E.: Aerosol indirect forcing in a global model with particle nucleation,
1321 Atmos. Chem. Phys., 9, 239-260, 2009.

1322 Wang, K., Zhang, Y., Nenes, A., and Fountoukis, C.: Implementation of dust emission and
1323 chemistry into the Community Multiscale Air Quality modeling system and initial application
1324 to an Asian dust storm episode, Atmos. Chem. Phys., 12, 10209-10237, doi:10.5194/acp-12-
1325 10209-2012, 2012.

1326 Wexler, A. S. and Seinfeld, J. H.: Second-generation inorganic aerosol model, Atmos. Environ.,
1327 25A, 2731-2748, 1991.

1328 Williams, J. E., Scheele, M. P., van Velthoven, P. F. J., Cammas, J.-P., Thouret, V. Galy-Lacaux,
1329 C., and Volz-Thomas, A.: The influence of biogenic emissions from Africa on tropical

tropospheric ozone during 2006: a global modeling study, Atmos. Chem. Phys., 9, 5729-5749, 2009.

Young, P. J., Archibald, A. T., Bowman, K. W., Lamarque, J.-F., Naik, V., Stevenson, D. S., Tilmes, S., Voulgarakis, A., Wild, O., Bergmann, D., Cameron-Smith, P., Cionni, I., Collins, W. J., Dalsøren, S. B., Doherty, R. M., Eyring, V., Faluvegi, G., Horowitz, L. W., Josse, B., Lee, Y. H., MacKenzie, I. A., Nagashima, T., Plummer, D. A., Righi, M., Rumbold, S. T., Skeie, R. B., Shindell, D. T., Strode, S. A., Sudo, K., Szopa, S., and Zeng, G.: Pre-industrial to end 21st century projections of tropospheric ozone from the Atmospheric Chemistry and Climate Model Intercomparison Project (ACCMIP), Atmos. Chem. Phys., 13, 2063-2090, doi:10.5194/acp-13-2063-2013, 2013.

Yu, F.: From molecular clusters to nanoparticles: Second generation ion-mediated nucleation model, Atmos. Chem. Phys., 6, 5193-5211, 2006.

Yu, F.: Ion-mediated nucleation in the atmosphere: Key controlling parameters, implications, and look-up table, J. Geophys. Res., 115, D03206, doi: 10.1029/2009JD012630, 2010.

Yu, F. and Luo, G.: Simulation of particle size distribution with a global aerosol model: Contribution of nucleation to aerosol and CCN number concentrations, Atmos. Chem. Phys., 9, 7691-7710, 2009.

Yu, F., Luo, G., Liu, X., Easter, R. C., Ma, X., and Ghan, S. J.: Indirect radiative forcing by ion-mediated nucleation of aerosol, Atmos. Chem. Phys., 12, 11451-11463, 2012.

Yu, F., Luo, G., Bates, T. S., Anderson, B., Clarke, A., Kapustin, V., Yantosca, R. M., Wang, Y., and Wu, S.: Spatial distributions of particle number concentrations in the global troposphere: simulations, observations, and implications for nucleation mechanisms, J. Geophys., Res., 115, D17205, doi:10.1029/2009JD013473, 2010.

Yu, F. and Turco, R. P.: Ultrafine aerosol formation via ion-mediated nucleation, Geophys. Res. Lett., 27, 883-886, doi: 10.1029/1999GL011151, 2000.

Yu, F. and Turco, R. P.: From molecular clusters to nanoparticles: The role of ambient ionization in tropospheric aerosol formation, J. Geophys., Res., 106, 4797-4814, doi: 10.1029/2000JD900539, 2001.

Yu, F., Wang, Z., Luo, G., and Turco, R. P.: Ion-mediated nucleation as an important global source of tropospheric aerosols, Atmos. Chem. Phys., 8, 2537-2554, 2008.

Zaveri, R. A., Easter, R. C., and Peters, L. K.: A computationally efficient multicomponent equilibrium solver for aerosols (MESA), J. Geophys. Res., 110, D24203, doi: 10.1029/2004JD005618, 2005.

Zender, C. S., Bian, H., and Newman, D.: The mineral Dust Entrainment And Deposition (DEAD) model: Description and 1990s dust climatology, J. Geophys. Res., 108(D14), 4416, doi: 10.1029/2002JD002775, 2003.

1366 Zhang, G. J., and McFarlane, N. A.: Sensitivity of climate simulations to the parameterization of
1367 cumulus convection in the Canadian Climate Centre general circulation model, Atmosphere-
1368 Ocean, 33, 407-446, 1995.

1369 Zhang, Y., Bischof, C. H., Easter, R. C., and Wu, P.-T.: Sensitivity analysis of a mixed-phase
1370 chemical mechanism using automatic differentiation, J. Geophys. Res., 103 (D15), 18,953-
1371 18,979, 1998.

1372 Zhang, Y., Seigneur, C., Seinfeld, J. H., Jacobson, M., Clegg, S. L., Binkowski, F. S.: A
1373 comparative review of inorganic aerosol thermodynamic equilibrium modules: similarities,
1374 differences, and their likely causes, Atmos. Environ., 34, 117-137, 2000.

1375 Zhang, Y., McMurry, P. H., Yu, F., and Jacobson, M. Z.: A comparative study of nucleation
1376 parameterizations: 1. Examination and evaluation of the formulations, J. Geophys. Res., 115,
1377 D20212, doi: 10.1029/2010JD014150, 2010.

1378 Zhang, Y., Chen, Y., Sarwar, G., and Schere, K.: Impacts of gas-phase mechanisms on weather
1379 research forecasting model with chemistry (WRF/Chem) predictions: Mechanism
1380 implementation and comparative evaluation, J. Geophys. Res., 117, D01301, doi:
1381 10.1029/2011JD015775, 2012a.

1382 Zhang, Y., Karamchandani, P., Glotfelty, T., Street, D. G., Grell, G., Nenes, A., Yu, F., and
1383 Bennartz, R.: Development and initial application of the global-through-urban weather
1384 research and forecasting model with chemistry (GU-WRF/Chem), J. Geophys. Res., 117,
1385 D20206, doi:10.1029/2012JD017966, 2012b.

1386 Zuend, A., Marcolli, C., Peter, T., and Seinfeld, J. H.: Computation of liquid-liquid equilibria and
1387 phase stabilities: implications for RH-dependent gas/particle partitioning of organic-inorganic
1388 aerosols, Atmos. Chem. Phys., 10, 7795-7820, doi:10.5194/acp-10-7795-2010, 2010.

Table 1. Simulation design and purposes

Run Index	Model Configuration	Purpose
MAM_SIM	Simple gas-phase chemistry coupled with default MAM7	A baseline run for the 1st set of simulations (see text)
MAM_CB05_GE	CB05_GE coupled with default MAM7	Differences of MAM_SIM and MAM_CB05_GE indicate the impacts of gas-phase chemical mechanisms
MAM_CON	Same as MAM_CB05_GE, but with explicit treatments for NO_3^-, Cl^-, and Na^+; HNO_3 and HCl condensation and aqueous-phase chemistry; species-dependent accommodation coefficients	A baseline run for the 2nd set of simulations; differences of MAM_SIM and MAM_CB05_GE indicate the impact of modified condensation and aqueous-phase chemistry treatments
MAM_CON/IMN	Same as MAM7_CON, but combine IMN with modified default nucleation parameterizations with a prefactor of 1.0×10^{-8}	Differences of MAM_CON and MAM_CON/IMN indicate the impacts of IMN and the lower prefactor for WP09
MAM_CON/ISO	Same as MAM7_CON, but with ISORROPIA II for aerosol thermodynamics under metastable conditions	Differences between MAM_CON and MAM_IMN/ISO indicate the impacts of explicit aerosol thermodynamics
MAM_NEWA	Same as MAM7_CON, but with all modified and new treatments and using a prefactor of 1.0×10^{-9} for default nucleation parameterization	Differences between MAM_CB05_GE and MAM_NEWA indicate the impacts of all new and modified treatments for inorganic aerosols
MAM_NEWB	Same as MAM_NEWA, but with ISORROPIA II under stable condition	Differences between MAM_NEWA and MAM_NEWB indicate the impacts of thermodynamic conditions on gas-aerosol partitioning
MAM_NEW/EMIS	Same as MAM7_NEW, but with adjusted emissions of SO_2, NH_3, BC, POM, and CO over CONUS, Europe, and East Asia	Differences between MAM_NEWA and MAM_NEW/EMIS indicate the impact of emissions
MAM_SIM_5Y	Same as MAM_SIM, but with prescribed SST for 2001-2005	A baseline run for 4th set of simulations
MAM_NEW_5YA	Same as MAM_NEW/EMIS, but with prescribed SST for 2001-2005	Differences between MAM_SIM_5Y and MAM_NEW_5YA indicate the indicate the impacts of all new and modified treatments for inorganic aerosols
MAM_NEW_5YB	Same as MAM_NEW/EMIS, but with fully-coupled model for 2001-2005	Difference between MAM_NEW_5YB and MAM_NEW_5YA indicate the impacts of processes from component models in the fully-coupled Earth system

Table 2. Datasets for model evaluation

Species/Variables	Dataset
Downwelling longwave radiation (LWD)	BSRN
Downwelling shortwave radiation (SWD)	BSRN
Outgoing longwave radiation (OLR)	NOAA/CDC
Cloud fraction (CF)	MODIS
Cloud optical thickness (COT)	MODIS
Cloud water path (CWP)	MODIS
Precipitating water vapor (PWV)	MODIS
Aerosol optical depth (AOD)	MODIS
Column cloud condensation nuclei (ocean) at S = 0.5% (CCN5)	MODIS
Cloud droplet number concentration (CDNC)	BE07
Shortwave cloud radiative forcing (SWCF)	CERES
Carbon monoxide (CO)	Europe: EMEP East Asia: NIES of Japan, TAQMN
Ozone (O_3)	CONUS: CASTNET Europe: Airbase, BDQA, EMEP East Asia: TAQMN
Sulfur dioxide (SO_2)	CONUS: CASTNET Europe: Airbase, BDQA, EMEP East Asia: MEP of China, NIES of Japan, TAQMN
Nitric acid (HNO_3)	CONUS: CASTNET Europe: EMEP
Ammonia (NH_3)	Europe: Airbase, EMEP
Nitrogen dioxide (NO_2)	Europe: Airbase, BDQA, EMEP East Asia: NIES of Japan, TAQMN
Sulfate (SO_4^{2-})	CONUS: CASTNET, IMPROVE, STN Europe: Airbase, EMEP
Ammonium (NH_4^+)	CONUS: CASTNET, IMPROVE, STN Europe: Airbase, EMEP
Nitrate (NO_3^-)	CONUS: CASTNET, IMPROVE, STN Europe: Airbase, EMEP
Chloride (Cl^-)	CONUS: IMPROVE Europe: Airbase, EMEP
Organic carbon (OC), Black carbon (BC), Total carbon (TC)	CONUS: IMPROVE, STN
Particulate matter with diameter less than 2.5 μm ($PM_{2.5}$)	CONUS: IMPROVE, STN Europe: BDQA, EMEP
Particulate matter with diameter less than 10 μm (PM_{10})	Europe: Airbase, BDQA, EMEP East Asia: MEP of China, NIES of Japan, TAQMN
Column CO	Globe: MOPITT
Column NO_2	Globe: GOME
Tropospheric ozone residual (TOR)	Globe: TOMS/SBUV
New particle formation rate (J)	Globe: Kulmala et al. (2004); Yu et al. (2008)

BSRN: Baseline Surface Radiation Network; NOAA/CDC: National Oceanic and Atmospheric Administration Climate Diagnostics Center; MODIS: Moderate Resolution Imaging Spectroradiometer; BE07: Bennartz, 2007; CERES: Clouds and Earth's Radiant Energy System; TOMS/SBUV: the Total Ozone Mapping Spectrometer/the Solar Backscatter UltraViolet; MOPITT: the Measurements Of Pollution In The Troposphere; GOME: Global Ozone Monitoring Experiment; CASTNET: Clean Air Status and Trends Network; IMPROVE: Interagency Monitoring of Protected Visual Environments; STN: Speciation Trends Network; EMEP: European Monitoring and Evaluation Program; BDQA: Base de Données sur la Qualité de l'Air; AirBase: European air quality database; MEP of China: Ministry of Environmental Protection of China; TAQMN: Taiwan Air Quality Monitoring Network; NIES of Japan: National Institute for Environmental Studies of Japan.

Table 3. Mean Bias (MB) and Normalized Mean Bias (NMB, in %) of Radiative/Cloud Predictions for the 2001 Simulations

Species/Variables	Dataset	Obs.	Simulations						
			MAM_ SIM	MAM_ CB05_GE	MAM_ CON	MAM_ CON/IMN	MAM_ CON/ISO	MAM_ NEWA	MAM_ NEW/EMIS
LWD (W m^{-2})[a]	BSRN	312.5	309.2/ -3.4/-1.1[c]	309.6/ -2.9/-0.9	308.4/ -4.2/-1.3	308.0/ -4.5/-1.4	308.3/ -4.2/-1.3	308.7/ -3.8/-1.2	309.1/ -3.5/-1.1
SWD (W m^{-2})[b]	BSRN	181.2	179.2/ -2.0/-1.1	177.0/ -4.2/-2.3	169.4/ -11.8/-6.5	170.2/ -11.0/-6.1	177.3/ -3.9/-2.2	174.5/ -6.8/-3.7	177.0/ -4.2/-2.3
OLR (W m^{-2})	NOAA-CDC	214.4	223.2/ 8.8/4.1	222.4/ 8.1/3.8	219.3/ 4.9/2.3	219.3/ 4.9/2.3	220.7/ 6.2/2.9	221.2/ 6.9/3.2	221.2/ 6.9/3.2
SWCF (W m^{-2})	CERES	-41.0	-37.8/ 3.2/7.9	-38.4/ 2.7/6.5	-43.2/ -2.2/-5.3	-43.3/ 2.3/-5.6	-40.4/ -0.7/1.6	-40.7/ -0.4/0.9	-40.5/ -0.6/1.4
CF (%)	MODIS	66.9	65.6/ -1.4/-2.0	65.9/ -1.0/-1.5	67.5/ 0.5/0.8	67.6/ 0.7/1.0	66.4/ -0.5/-0.8	66.5/ -0.4/-0.6	66.6/ -0.3/-0.5
COT	MODIS	17.1	6.9/ -10.2/-59.5	7.1/ -10.1/-58.8	8.7/ -8.4/-49.2	8.8/ -8.3/-48.4	7.7/ -9.4/-55.1	7.7/ -9.4/-54.9	7.7/ -9.4/-55.2
CWP (g m^{-2})	MODIS	148.1	33.0/ -115.1/ -77.7	33.5/ -114.7/ -77.4	42.3/ -105.8/ -71.4	42.7/ -105.4/ -71.2	36.4/ -111.7/ -75.4	36.5/ -111.7/ -75.4	36.2/ -111.9/ -75.5
PWV (cm)	MODIS	1.9	1.9/ -2.5×10^{-2}/ -1.3	1.9/ -1.8×10^{-2}/ -0.9	1.9/ -3.3×10^{-2}/ -1.7	1.9/ -3.9×10^{-2}/ -2.0	1.9/ -1.8×10^{-2}/ -0.9	1.9/ -1.4×10^{-2}/ -0.7	1.9/ -1.2×10^{-2}/ -0.6
AOD	MODIS	1.5×10^{-1}	9.8×10^{-2}/ -5.5×10^{-2}/ -36.1	1.0×10^{-1}/ -5.2×10^{-2}/ -33.9	1.2×10^{-1}/ -3.0×10^{-2}/ -19.8	1.3×10^{-1}/ -2.6×10^{-2}/ -17.1	1.0×10^{-1}/ -5.3×10^{-2}/ -34.4	1.0×10^{-1}/ -5.0×10^{-2}/ -32.9	1.0×10^{-1}/ -5.2×10^{-2}/ -34.0
Column CCN5 (ocean) (cm^{-2})	MODIS	2.4×10^{8}	5.8×10^{7}/ -1.9×10^{8}/ -76.4	5.2×10^{7}/ -1.9×10^{8}/ -78.6	1.8×10^{8}/ -6.7×10^{7}/ -27.5	2.0×10^{8}/ -4.6×10^{7}/ -18.8	9.1×10^{7}/ -1.5×10^{8}/ -62.7	8.5×10^{7}/ -1.6×10^{8}/ -65.3	8.2×10^{7}/ -1.6×10^{8}/ -66.6
CDNC (cm^{-3})	BE07	113.1	45.5/ -67.7/-59.9	46.7/ -66.5/-58.8	89.7/ -23.4/-20.7	93.1/ -20.0/-17.7	65.0/ -48.1/-42.5	66.7/ -46.4/-41.0	67.0/ -46.1/-40.8

[a]The pair of observation and simulation is removed in the statistical calculation if the observed LWD value is lower than 50 W m^{-2} or higher than 700 W m^{-2} (http://www.pangaea.de).

[b]The pair of observation and simulation is removed in the statistical calculation if the observed SWD value is lower than -10 or higher than 3000 W m^{-2} (http://www.pangaea.de).

[c]The values of modeled results (Sim), MBs, and NMBs are expressed as Sim/MB/NMB.

Table 4. Mean Bias (MB) and Normalized Mean Bias (NMB, in %) of Chemical Predictions for the 2001 Simulations

Species/ variables[a]	Domain	Obs.	Simulations							
			MAM_SIM	MAM_CB05_GE	MAM_CON	MAM_CON/IMN	MAM_CON/ISO	MAM_NEWA	MAM_NEWB	MAM_NEW/ EMIS
CO	Europe	123.0	-	112.4/-10.6/-8.6	115.0/-8.0/-6.5	107.9/-15.1/-12.3	114.0-9.0/-7.3	118.8/-4.2/-3.4	113.6/-9.4/-7.6	137.9/14.9/12.1
	East Asia	0.6	-	0.1/-0.5/-82.1	0.1/-0.5/-82.0	0.1/-0.5/-81.8	0.1/-0.5/-81.8	0.1/-0.5/-82.0	0.1/-0.5/-81.7	0.1/-0.5/-78.7
SO_2	CONUS	3.9	14.2/10.3/264.8[b]	14.4/10.5/270.1	15.6/11.7/301.2	15.1/11.2/286.1	15.4/11.5/295.8	15.3/11.4/291.8	15.3/11.4/293.0	9.8/5.9/152.2
	Europe	6.8	13.4/6.6/97.5	13.8/7.0/103.2	15.2/8.4/123.0	13.6/6.8/100.3	14.6/7.8/114.7	15.7/8.9/130.7	14.5/7.7/114.0	6.8/0.0/0.3
	East Asia	12.5	4.6/-7.9/-63.0	4.8/-7.7/-61.3	4.8/-7.7/-61.4	4.8/-7.7/-61.8	4.9-7.6/-61.0	4.8/-7.7/-61.2	4.8/-7.7/-61.2	5.8/-6.7/-53.4
NH_3	Europe	9.4	1.7/-7.7/-82.0	1.8/-7.6/-80.8	1.2/-8.2/-86.8	1.1/-8.3/-87.8	1.4/-8.0/-84.7	1.5/-7.9/-84.3	1.1/-8.3/-84.0	2.1/-7.3/-77.5
NO_2	Europe	20.2	-	4.6/-15.6/-77.0	5.2/-15.0/-74.1	4.7/-15.5/-76.5	5.0/-15.2/-75.2	5.2/-15.0/-74.1	4.9/-15.3/-75.7	4.9/-15.3/-75.9
	East Asia	14.0		1.6/-12.4/-88.4/	1.7/-12.3/-88.0	1.7/-12.3/-88.2	1.6/-12.4/-88.4	1.7/-12.3/-88.3	1.6/-12.4/-88.5	1.7/-12.3/-88.2
O_3	CONUS	34.6	-	44.6/10.0/28.9	42.6/8.0/23.0	42.5/7.9/22.7	44.4/9.8/28.4	44.1/9.5/27.4	43.7/9.1/26.4	44.4/9.8/28.1
	Europe	53.5	-	90.2/36.7/68.6	84.4/30.9/57.7	84.5/31.0/58.0	87.6/34.1/63.7	87.0/33.5/62.7	87.7/34.2/63.9	88.4/34.9/65.2
	East Asia	26.4		42.8/16.4/62.2	42.7/16.3/61.7	40.7/14.3/54.3	42.6/16.2/65.9	42.1/15.7/59.6	43.0/16.6/63.0	42.5/16.1/61.2
HNO_3	CONUS	1.5	-	2.5/1.0/68.1	0.6/-0.9/-60.2	0.6/-0.9/-59.7	1.7/0.2/15.8	1.8/0.3/17.7	1.8/0.3/19.0	1.6/0.1/4.1
	Europe	0.5	-	1.8/1.3/268.5	0.3/-0.2/-34.1	0.3/-0.2/-35.8	0.9/0.4/86.1	0.9/0.4/83.6	1.0/0.5/103.8	0.9/0.4/73.8
SO_4^{2-}	CONUS	2.6	2.5/-0.1/-5.1	2.4/-0.2/-7.2	$2.6/4.4\times10^{-2}$/1.7	$2.6/4.2\times10^{-2}$/1.6	2.4/-0.2/-7.9	2.4/-0.2/-6.3	2.5/-0.1/-5.5	1.9/-0.7/-28.4
	Europe	2.2	3.0/0.8/36.5	2.9/0.7/33.1	3.1/0.9/40.3	3.0/0.8/35.8	2.9/0.7/32.6	3.1/0.9/39.4	3.0/0.8/36.8	2.0/-0.2/-7.2
NH_4^+	CONUS	1.4	1.0/-0.4/-32.1	0.8/-0.6/-39.6	1.7/0.3/20.0	1.7/0.3/19.7	1.3/-0.1/-6.4	1.3/-0.1/-6.5	1.3/-0.1/-4.3	1.2/-0.2/-13.1
	Europe	1.2	1.1/-0.1/-9.1	1.0/-0.2/18.3	2.2/1.0/85.0	2.0/0.8/65.7	1.8/0.6/49.4	1.9/0.7/54.8	1.7/0.5/37.7	1.6/0.4/32.5
NO_3^-	CONUS	1.0	-	-	3.0/2.0/198.2	2.9/1.9/192.7	$1.0/-4.8\times10^{-2}$/-4.8	0.9/-0.1/-9.6	$1.0/-2.2\times10^{-2}$/-2.1	$1.0/4.0\times10^{-3}$/0.4
	Europe	2.0	-	-	3.4/1.4/67.8	3.0/1.0/49.4	1.9/-0.1/-4.3	$2.0/-4.0\times10^{-2}$/-2.0	1.8/-0.2/-12.5	2.1/0.1/5.2
Cl^-	CONUS	0.1	-	-	0.5/0.4/359.9	0.5/0.4/373.1	$0.1/-1.5\times10^{-2}$/-14.5	$0.1/-1.8\times10^{-2}$/-17.5	$0.1/-1.5\times10^{-2}$/-12.1	$0.1/-2.8\times10^{-3}$/-2.8
	Europe	0.7	-	-	1.4/0.7/102.8	1.3/0.6/89.9	$0.7/2.1\times10^{-3}$/0.3	$0.7/1.4\times10^{-2}$/2.0	0.6/-0.1/-14.5	-4.7×10^{-2}/-6.7
BC	CONUS	0.6	0.3/-0.3/-54.6	0.3/-0.3/-55.8	0.3/-0.3/-54.7	0.3/-0.3/-54.6	0.3/-0.3/-53.8	0.3/-0.3/-54.3	0.3/-0.3/-54.9	0.4/-0.2/-29.4
OC	CONUS	1.1	0.8/-0.3/-22.7	1.0/-0.1/-12.1	1.0/-0.1/-11.4	1.0/-0.1/-11.9	1.0/-0.1/-8.6	1.0/-0.1/-9.1	1.0/-0.1/-11.3	$1.0/5.6\times10^{-3}$/0.5
TC	CONUS	2.5	1.3/-1.2/-47.9	1.4/-1.1/-43.1	1.4/-1.1/-42.2	1.4/-1.1/-42.5	1.4/-1.0/-40.9	1.5/-1.0/-41.1	1.4/-1.1/-42.5	1.6/-0.9/-35.0
$PM_{2.5}$	CONUS	7.9	4.9/-3.0/-37.6	5.0/-2.9/-36.8	9.5/1.6/20.1	6.6/1.3/16.7	7.8/-0.1/-1.7	6.9/-1.0/-13.2	7.2/-0.7/-8.8	6.8/-1.1/-13.5
	Europe	14.5	8.4/-6.1/-41.8	7.9/-6.6/-45.3	13.7/-0.8/-5.5	14.4/-0.1/-0.9	11.0/-3.5/-24.4	11.9/-2.6/-17.7	10.9/-3.6/-24.9	10.6/-3.9/-27.2
PM_{10}	Europe	25.7	17.5/-8.2/-31.8	16.5/-9.2/-35.8	22.5/-3.2/-12.3	23.0/-2.7/-10.5	20.1/-4.8/-18.5	21.4/-4.3/-16.6	20.7/-5.0/-19.4	20.9/-4.8/-18.8
	East Asia	118.5	38.5/-80.0/-67.5	44.9/-73.6/-62.1	55.9/-62.6/-52.8	58.8/-57.7/-48.7	48.5/-70.0/-59.1	65.5/-53.0/-44.7	55.6/-62.9/-53.1	48.2/-70.3/-59.3
Col.CO	Globe	1.3×10^{18}	- --	1.2×10^{18}/ -7.4×10^{16}/-5.7	1.2×10^{18}/ -5.7×10^{16}/-4.4	1.2×10^{18}/ -6.3×10^{16}/-4.8	1.2×10^{18}/ -6.4×10^{16}/-4.9	1.2×10^{18}/ -6.3×10^{16}/-4.8	1.2×10^{18}/ -5.6×10^{16}/-4.3	1.3×10^{18}/ 2.3×10^{16}/1.8
Col.NO_2	Globe	4.7×10^{14}	-	6.7×10^{14}/ 1.9×10^{14}/40.5	6.2×10^{14}/ 1.4×10^{14}/30.4	6.2×10^{14}/ 1.4×10^{14}/30.0	6.5×10^{14}/ 1.8×10^{14}/37.5	6.5×10^{14}/ 1.8×10^{14}/37.2	6.5×10^{14}/ 1.8×10^{14}/37.9	6.5×10^{14}/ 1.8×10^{14}/37.3
TOR	Globe	30.3	29.8/-0.5/1.6	29.2/-1.1/-3.7	27.6/-2.7/-9.0	27.4/-2.9/-9.6	28.8/-1.5/-4.9	28.7/-1.6/-5.2	28.6/-1.5/-5.0	28.6-1.5/-4.9
J	Globe	0.6	0.003/-0.6/-99.6	0.1/-0.5/-99.5	0.5/-0.1/-12.8	0.3/-0.3/-49.6	0.8/0.2/36.1	0.3/-0.3/-53.1	0.3/-0.3/-51.7	0.3/-0.3/-62.0

[a]The units are CO, ppb (over Europe) and ppm (over East Asia); SO_2, ppb (over East Asia) and μg m^{-3} (over CONUS and Europe); O_3, ppb (over CONUS) and μg m^{-3} (over Europe); column CO and NO_2, molecules cm^{-2}; TOR, DU; J, $cm^{-3}s^{-1}$. All other concentrations are in μg m^{-3}. [b]The values of modeled results (Sim), MBs, and NMBs are expressed as Sim/MB/NMB.

Table 5. The observed values and the mean bias (MB) and normalized mean bias (NMB, in %) of predictions of O_3 NO_2, and HNO_3 mixing ratios over Europe in MAM_NEWA

	Network		Obs ($\mu g\ m^{-3}$)	Sim ($\mu g\ m^{-3}$)	MB/NMB
Winter	Airbase			75.2	37.5/99.6[a]
		NO_2	26.0	7.6	-18.4/-70.9
	BDQA	O_3	31.0	74.2	43.2/139.2
		NO_2	30.6	5.6	-25.0/-81.9
	EMEP	O_3	50.7	75.7	25.0/49.3
		NO_2	9.0	8.3	-0.7/-7.8
		HNO_3	0.5	0.5	-4.9×10^{-3}/1.0
Spring	Airbase	O_3	63.1	100.8	37.7/59.7
		NO_2	20.0	4.6	-15.4/-77.1
	BDQA	O_3	59.6	98.9	39.3/65.9
		NO_2	23.6	3.1	-20.5/-87.0
	EMEP	O_3	75.0	101.9	26.9/35.9
		NO_2	5.9	4.9	-1.0/-17.2
		HNO_3	0.4	0.9	0.5/144.5
Summer	Airbase	O_3	64.9	93.5	28.6/44.0
		NO_2	16.2	4.4	-11.8/-72.8
	BDQA	O_3	64.5	94.5	30.0/46.5
		NO_2	18.7	3.6	-15.1/-80.9
	EMEP	O_3	72.2	91.2	19.0/26.3
		NO_2	4.7	4.4	-0.3/-6.2
		HNO_3	0.5	1.3	0.8/169.6
Autumn	Airbase	O_3	40.5	79.5	39.0/96.4
		NO_2	21.7	5.3	-16.4/-75.6
	BDQA	O_3	35.7	80.9	45.2/126.5
		NO_2	24.8	3.7	-21.1/-85.2
	EMEP	O_3	51.7	78.2	26.5/51.2
		NO_2	6.6	5.2	-1.4/-21.1
		HNO_3	0.6	0.9	0.3/45.0

[a]The values of MBs and NMBs are expressed as MB/NMB.

Table 6. Statistical Performance of Radiative/Cloud Predictions (Average of the 5-yr (2001-2005) Simulations)

Species/Variables	Dataset	Obs.	Simulations		
			MAM_SIM_5Y	MAM_NEW_5YA	MAM_NEW_5YB
LWD (W m^{-2})[a]	CERES	307.6	302.9/-4.7/-1.5/2.9/11.6[c]	303.9/-3.6/-1.1/2.8/11.3	304.4/-3.1/-1.0/2.9/11.3
SWD (W m^{-2})[b]	CERES	163.9	169.9/5.9/3.6/7.0/14.1	166.5/2.5/1.5/6.5/13.8	167.0/3.1/1.9/6.7/13.7
OLR (W m^{-2})	NOAA-CDC	215.9	222.5/6.6/3.1/3.5/8.9	220.7/4.8/2.2/3.4/9.1	221.4/5.5/2.6/3.5/9.0
SWCF (W m^{-2})	CERES	-41.0	-38.8/2.2/-5.4/-21.5/12.0	-41.5/-0.5/1.2/-21.4/12.5	-40.8/0.2/-0.5/-22.2/12.4
CF (%)	MODIS	67.1	66.6/-0.6/-0.8/15.2/13.3	67.3/0.2/0.3/14.7/13.0	66.6/-0.6/-0.9/15.5/13.7
COT	MODIS	17.3	7.1/-10.3/-59.3/70.2/15.1	7.9/-9.4/-54.5/65.7/14.6	7.8/-9.6/-55.2/65.6/14.5
CWP (g m^{-2})	MODIS	86.0	38.2/-47.8/-55.5/55.7/52.9	43.2/-42.8/-49.8/50.0/49.2	43.4/-42.6/-49.5/49.7/49.2
PWV (cm)	MODIS	1.93	1.96/0.03/1.5/11.6/0.3	1.99/0.06/2.9/10.9/0.3	1.97/0.04/1.8/13.8/0.3
AOD	MODIS	0.2	0.1/-0.07/-44.1/54.5/0.1	0.1/-0.06/-39.2/51.3/0.1	0.1/-0.06/-36.3/49.5/0.1
Column CCN5 (ocean) (cm^{-2})	MODIS	2.5×10^8	5.3×10^7/-1.9×10^8/ -78.6/78.6/5.7×10^8	8.6×10^7/1.6×10^8/ -65.2/65.2/5.5×10^8	8.6×10^7/1.6×10^8/ -65.3/65.3/5.5×10^8
CDNC (cm^{-3})	BE07	112.6	44.2/-68.3/-60.7/61.6/84.3	69.2/-43.4/-38.6/44.2/66.8	68.8/-43.8/-38.9/45.5/67.9

[a] The pair of observation and simulation is removed in the statistical calculation if the observed LWD value is lower than 50 W m^{-2} or higher than 700 W m^{-2} (http://www.pangaea.de).

[b] The pair of observation and simulation is removed in the statistical calculation if the observed SWD value is lower than -10 or higher than 3000 W m^{-2} (http://www.pangaea.de).

[c] The values are expressed as Sim/MB/NMB/NME/RMSE. Sim: simulated values; MB: mean bias; NMB: normalized mean bias (%); NME: normalized mean error (%); RMSE: root mean squared error.

Table 7. Statistical Performance of Chemical Predictions (Average of from the 5-yr (2001-2005) Simulations)

Species/ variables[a]	Domain	Obs.	Simulations		
			MAM_SIM_5Y	MAM_NEW_5YA	MAM_NEW_5YB
CO	East Asia	562.0	-	139.7/-422.3/-75.1/75.1/451.8[b]	137.0/-425.0/-75.6/75.6/454.0
SO_2	CONUS	3.4	9.6/6.2/183.9/184.6/9.9	10.1/6.7/198.8/199.1/10.6	10.3/6.9/203.1/203.5/10.9
	Europe	6.6	6.0/-0.6/-9.3/73.3/7.9	6.6/-0.06/-0.9/77.2/8.3	6.2/-0.4/-5.5/74.6/8.0
	East Asia	3.4	3.4/0.04/1.1/76.0/5.0	3.4/0.01/0.4/76.2/5.0	3.4/-0.05/-1.6/73.1/4.8
NH_3	Europe	6.3	3.0/-3.3/-52.0/81.0/25.3	2.4/-3.9/-61.3/79.7/25.3	2.4/-3.9/-62.0/79.3/25.3
NO_2	Europe	23.5	-	5.8/-17.7/-75.4/76.5/21.5	5.5/-18.0/-76.7/77.7/21.7
	East Asia	13.5	-	2.3/-11.2/-83.3/83.3/12.2	2.3/-11.2/-83.6/83.6/12.2
O_3	CONUS	35.1	-	43.9/8.8/25.1/27.3/11.3	44.1/9.0/25.7/27.7/11.6
	Europe	52.7	-	86.6/33.9/64.5/64.6/36.4	89.2/36.5/69.3/69.4/38.8
	East Asia	27.4	-	45.6/18.2/66.4/66.4/19.2	45.5/18.1/66.0/66.0/19.1
HNO_3	CONUS	1.4	-	1.6/0.2/16.3/39.5/0.7	1.6/0.2/12.1/38.2/0.7
	Europe	0.7	-	1.0/0.3/45.8/83.5/0.8	1.0/0.3/37.9/79.8/0.8
SO_4^{2-}	CONUS	2.6	2.3/-0.3/-13.4/26.9/1.0	2.3/-0.3/-13.1/23.0/0.8	2.3/-0.3/-12.8/24.2/0.9
	Europe	2.3	2.3/-0.04/-1.9/37.3/1.4	2.0/-0.3/-11.1/34.1/1.3	2.0/-0.3/-13.0/35.5/1.4
NH_4^+	CONUS	1.2	0.9/-0.3/-20.8/33.4/55.0	1.5/0.3/22.2/43.2/0.8	1.5/0.3/26.4/44.3/0.8
	Europe	1.0	0.8/-0.2/-16.8/36.9/0.5	1.6/0.6/62.8/68.7/0.9	1.5/0.5/53.8/60.3/0.8
NO_3^-	CONUS	1.1	-	1.6/0.5/41.3/85.4/1.4	1.6/0.5/49.8/90.2/1.5
	Europe	1.8	-	2.3/0.5/30.3/51.1/1.2	2.2/0.4/24.7/47.0/1.1
Cl^-	CONUS	0.1	-	$0.1/3.1\times10^{-3}/2.7/105.8/0.4$	$0.1/8.7\times10^{-3}/7.8/110.1/0.4$
	Europe	0.3	-	2.4/2.1/681.2/681.2/2.9	2.3/2.0/663.3/663.6/2.8
BC	CONUS	0.4	0.3/-0.1/-17.9/44.4/0.3	0.3/-0.1/-15.6/44.0/28.2	0.3/-0.1/-17.7/44.3/0.2
OC	CONUS	1.2	0.9/-0.3/-23.2/59.3/1.0	1.1/-0.1/-7.7/56.7/1.0	1.1/-0.1/-11.0/54.3/0.9
TC	CONUS	3.1	1.4/-1.7/-54.4/62.8/2.8	1.7/-1.4/-45.7/57.1/2.6	1.6/-1.5/-47.1/57.1/2.7
$PM_{2.5}$	CONUS	8.8	7.2/-1.6/-17.9/37.0/4.3	9.2/0.4/4.1/33.5/3.9	8.7/-0.1/-1.1/29.4/3.6
	Europe	14.6	6.7/-7.9/-53.9/54.6/10.6	9.7/-4.9/-33.8/37.6/8.6	10.0/-4.6/-31.7/36.1/8.4
PM_{10}	Europe	26.3	15.1/-11.2/-42.6/46.8/15.9	18.7/-7.6/-28.8/36.1/13.9	19.9/-6.4/-24.4/33.5/13.1
	East Asia	107.9	45.4/-62.5/-58.0/59.3/70.7	52.5/-57.4/-53.2/54.2/66.0	57.8/-50.1/-46.5/50.0/61.6
Col.CO	Globe	1.4×10^{18}	-	1.3×10^{18}/-1.4×10^{17}/ -10.2/16.5/3.1×10^{17}	1.2×10^{18}/-1.5×10^{17}/ -11.0/17.2/3.2×10^{17}
Col.NO_2	Globe	5.3×10^{14}	-	8.4×10^{14}/3.1×10^{14}/ 59.2/70.0/5.4×10^{14}	8.3×10^{14}/3.0×10^{14}/ 57.6/69.2/5.4×10^{14}
TOR	Globe	30.4	29.9/-0.5/1.6/16.3/6.1	30.5/0.1/0.4/15.0/5.8	29.9/-0.5/-1.7/16.4/6.1

[a]The units are CO, ppm (over East Asia); SO_2, ppb (over East Asia) and μg m^{-3} (over CONUS); O_3, ppb (over CONUS) and μg m^{-3} (over Europe); column CO and NO_2, molecules cm^{-2}; TOR, DU. All other concentrations are in μg m^{-3}.

[b]The values are expressed as Sim/MB/NMB/NME/RMSE. MB: mean bias; NMB: normalized mean bias (%); NME: normalized mean error (%); RMSE: root mean squared error.

Table 8. Global Burdens of Major Gaseous and Aerosol Species from the 5-yr (2001-2005) Simulations

	MAM_SIM_5Y	MAM_NEW_5YA	Previous studies
Tropospheric CO (Tg) [a]	N.A.[c]	322.06	337-354 [d]
Tropospheric O_3 (DU) [a]	29.7 [c]	30.5	34.04 [e]
Tropospheric O_3 (Tg) [a]	324.14 [c]	332.87	372 [e]
DMS (Tg S)	0.051	0.058	0.067 [f]
SO_2 (Tg S)	0.276	0.281	0.34 [f]
H_2SO_4 (Tg S)	3.8×10^{-4}	1.9×10^{-3}	4.2×10^{-4} [f]
Tropospheric NO_x [a, b]	N.A. [c]	0.116 Tg N (8.24×10^{14} molecules cm^{-2})	7.6×10^{14} molecules cm^{-2} [g]
NOy (Tg N) [b]	N.A. [c]	3.26	N.A. [c]
NH3 (Tg N)	0.074	0.059	0.064 [f]
VOCs (Tg C) [b]	N.A. [c]	7.63	N.A. [c]
Tropospheric HCHO (Tg C) [a]	N.A. [c]	0.391	0.335-0.349 [d]
SO_4^{2-} (Tg S)	0.36	0.39	0.84 [e] ,0.47 [f], 0.66 [h]
NO_3^- (Tg N)	N.A. [c]	0.11	0.01-0.14 i
NH_4^+ (Tg N)	0.20	0.21	0.24 [f], (0.27-0.44) [i]
Na^+ (Tg)	2.93	3.04	2.98 [e], (0.38-5.19) [i]
Cl^- (Tg)	4.52	4.47	4.60 [e], (0.59-8.02) [i]
BC (Tg)	0.091	0.076	0.28 [e], 0.093 [f]
OC (Tg)	0.45	0.61	1.28 [e]
POM (Tg)	0.63	0.48	0.68 [f], 1.70 [h]
SOA (Tg)	N.A. [c]	0.38	1.15 [f], 0.59 [j]
Dust (Tg)	25.78	26.43	24.7 [f], (7.9-35.9) [i]

[a] CESM/CAM5 simulations use 30 model layers, with atmospheric pressures from ~1000 mb (layer 30) to ~3 mb (layer 1). Troposphere refers to model layers below tropopause height.

[b] $NO_x = NO + NO_2$; $NO_y = NO_x$ + nitrogen trioxide (NO_3) + dinitrogen pentoxide (N_2O_5) + nitrous acid (HONO) + nitric acid (HNO_3) + pernitric acid (HNO_4) + peroxyacyl nitrate (PAN) + $\geq C_3$ peroxyacyl nitrate (PANX) + other organic nitrate (NTR); VOCs-volatile organic compounds including acetaldehyde (ALD2), carboxylic acid(AACD), long-chain alkanes (ALKH), Cresol and higher phenols (CRES), ethene (ETH), ethane (ETHA), ethanol (ETOH), formaldehyde (FORM), internal olefinic carbon bond (IOLE), methanol (MEOH), olefinic carbon bond (OLE), paraffin carbon bond (PAR), polycyclic aromatic hydrocarbons (PAH), toluene (TOL), xylene (XYL), isoprene (ISOP), and terpene (TERP).

[c] N.A – not available, it refers to the species that are not treated in MAM_SIM_5Y or species having no burden data from previous studies. Tropospheric O_3 burden in MAM_SIM_5Y is from climatology. N.A. in SOA is due to no SOAG emission for MAM_SIM_5Y.

[d] Williams et al. (2009)

[e] Horowitz et al. (2006)

[f] Liu et al. (2012)

[g] Larmarque et al. (2006)

[h] Textor et al. (2006)

[i] Tsigaridis et al. (2006)

[j] Heald et al. (2008)

Figure captions

Figure 1a. Absolute differences of H_2O_2, SO_2, SO_4^{2-}, and SOA between MAM_CB05_GE and MAM_SIM for 2001.

Figure 1b. Absolute differences between the mixing ratios of surface OH, HO_2, NO_3, and O_3 predicted from MAM_CB05_GE and climatology values used in MAM_SIM for 2001.

Figure 2. Spatial distributions of CO, O_3, NO_2, HNO_3, HCl, and isoprene (ISOP) at surface simulated by MAM_CB05_GE for 2001.

Figure 3. Spatial distributions of total ammonium, total sulfate, total nitrate, total chloride, $PM_{2.5}$, NH_3, SO_2, H_2SO_4, HNO_3, and HCl at surface between MAM_CON and MAM_CB05_GE for summer (June, July, and August (JJA)), 2001.

Figure 4. Vertical distributions of new particle formation rate (J) (row 1) and aerosol number (PM_{num}) (row 3) simulated by MAM_CON/IMN for 2001. The overlay plots in row 2 show the distributions of simulated and observed J in bottom 1000-m in the atmosphere. Circles on overlay plots represent observations for J. Different colors of circles represent different values of J, using the same color scale as simulated J.

Figure 5. Absolute differences of $PM_{2.5}$, AOD, column CCN5, CF, COT, and SWCF between MAM_CON/IMN and MAM_CON for 2001.

Figure 6a. Absolute differences of major PM species and their gas precursors between MAM_CON/ISO and MAM_CON for summer, 2001.

Figure 6b. Absolute differences of major PM species and their gas precursors between MAM_CON/ISO and MAM_CON for winter, 2001.

Figure 7. The spatial distributions of TCAT/TSO4 at surface in MAM_CON and MAM_CON/ISO and their absolute differences (MAM_CON/ISO - MAM_CON) for summer and winter, 2001.

Figure 8. Absolute differences of major aerosol species and their gas precursors between metastable (MAM_NEWA) and stable (MAM_NEWB) conditions.

Figure 9. Absolute differences of major aerosol species and their gas precursors, new particle formation rate (J), and aerosol number between MAM_NEW_5YA and MAM_SIM_5Y for 2001-2005.

Figure 10. Absolute differences of major cloud and radiative variables between MAM_NEW_5YA and MAM_SIM_5Y for 2001-2005.

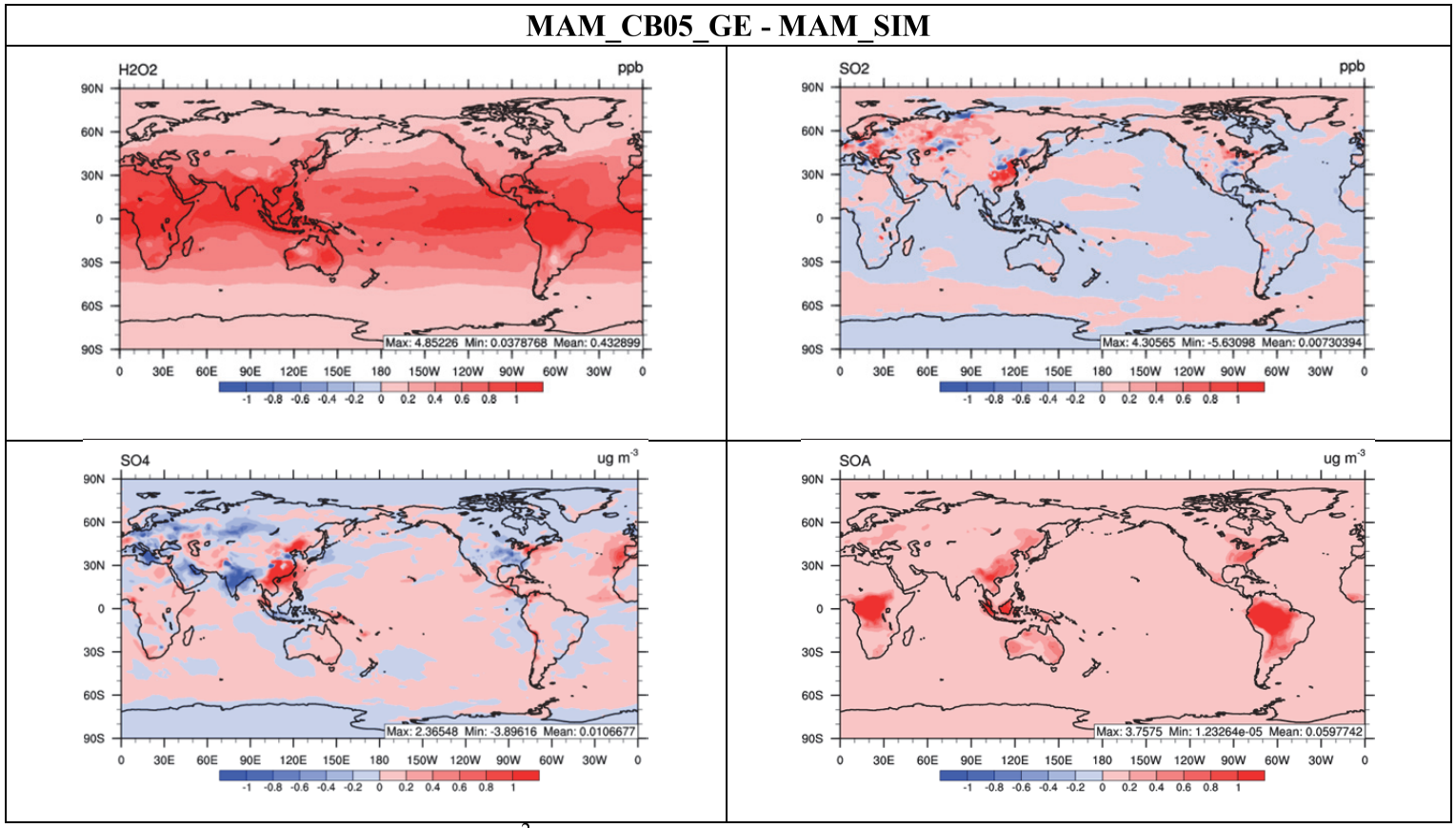

Figure 1a. Absolute differences of H_2O_2, SO_2, SO_4^{2-}, and SOA between MAM_CB05_GE and MAM_SIM for 2001.

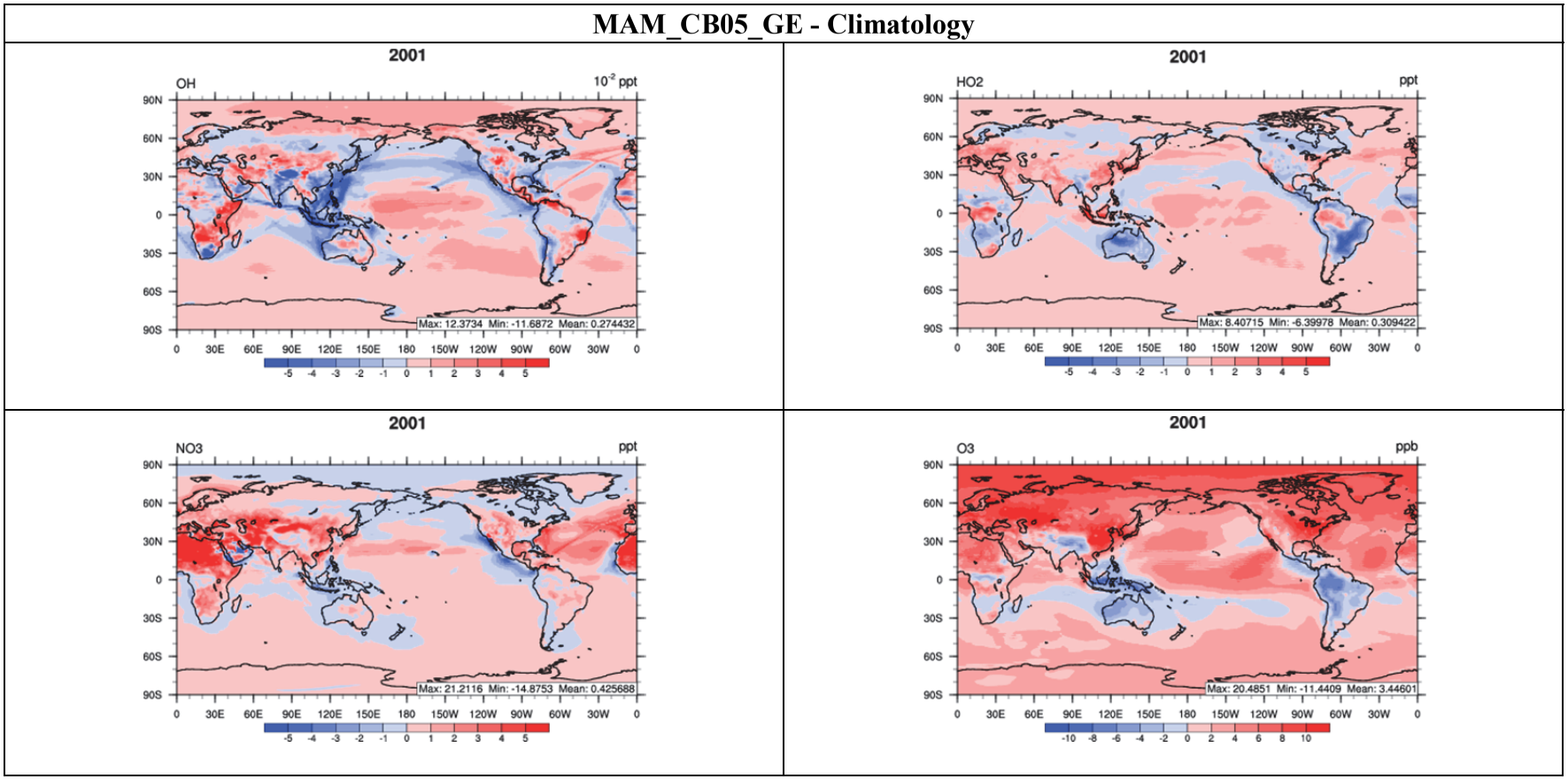

Figure 1b. Absolute differences between the mixing ratios of surface OH, HO_2, NO_3, and O_3 predicted from MAM_CB05_GE and climatology values used in MAM_SIM for 2001.

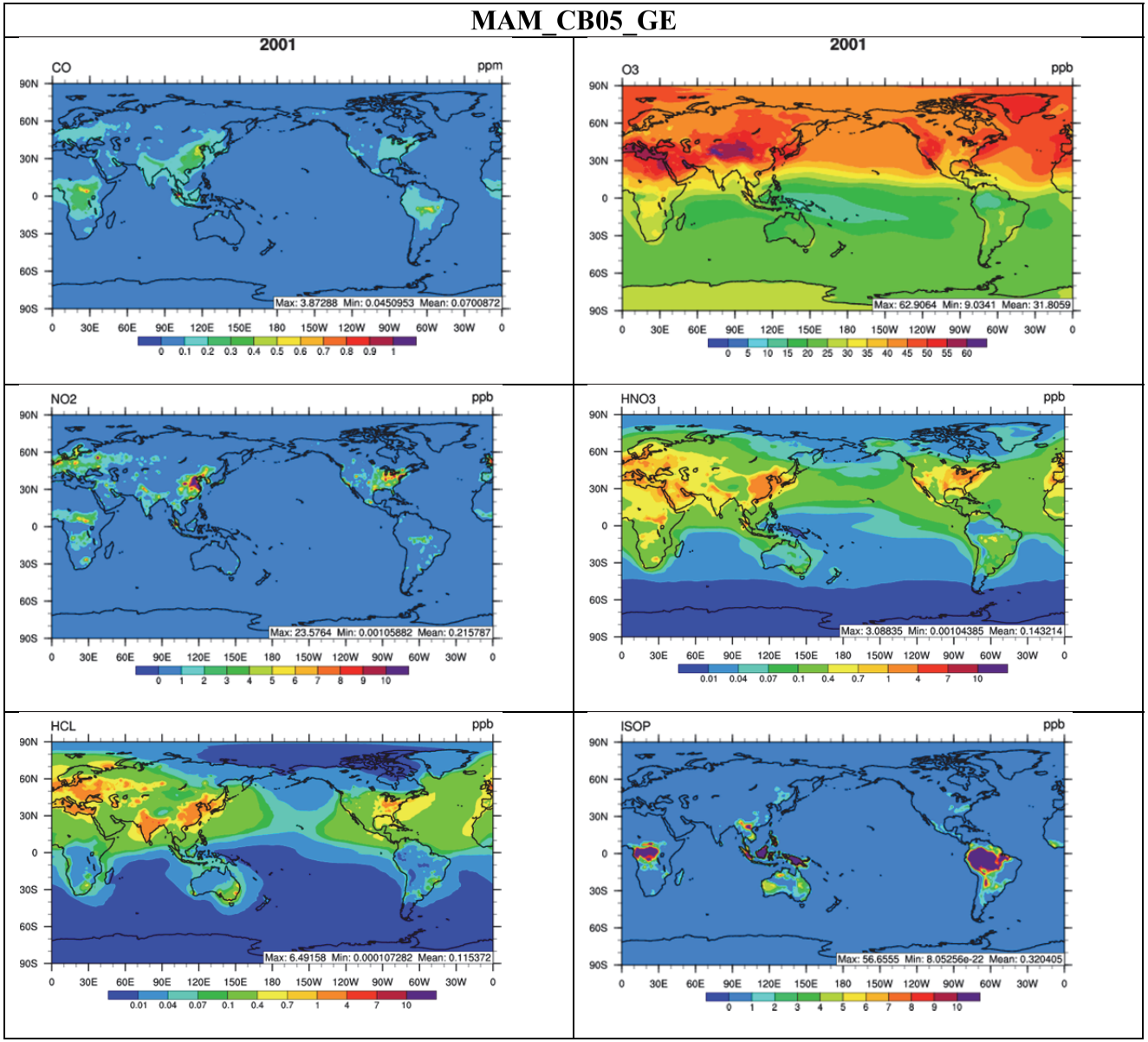

Figure 2. Surface distribution of CO, O_3, NO_2, HNO_3, HCl, and isoprene (ISOP) in MAM_CB05_GE for 2001.

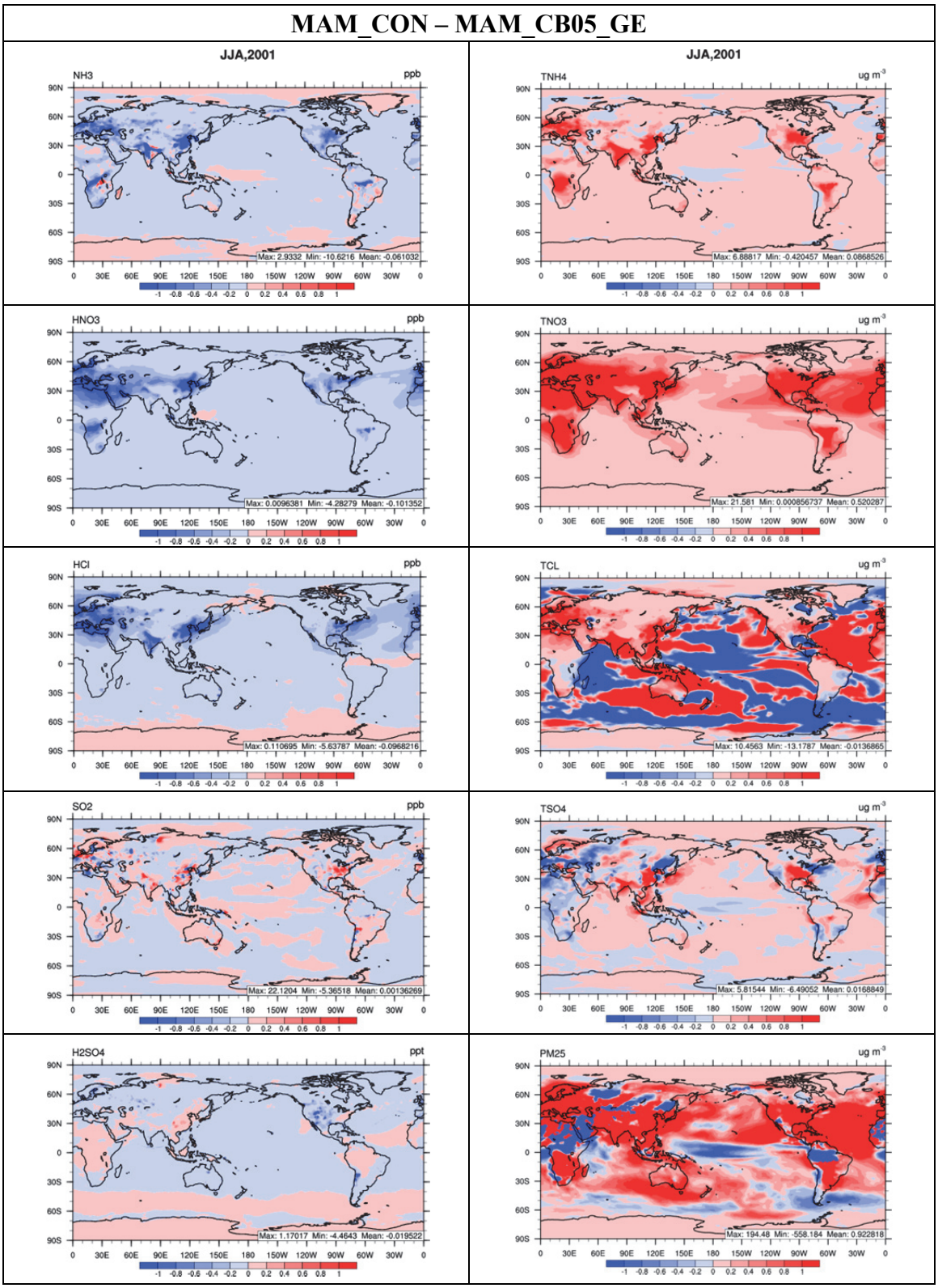

Figure 3. Surface distribution of total ammonium, total sulfate, total nitrate, total chloride, $PM_{2.5}$, NH_3, SO_2, H_2SO_4, HNO_3, and HCl between MAM_CON and MAM_CB05_GE for summer (June, July, and August (JJA)), 2001.

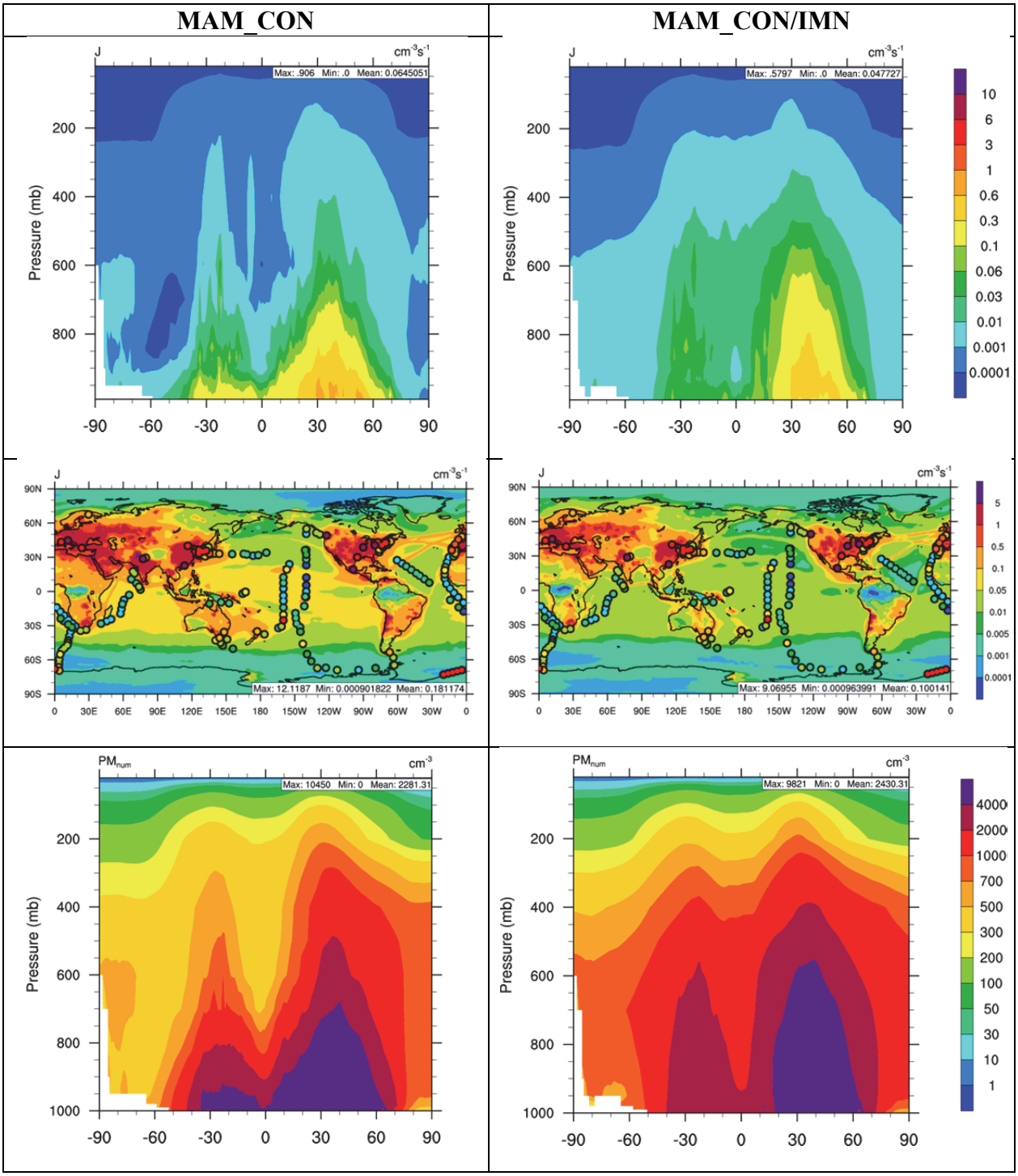

Figure 4. Vertical distribution of new particle formation rate (J) and aerosol number (PM_{num}) simulated by MAM_CON/IMN for 2001. The overlay plots show the distribution of J in bottom 1000-m. Circles on overlay plots represent observations for J. Different colors of circles represent different values of J, using the same color scale as simulated J.

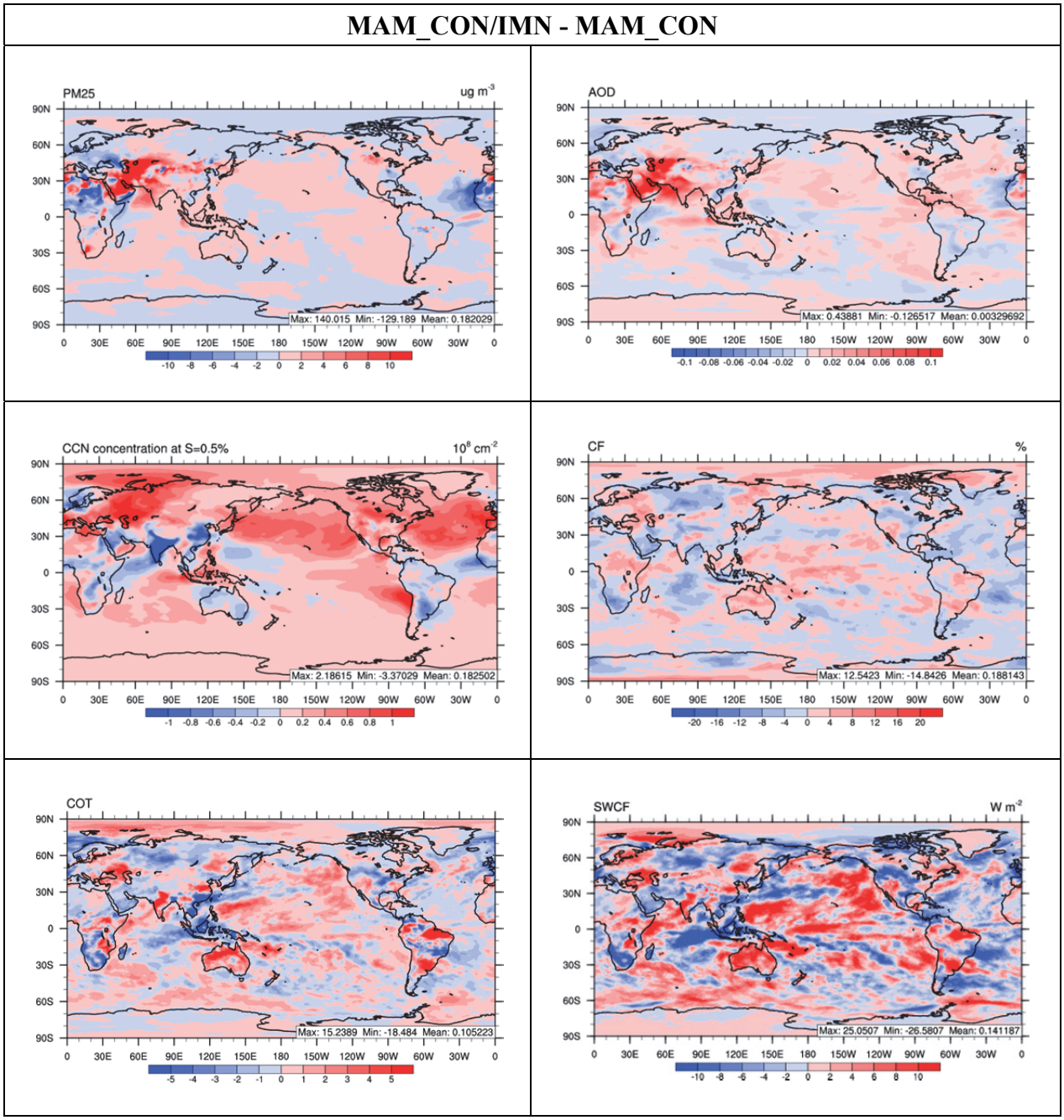

Figure 5. Absolute differences of $PM_{2.5}$, AOD, column CCN5, CF, COT, and SWCF between MAM_CON/IMN and MAM_CON for 2001.

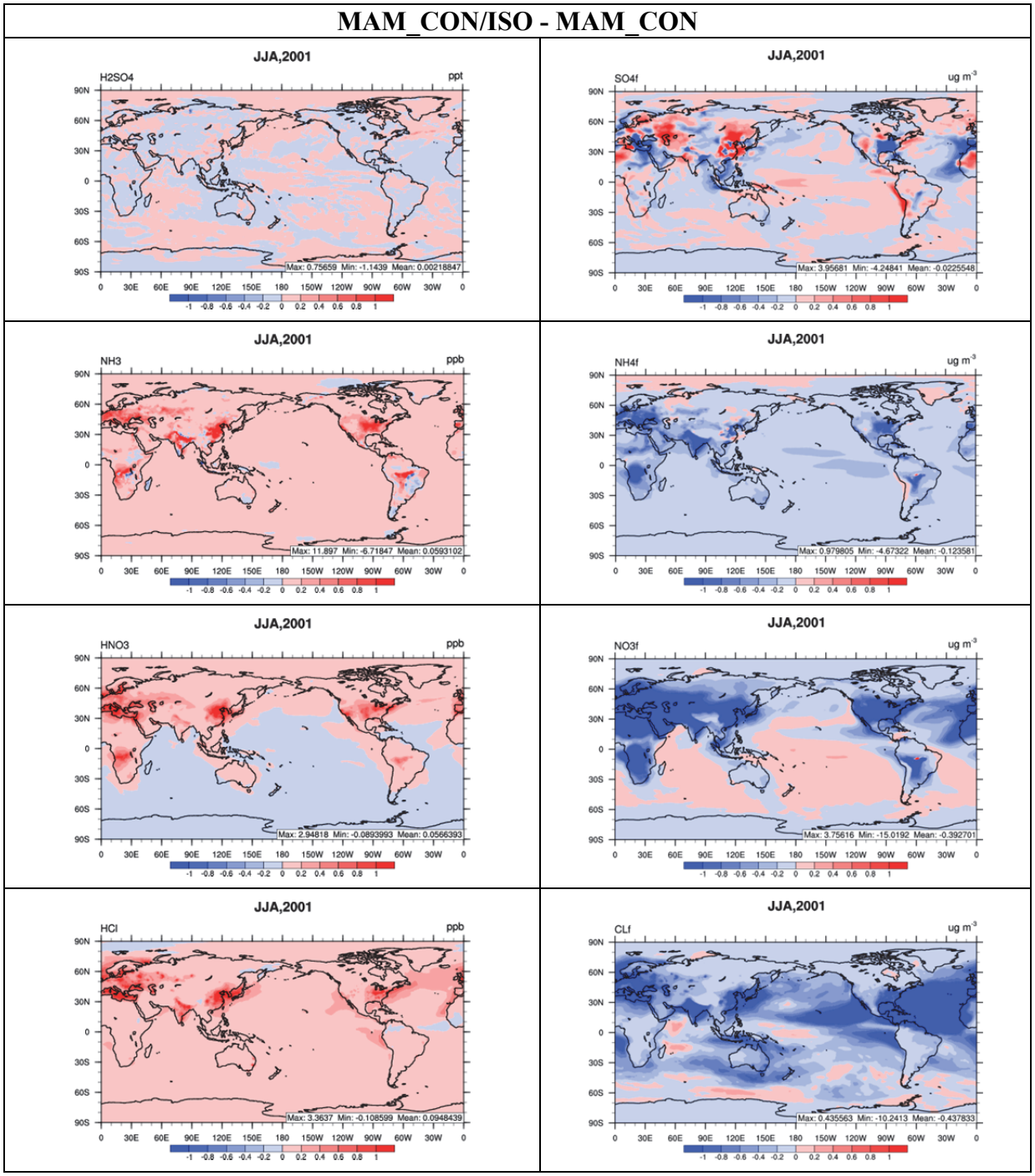

Figure 6a. Absolute differences of major PM species and their gas precursors between MAM_CON/ISO and MAM_CON for summer, 2001.

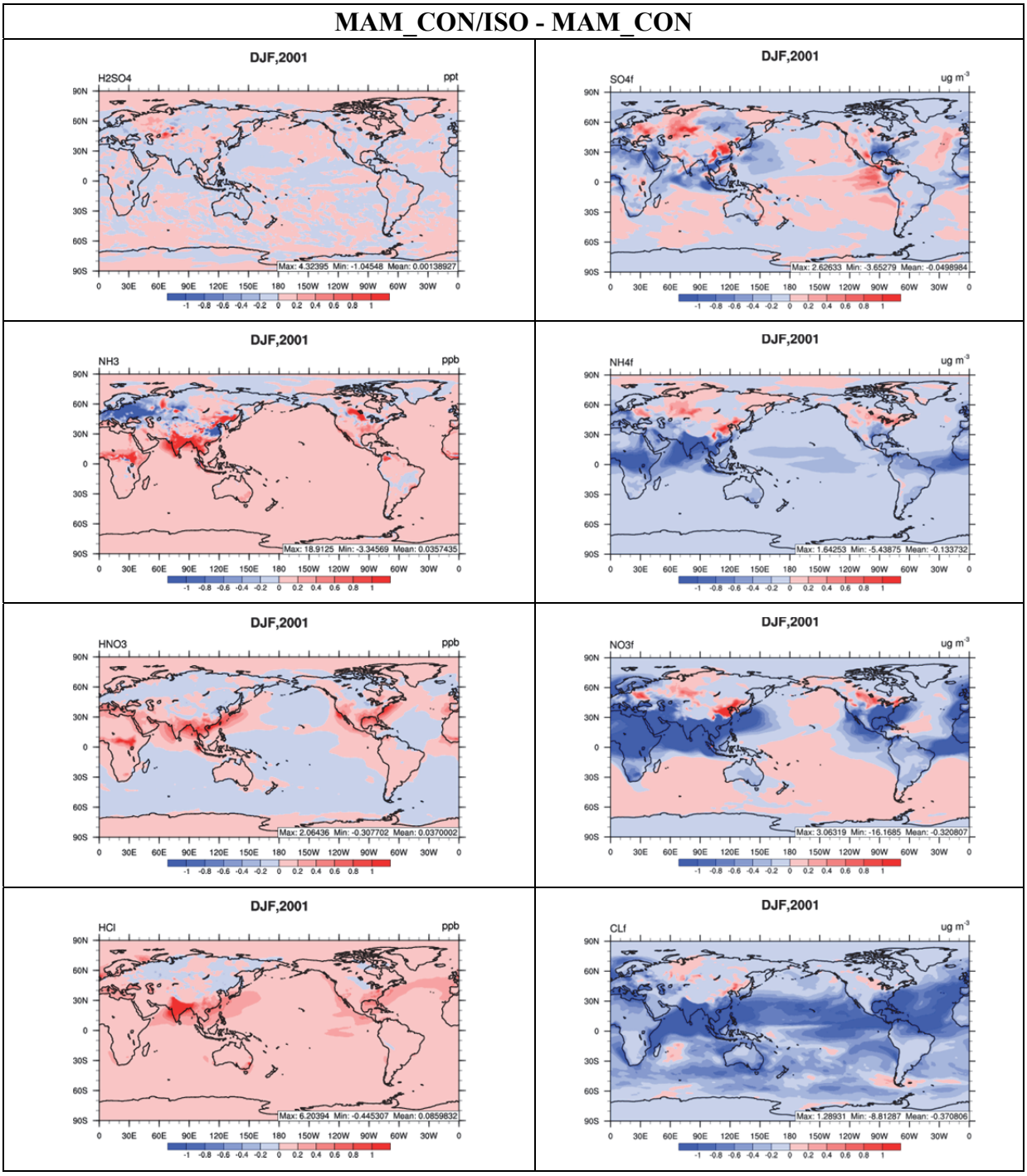

Figure 6b. Absolute differences of major PM species and their gas precursors between MAM_CON/ISO and MAM_CON for winter, 2001.

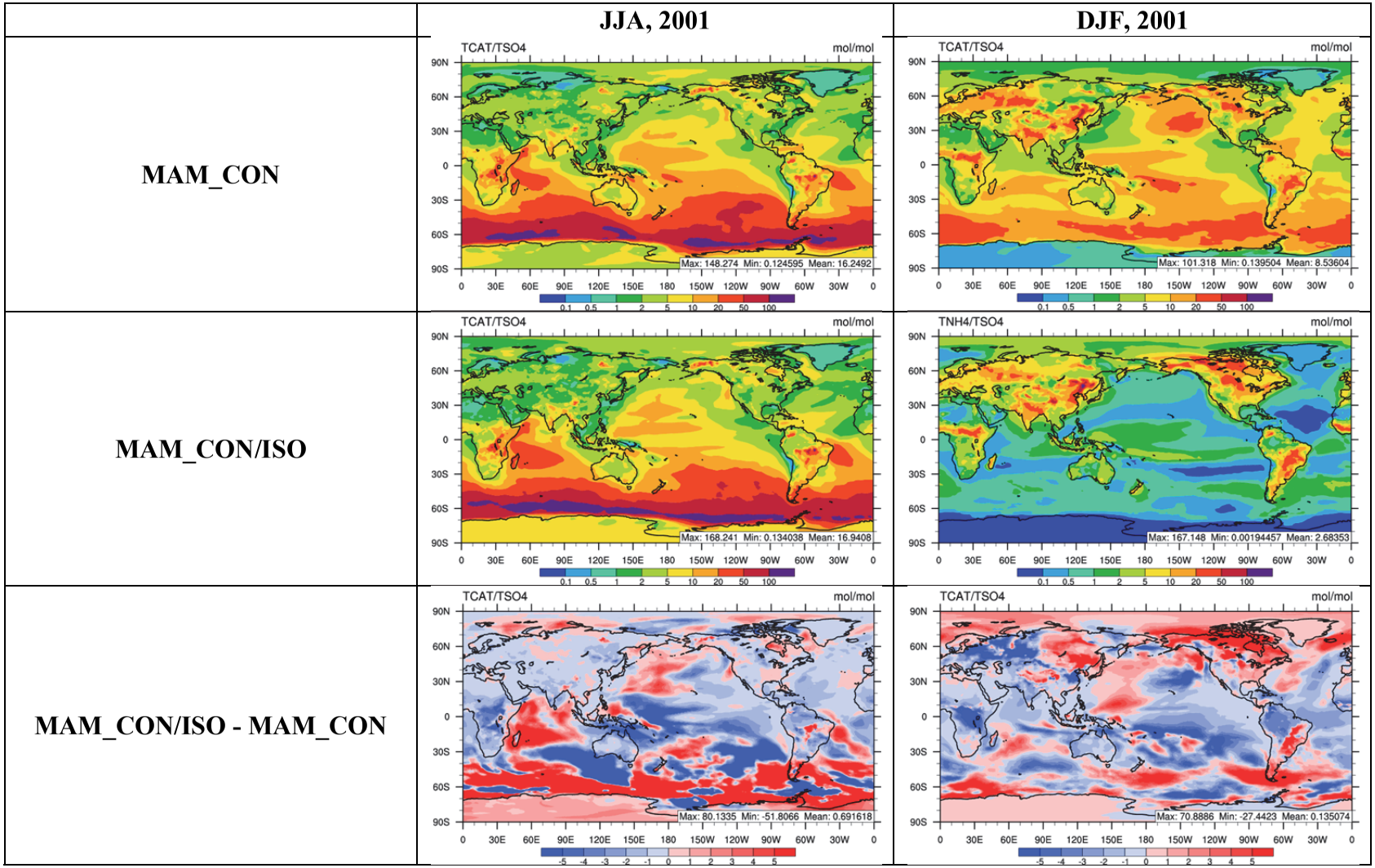

Figure 7. Surface distribution of TCAT/TSO4 in MAM_CON and MAM_CON/ISO and absolute differences of TCAT/TSO4 between MAM_CON/ISO and MAM_CON for summer and winter, 2001

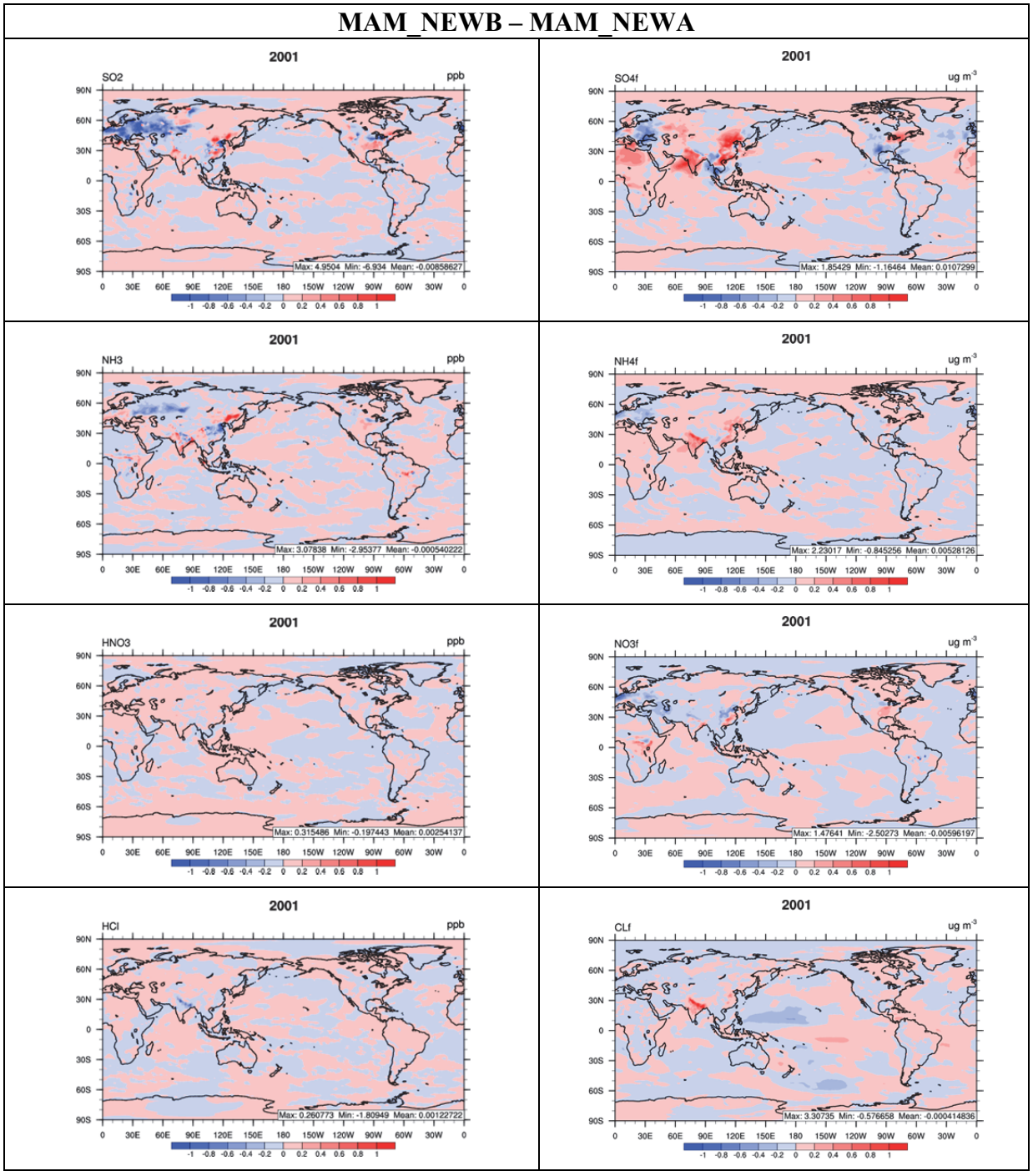

Figure 8. Absolute differences of major aerosol species and their gas precursors between metastable and stable conditions.

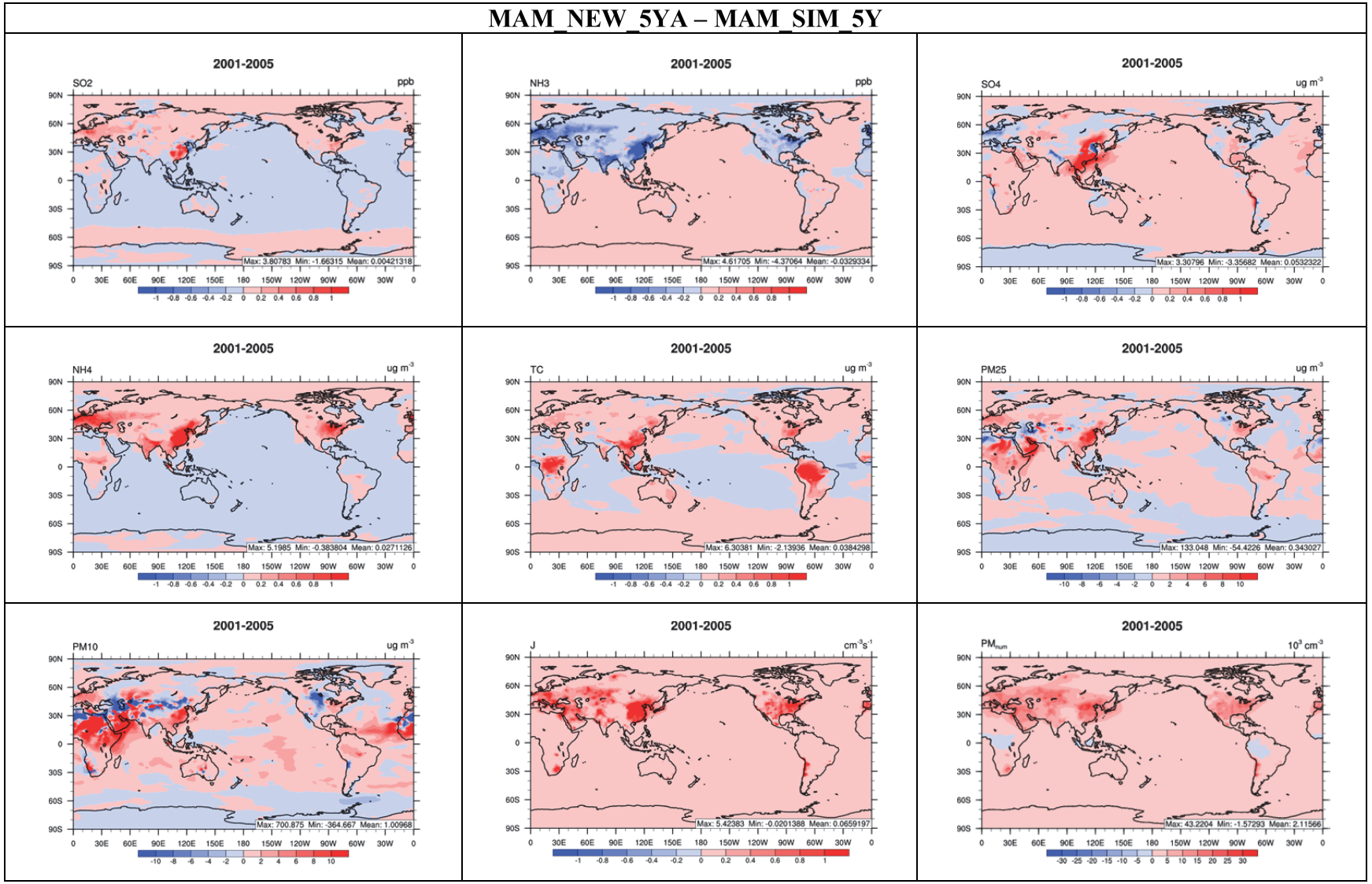

Figure 9. Absolute differences of major aerosol species and their gas precursors, new particle formation rate, and aerosol number between MAM_NEW_5YA and MAM_SIM_5Y for 2001-2005.

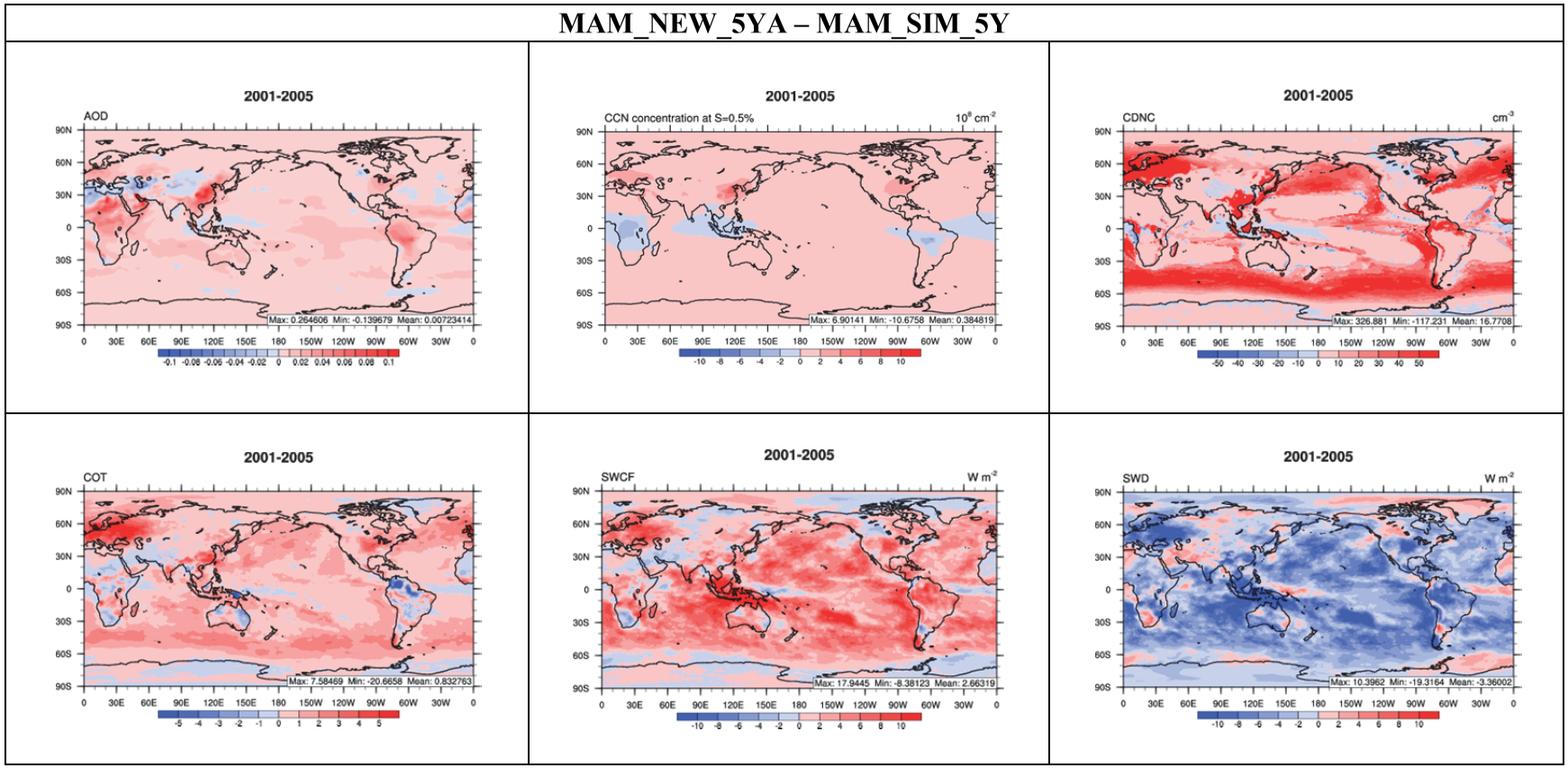

Figure 10. Absolute differences of major cloud and radiative variables between MAM_NEW_5YA and MAM_SIM_5Y for 2001-2005.